Sensitivity Analysis for Nonsmooth Mechanical Systems with Simultaneous Impacts and Spatial Friction

M. Bouma (0784690)
Department of Mechanical Engineering
Dynamics and Control group
Eindhoven University of Technology
DC 2019.003

Project Supervisor
prof. dr. ir. N. van de Wouw

Co-Supervisors
dr. ir. A. Saccon
dr. ir. M.W.L.M. Rijnen

Committee
prof. dr. ir. N. van de Wouw ∗
dr. ir. A. Saccon ∗
dr. ir. M.W.L.M. Rijnen ∗
dr. ir. D.J. Antunes †

∗ Eindhoven University of Technology (Dynamics and Control)
† Eindhoven University of Technology (Control Systems Technology)

January 9, 2019

Abstract

Everyday we touch, grab, or throw objects in our environment. This interaction with our environment comes natural to us; we do this without actively thinking about it. This is not the case for robots. To avoid complexity of the controller, many solutions for physically interacting robots require the contact to happen at zero relative velocity. Such movements, however, are very unnatural and hinder the robot in situations where speed is of significance, e.g., an industrial robot aiming to reach a certain throughput or a quadruped performing running motions. This thesis works towards a control strategy capable of handling contacts at non-negligible speed, increasing the performance of physically interacting robots and achieving more fluent, natural motions.

Acknowledgments

Contents

Chapter 1

Introduction

1.1 High performance physical interaction in robotics

In many applications of mechanical systems, and particularly in robotics, physical interaction with the environment is necessary to function. Humanoid robots, quadrupeds, and industrial robots are some examples of robots that repeatedly interact with their environment. Common control strategies that are available for these applications are limiting in performance. To avoid complexity of the controller, they often assume contact with their environment to happen at zero relative speed. Such motions are unnatural and makes the robots less suitable for situations where speed is of significance, e.g., an industrial robot aiming to reach a certain throughput or a quadruped performing running motions. Examples of such robots the SimLab quadruped [1] and the ABB IRB 360 FlexPicker [2], which are depicted in Figure 1.1. In such cases, performance is severely limited by zero velocity contact constraints. Therefore, it is clear that the field of robotics can benefit from control strategies that are capable of handling non-zero relative velocity. Such controllers, however, are more complex than the controllers that require zero velocity contact situations.

When two bodies make physical contact at non-zero velocity, impact occurs. Impact is a complex physical event that is characterized by dynamics at short timescales, high force levels, high energy dissipation rates, and large accelerations and decelerations. Due to the small timescale at which

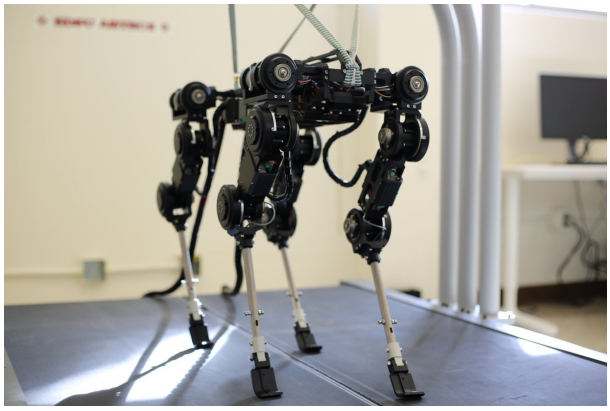

(a) *SimLab quadruped used at Virginia Tech [1].*

(b) *The ABB IRB 360 FlexPicker [2].*

Figure 1.1: *Two examples of robots with physical interaction that can benefit from high performance control strategies.*

impacts happen, their effect is often modeled as instantaneous. In such a modeling setting, the contact forces are impulsive and the velocity experiences jumps during an impact. Such a modeling approach is pursued within *nonsmooth mechanics*. Nonsmooth mechanical systems with impact are systems that have discontinuities in their state-evolution. In nonsmooth mechanics, a unilateral constraint is a constraint that prevents two bodies from penetrating. Mechanical systems with unilateral constraints are an example of systems that can exhibit nonsmooth behavior, as they experience velocity jumps when their unilateral constraints are closed at non-zero velocities. Control strategies for such systems are necessary to achieve higher performance.

1.2 Nonsmooth modeling frameworks

Nonsmooth systems can be described by several mathematical frameworks, e.g., singularly perturbed systems, hybrid systems, complementarity systems, and (measure-)differential inclusions [3]. The singular perturbation framework approximates the nonsmooth behaviour using a singularly perturbed smooth system. In this way, the singularly perturbed system can be evaluated numerically using a single smooth differential equation. However, due to the smooth approximation, the system becomes excessively stiff and needs extremely small time-steps in numerical simulation.

More suitable for numerical evaluation are differential inclusions, which are applicable to systems with a discontinuous right-hand side but a time-continuous state-evolution (also called Filippov-systems [4]). A common example of Filippov-systems are systems experiencing dry friction. The differential inclusion provides a description of the nonsmooth dynamics in a single inclusion. However, mechanical systems with unilateral constraints and impact do not satisfy the requirement of having a time-continuous state-evolution. A measure-differential inclusion describes the continuous as well as the impulsive dynamics of a nonsmooth system [5]. In this way, measure-differential inclusions are suitable for systems with time-discontinuities in their state-evolution [6,7]. Using this approach, the dynamics can be accurately integrated using the timestepping method [8].

From a control point-of-view, the complementarity framework is often considered. This framework describes nonsmoothness through a combination of differential equations and inequalities [9, 10]. In [11], the complementarity problem is used to describe mechanical systems with unilateral constraints. It plays a key role in mathematical programming, and several solutions for trajectory tracking using complementarity systems exist [12, 13].

In recent years, the hybrid systems framework has drawn more interest for solving the trajectory tracking problem of nonsmooth systems [14,15]. A hybrid system is a dynamical system that exhibits both continuous and discrete dynamics behaviour, where it reinitializes the state and switches (discrete behaviour) between several differential equations (continuous behaviour) [16]. According to [17], the hybrid systems framework is suitable for the modeling of mechanical systems with unilateral constraints as well as robotics. In a hybrid dynamical model guard sets are defined, which, when entered by the state of the system, will cause the dynamics to switch from one differential equation to another and possibly reinitialize the state. This makes it a rather intuitive approach to the modeling of nonsmoothness.

A known difficulty with the hybrid system framework however, is a phenomenon called *Zeno-behaviour*. One speaks of Zeno-behaviour when an infinite amount of guard activations happens in a finite time. A classic example is the bouncing ball. Measure-differential inclusions with a timestepping scheme would be more suitable in such a situation, since the combined effect of several state resets is captured in a single time step. An advantage of using the hybrid systems framework, is that it is a more intuitive description of the dynamics whereas measure-differential inclusions are more abstract. The stability analyses for these frameworks are well-developed, i.e., [16, 18, 19] for

hybrid systems, [20–22] for measure differential inclusions, and [7, 23, 24] for linear complementarity problems.

1.3 Tracking control for nonsmooth systems

Legged robotic systems account for a substantial part of the research done into the trajectory tracking control of mechanical systems with unilateral constraints. Many results in this area deal with the stability of periodic orbits of systems with impacts. In [25], a first big step has been made into modeling and controlling a one-legged hopping robot. In this research, the energy-loss during impact is modeled through damping and coupling effects are modeled as perturbations. Other pioneering works can be found in [26–28].

In [15, 29], the hybrid framework is adopted to find stable walking gaits for biped robots. Using Poincaré maps, the stability of periodic orbits with discontinuities of under-actuated systems are analyzed. Phases can be distinguished where the system is fully actuated and where the system is under-actuated. The fully actuated phase can then be used to stabilize the periodic trajectory despite the under-actuated phase. This work is continued in [30], generating control laws using data of walking humans, and in [31] the energy-efficiency of generated walking gaits has been the focus. An example of a humanoid robot on which such controllers have been implemented is Agility Robotics' Cassie [32], which is depicted in Figure 1.2. An extensive survey in the field of bipedal robotic walking can be found in [33]. The analysis of stable walking gaits is applied to the MIT Cheetah in [14], where a stability analysis and controller design is presented for the trot-running of a quadrupedal robot.

Considerable progress has been made in the field of walking robots and billiards, yet it is easy to think of an example where nonperiodic trajectories are of interest. Under the assumption that the state trajectory jumps at the exact same time as the reference trajectory, the trajectory tracking problem for nonsmooth systems has been solved for several types of systems. The tracking problem for Lur'e type systems has been analyzed in [34, 35], using MDI's to describe nonsmooth and impulsive dynamics. This work uses the convergence property to provide a solution to the tracking problem, where the solution may be time-varying and exhibit state-jumps. In [12], a passivity-based approach is used to solve the tracking control problem of complementarity Lagrangian systems. Asymptotic

Figure 1.2: *The bipedal robot Cassie developed by Agility Robotics [32].*

stability is achieved for Lagrangian systems with unilateral constraints. The same approach has been applied to the hybrid system framework in [36], which results in a control law that can guarantee stability of a trajectory with multiple impacts. By embedding the reference trajectory with discontinuities into a set, Lyapunov tools can be used to analyze stability as in [37,38]. In [39], a stability analysis of systems with impacts and friction has been presented. The results are obtained using the measure-differential inclusion framework, resulting in a smooth control law. The planning and control of non-periodic bipedal locomotion with impacts and friction is discussed in [40].

In the prior discussed work, the tracking problem has been solved under the assumption that the jump of the state trajectory occurs at the same time-instant as the jump of the reference trajectory, i.e., in [36, 38, 39]. In reality, especially in high velocity conditions, the time-instant of the state jump and that of the reference trajectory jump are noncoincident more often than not. In this case a phenomenon called *peaking* occurs [41]. Spikes in the tracking error will arise around the jump times, generating large actuation forces and contradict stability.

Solutions to peaking of the tracking error exist for periodic orbits in [42, 43], where the results are compatible with a mismatch in reference jump-time and state jump-time for infinite time periodic trajectories with infinitely many state-jumps. Such trajectories are often found in so-called *Birkhoff Billiards* where the coefficient of restitution is 1. [44] also presents results for billiards, applicable to a large class of trajectories than [42, 43]. In [41, 45], a novel definition of the tracking error is introduced, using a distance function which is not sensitive to jumps of the state and the reference trajectory. Lyapunov-based conditions for the global asymptotic stability of nonsmooth trajectories have been derived. Another solution for the problem of a jump-time mismatch is proposed in [46] in the form of a distance function similar to [41,45] based on a quotient metric. When a state jump happens at a different time than the reference jump, this approach applies the jump map to the reference to be able to compare the state to the reference. In [47], a novel controller design using gluing functions is introduced to connect the start and end point of a jump in the state space. After gluing, the system can be considered a continuous or piecewise continuous function without state jumps. In [48], a tracking error is defined by taking the smallest of two values: the ante-impact tracking error and post-impact tracking error.

The solutions to the peaking behavior mentioned in the section above do not always appear to be the best choice. It is beneficial to have some control over how the tracking error is defined, and particularly what the reference trajectory is, around the jump times. For this reason, a more intuitive and controllable solution to the peaking behavior is introduced in the following section.

1.4 Reference spreading control

By extending the reference trajectory segments and considering the error between the reference trajectory and the state trajectory that have encountered the same number of jumps, [49, 50] have introduced a novel notion of error for systems with state jumps. This way, an ante-event state trajectory can always be compared to an ante-event reference trajectory and a post-event state trajectory can always be compared to a post-event reference trajectory, even when the event times do not coincide. The extensions are defined by integrating the vector field, forwards and backwards, past the event times. Consequentially, the input during the extension can be chosen in a particular manner to find a desired extension of the reference trajectory. Due to this flexibility, one has more control over the behavior around events. These extensions will, similar to the solutions presented in previous section, avoid peaking of the tracking error. The authors of [49, 50] then use that notion of error as the basis for extending the sensitivity analysis, as introduced in [51], to the hybrid system framework. Subsequently, these results are used to obtain a local approximation of

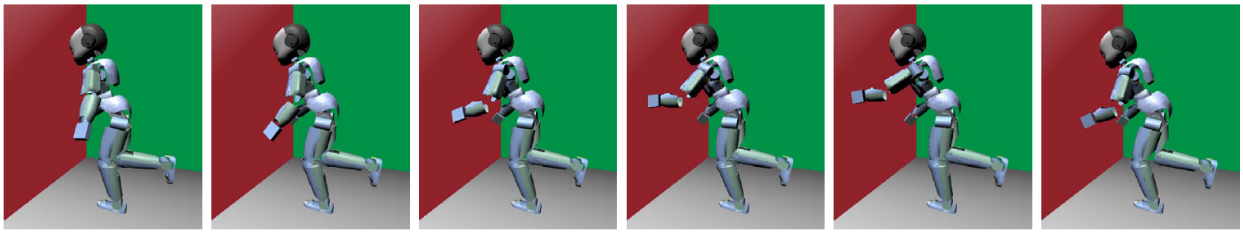

Figure 1.3: *Snapshots of the motion the iCub robot makes in the simulation done in [56] using reference spreading control.*

the perturbed state dynamics. This analysis gives insight in how the system behaves under the presence of perturbations, which is useful for controller design. Experimental results for this control law are presented in [52], where a 1-DOF robot arm performs an impacting trajectory using the control law as proposed in [49]. In [53], a control strategy for hybrid systems with state triggered jumps is used on a hopping robotic leg model from [54]. This control strategy is named *reference spreading control* in [55], due to the extensions made on the reference trajectories in the notion of error. In [56], the reference spreading control law is used in simulations with an iCub robot. The iCub robot balances on one foot and keeps himself standing upright by making and breaking contact with a wall using one of its arms. Some snapshots of the motion are depicted in Figure 1.3. As mentioned earlier, a vast amount of works in literature assume that the exact impact time is known. This is extremely limiting during implementation of the control law. Using the reference spreading approach, the impact time of the state is allowed to deviate from that of the reference, making implementation of the control law in practical applications more viable while still allowing for state-jumps.

As is the case in the simulations with the iCub in Figure 1.3, impacts are often modeled using a one-point contact between two bodies. However, in practice, more complex geometries can make contact with each other. The feet of Cassie in Figure 1.2 for example, have a clear resemblance to human feet, which often results in distinct heel and toe strikes during walking motions. A more realistic contact geometry is used in [57], in which the foot strike of a humanoid bipedal robot is modeled using multiple impacts. One strike is modeled by a heel impact, a toe impact, a heel release, and finally a toe release, resulting in a more realistic model of the walking gait of the bipedal robot. In such a movement, the order of impacts is known.

When considering a trajectory with multiple contacts closing at one time-instant, the problem becomes more complex. Imagine for example the iCub in [56] having a physically realistic geometry at the end of its arm, as illustrated in Figure 1.4. The arm can first make a point contact, then a line contact, and finally a surface contact to make full contact with the wall. It can also track a trajectory where the surface of the arm makes a surface contact with the wall at one time-instant. Such events can be considered as multiple impacts happening at the same time-instant and are called *simultaneous impacts*. One can imagine that a small perturbation can significantly change the behavior of a simultaneous impact. Instead of the expected single jump in the state, a perturbation can cause the state to have multiple jumps. Also the order of impacts of the several parts of the arm is not known beforehand. In Figure 1.4, a planar representation of the wrist of the iCub robot is illustrated. This image clearly visualizes the effect a perturbation has on a trajectory with simultaneous impacts. The approach used in [57] is not suitable for these situations.

The phenomenon of simultaneous impacts is first introduced in [58], where the first step is taken into solving the trajectory tracking problem for such impacts. A hybrid system framework is used to model the impacts, where multiple guards can be activated at once. The reference spreading control

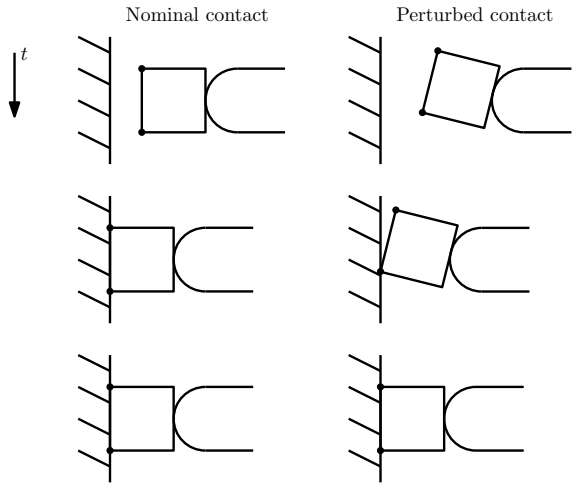

Figure 1.4: *A planar illustration of the end effector of the wrist of the iCub robot. On the left: a nominal trajectory is illustrated (from top to bottom), where a simultaneous impact happens at the points indicated by black dots. The wrist immediately makes a line-contact with the surface. On the right: the trajectory is perturbed, which results in two subsequent impacts instead of one simultaneous impact.*

in [53, 55] and the sensitivity analysis to approximate a system's behavior around trajectories with single guard activation, as introduced in [49], are extended to be suitable for simultaneous guard activation. The results of the sensitivity analyses are used to find a first-order approximation of the perturbed trajectory, which can be used to find suitable feedback gains. In addition to an impulse perpendicular to the impact-surface, taking friction into account will result in a tangential impulse. Also, the release phase is not considered in [58]. During the release phase, no discontinuity in the state-evolution is seen, only a change in the number of active constraints on the system occurs. Therefore, this research aims at applying the reference spreading control strategy and sensitivity analysis to systems experiencing both impacts including friction and releasing motions.

1.5 Research objectives and contribution

The research objective of this work is to extend the work presented in [59] in two ways: extending the sensitivity analysis to friction cases and release cases. In this section, the research objective is further elucidated as well as the subsequent contribution of this thesis.

Simultaneous impacts with friction

Friction elements are often disregarded when analyzing impacts. However, to set up a unifying theory, friction elements should not be ignored. Tangential impulses can have a considerable effect on a system's dynamics. Particularly for walking motions, the frictional element of an impact is of significant importance. The impact laws used in the work of [58] can be extended using one of the several available friction laws [22]. To supplement impact laws with a tangential element, often a Coulomb friction law is used [60]. In addition to the tangential impulse, a Filippov-like discontinuity will be present due to Coulomb friction. This work will include a Coulomb friction law in order to achieve more accurate models and controllers for mechanical systems with unilateral constraints. Therefore, the research objective associated with frictional simultaneous impacts is defined as:

Find a model suitable to describe mechanical systems with unilateral constraints and spatial friction. The sensitivity analysis and mathematical notation presented in [59] shall be extended to be compatible with such models.

Simultaneous releases

The release of two bodies is based on a force equilibrium. For this reason, the conditions that determine whether release happens is not only state dependent, but also input dependent. In [53] and [61], tracking of trajectories with events experiencing input-based triggers has been extensively researched. However, these results only include subsequent events. The release phase for simultaneous events is not yet investigated. In [58], only the establishment of contact is simulated while release is excluded. Extending the sensitivity analysis in [58] to be suitable for simultaneous releases would make it possible to simulate and control one trajectory with several simultaneous impacts and releases. Therefore, the research objective associated with simultaneous releases is defined as:

Extending the sensitivity analysis presented in [59] such that it is suitable for input-triggered events.

1.6 Report outline

The modeling of mechanical systems with unilateral constraints and spatial friction is discussed in Chapter 2. The generic dynamics of a mechanical system including contact and friction laws are derived, eventually resulting in a hybrid system with impulsive effects. Then, in Chapter 3, a tracking control strategy for hybrid systems with isolated state-and-input-triggered events is presented. In Chapter 4, this tracking control strategy is extended to trajectories involving simultaneous impacts. An example of a mechanical system with unilateral constraints and spatial friction is given in Chapter 5, which is used for a numerical validation of the presented control strategy. Finally, in Chapter 6, conclusions are drawn and recommendations for future research are provided.

Chapter 2

Mechanical Systems with Unilateral Constraints and Spatial Friction

In this chapter, several modeling approaches for mechanical systems with unilateral constraints and spatial friction are presented. We start by presenting a general representation of mechanical systems. Then, several formulations of contact and friction laws are introduced in the form of complementarity conditions. The complementarity problem formulation is a complete and often used formulation for mechanical systems with unilateral constraints. This complementarity formulation is then transformed into a hybrid system formulation, that will be used in this work to analyze the tracking of trajectories of mechanical systems with unilateral constraints and spatial friction. While the hybrid system formulation is restrictive in modeling, it is a powerful tool for the control of systems with a special class of trajectories. Since the analysis that will be presented in this work is done with controller design in mind, the analysis will be presented in the hybrid system framework.

2.1 General system definition

When a unilateral constraint is activated, the differential equation that describes the dynamics of the system can change. The state even goes through a reinitialization when the constraint is activated with non-zero velocity. Two bodies already in contact can also experience changes in their dynamics, as a result from the friction between these bodies. This behavior can be described by dynamics consisting of a continuous part and a discrete part; the continuous part describes the flow of the state, and the discrete part describes the reinitialization of the state. The occurrence of a change in differential equation and a possible state reinitialization are referred to as *events*. To be able to detect when the system goes through a such an event, contact points are defined on the bodies. These contact points can activate and deactivate unilateral constraints, which corresponds with opening and closing contact with another body. A contact point that has activated a unilateral constraint can transition between stick and slip. A contact point in stick has a tangential relative velocity of zero, whereas a contact point in stick has a nonzero tangential relative velocity. The *mode* of the contact point is defined. The mode determines if a contact point is in contact or not, and if it is in stick or slip when the contact point is in contact. Using these contact points, a method is presented to model mechanical systems with unilateral constraints and spatial friction.

Let us now consider a mechanical system whose current configuration is described by the generalized coordinates $\boldsymbol{q} \in \mathbb{R}^n$ and whose generalized velocity is denoted $\boldsymbol{\nu} \in \mathbb{R}^n$ with $\boldsymbol{\nu} = \dot{\boldsymbol{q}}$ almost everywhere. The configuration space of the system is restricted using c unilateral constraints for

modeling contact, using the set of contact points $\mathcal{I} = \{\iota_1, \iota_2, \ldots, \iota_c\}$. The set $\mathcal{I}_{\text{cl}}$ is defined as the set of c_{cl} closed contact points, i.e., for a contact $\iota \in \mathcal{I}_{\text{cl}}$ the corresponding unilateral constraint is active. The set of potential contact points for which this geometric constraint is inactive, or open contact points, we define as $\mathcal{I}_{\text{op}} := \{\iota \mid \iota \notin \mathcal{I}_{\text{cl}}\}$. Note that in a physics-based engine the set $\mathcal{I}_{\text{op}}$ is often undefined, because not all contact points are tracked. Only the contact points generating reaction forces are tracked. The set $\mathcal{I}_{\text{op}}$ is only defined for convenience when the mode of the system is discussed. When a unilateral constraint is activated at a nonzero relative velocity, impact happens. For the unilateral constraint not to be violated, a jump in the velocity has to occur. These impact-times are denoted τ_j, where $j \in \{1, 2, \ldots, N\}$ is a counter for unilateral constraint activations, with N the number of jumps in a trajectory.

Consider Figure 2.1 showing two bodies. A contact point ι is defined on one of the bodies, at which a plane tangent to the surface of the body is spanned. In the direction normal to this plane, the contact distance $\mathrm{h}_{n,\iota}(\boldsymbol{q})$ is defined. The contact distance is the minimal distance between the contact point and the surface that it can make contact with. For the relative normal velocity $\mathrm{v}_{n,\iota} \in \mathbb{R}$ of contact point ι follows that

$$\mathrm{v}_{n,\iota} = \frac{\partial \mathrm{h}_{n,\iota}}{\partial \boldsymbol{q}} \frac{\mathrm{d}\boldsymbol{q}}{\mathrm{d}t} = \boldsymbol{w}_{n,\iota}^T \dot{\boldsymbol{q}}, \tag{2.1}$$

with $\boldsymbol{w}_{n,\iota}^T \in \mathbb{R}^n$ representing the Jacobian of the normal velocity $\mathrm{v}_{n,\iota}$. The relative tangential velocity $\mathbf{v}_{t,\iota} \in \mathbb{R}^2$ is defined in the tangent plane of contact point ι. Similar to the normal direction, $\mathbf{h}_{t,\iota} = \begin{bmatrix} \mathbf{h}_{t_1,\iota} & \mathbf{h}_{t_2,\iota} \end{bmatrix}^T$, where $\mathbf{h}_{t_1,\iota}$ and $\mathbf{h}_{t_2,\iota}$ are the contact distances in t_1 direction and t_2 direction, respectively. It then follows that the relative tangential velocity is given by

$$\mathbf{v}_{t,\iota} = \frac{\partial \mathbf{h}_{t,\iota}^T}{\partial \boldsymbol{q}} \frac{\mathrm{d}\boldsymbol{q}}{\mathrm{d}t} = \boldsymbol{W}_{t,\iota}^T \dot{\boldsymbol{q}}, \tag{2.2}$$

with $\boldsymbol{W}_{t,\iota}^T \in \mathbb{R}^{n \times 2}$ representing the Jacobian of the tangential relative velocity $\mathbf{v}_{t,\iota}$.

Then, the continuous dynamics of a mechanical system with unilateral constraints and spatial friction are of the form

$$\boldsymbol{M}(\boldsymbol{q})\dot{\boldsymbol{\nu}} + \boldsymbol{C}(\boldsymbol{q}, \boldsymbol{\nu}) = \boldsymbol{S}(\boldsymbol{q})\boldsymbol{u} + \sum_{\iota \in \mathcal{I}_{\text{cl}}} \boldsymbol{w}_{n,\iota}(\boldsymbol{q})\lambda_{n,\iota} + \boldsymbol{W}_{t,\iota}(\boldsymbol{q})\boldsymbol{\lambda}_{t,\iota}, \tag{2.3}$$

(Contact Law),

(Friction Law),

with $\boldsymbol{q}, \boldsymbol{\nu} \in \mathbb{R}^n$ and $\boldsymbol{u} \in \mathbb{R}^m$. In (2.3), $\boldsymbol{M}(\boldsymbol{q}) \in \mathbb{R}^{n \times n}$ is the mass matrix of the system, $\boldsymbol{C}(\boldsymbol{q}, \boldsymbol{\nu}) \in \mathbb{R}^n$ contains the centripetal, Coriolis, stiffness and damping related forces, and gravitational forces in the system and $\boldsymbol{S}(\boldsymbol{q}) \in \mathbb{R}^{n \times m}$ represents the generalized directions of the input forces $\boldsymbol{u}$. $\lambda_{n,\iota} \in \mathbb{R}$ and $\boldsymbol{\lambda}_{t,\iota} \in \mathbb{R}^2$ are the normal and tangential reaction forces, respectively, of contact point ι with $\boldsymbol{w}_{n,\iota} \in \mathbb{R}^n$ and $\boldsymbol{W}_{t,\iota} \in \mathbb{R}^{n \times 2}$ the transposed corresponding Jacobians. To make the system description in (2.3) complete, a contact law and friction law is required. These laws will be discussed in Section 2.2.

As mentioned above, when a unilateral constraint is activated, impulsive dynamics can cause a jump in the generalized velocity of the system. The impulsive dynamics, derived in [22, Section 5.4], are of the form

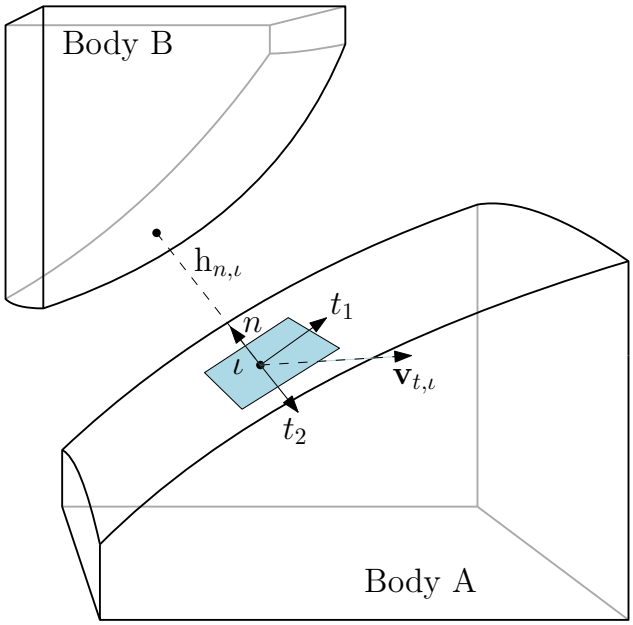

Figure 2.1: *An illustration of two bodies about to make contact. The contact distance* $\mathrm{h}_{n,\iota}$ *and the relative tangential velocity* $\mathbf{v}_{t,\iota}$ *for contact point* ι *are illustrated, which are defined on the surface of Body A.*

$$\boldsymbol{M}(\boldsymbol{q})(\boldsymbol{\nu}^+ - \boldsymbol{\nu}^-) = \sum_{\iota \in \mathcal{I}_{\mathrm{cl}}} \boldsymbol{w}_{n,\iota}(\boldsymbol{q})\Lambda_{n,\iota} + \boldsymbol{W}_{t,\iota}(\boldsymbol{q})\boldsymbol{\Lambda}_{t,\iota}, \tag{2.4}$$

(Impulsive Contact Law),

(Impulsive Friction Law),

with $\Lambda_{n,\iota}$ and $\boldsymbol{\Lambda}_{t,\iota}$ the normal and tangential impulsive reaction forces, respectively, of contact point ι. These dynamics are impulsive, and happen at one instance in time. In (2.4), $\boldsymbol{\nu}^-$ and $\boldsymbol{\nu}^+$ denote the left, respectively the right limit of the generalized velocity $\boldsymbol{\nu}$ at the time of impact τ_j. The expression moreover states that, similarly to the continuous dynamics (2.3), constitutive laws for contact and friction are required. These will be discussed in the following. First a complementarity problem formulation of mechanical systems with unilateral constraints is given, from which later a proximal point formulation and a hybrid system formulation are derived. For more information on modeling of multibody systems, the reader is referred to [22] and [62].

2.2 Model formulation including set-valued force laws

Mechanical systems with unilateral constraints can conveniently be described using so-called complementarity constraints or set-valued force laws. Particularly impacts and frictional effects are often described using these complementarity constraints, introducing a nonsmoothness into the mechanical system. In this section, the contact and friction laws required to describe a mechanical system with unilateral constraints and spatial friction are presented in a complementarity fashion. First, the contact case is handled in Section 2.2.1, where the complementarity constraints describing contact behavior for both flow and impulsive situations are presented. In Section 2.2.2, the complementarity constraints for frictional effects are presented, similar to the contact case, for both flow

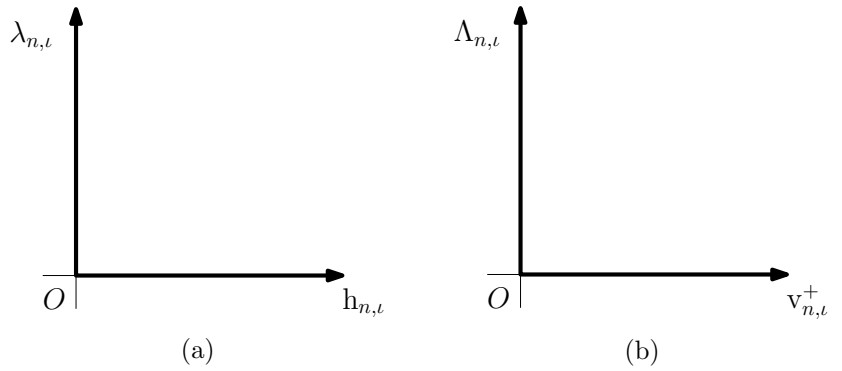

Figure 2.2: *In* (a) *Signorini's contact law and in* (b) *Newton's impact law without restitution.*

and impulsive situations. Finally, a complete complementarity description of mechanical system with unilateral constraints and spatial friction is presented in Section 2.2.3.

2.2.1 Signorini's contact law and Newton's impact law

To describe the contact interaction between rigid bodies, Signorini's contact law is used. Since we assume that the bodies composing the system are rigid and therefore impenetrable, and that the reaction forces caused by contact cannot prevent two or more bodies from seperating, both the contact distance $\mathrm{h}_{n,\iota}$ and and reaction force $\lambda_{n,\iota}$ cannot become negative. For a contact point $\iota \in \mathcal{I}$, two situations are then possible, i.e.,

1. $\mathrm{h}_{n,\iota} = 0 \ \wedge \ \lambda_{n,\iota} \geq 0$ (closed-contact)
2. $\mathrm{h}_{n,\iota} > 0 \ \wedge \ \lambda_{n,\iota} = 0$ (open-contact)

These situations are illustrated in Figure 2.2a, from which can be seen that the two situations are orthogonal. This behavior can be summarized in the complementarity condition, as presented in [22, Section 5.3.1],

$$0 \leq \mathrm{h}_{n,\iota} \perp \lambda_{n,\iota} \geq 0, \tag{2.5}$$

where the symbol $\perp$ is used to express the orthogonality between the constraints on $\mathrm{h}_{n,\iota}$ and $\lambda_{n,\iota}$. The complementarity condition (2.5) is called Signorini's contact law. A separate model is required for describing the contact dynamics during an impact event. As mentioned above, when contact is established at nonzero velocity, a jump in the velocity is generally seen. To describe this impact effect, Newton's impact law is used. Newton's impact law relates the normal velocities at the contact points after impact to the normal velocities just before the impact using a so-called coefficient of restitution e. Mathematically, Newton's impact law can be expressed as

$$\mathrm{v}^+_{n,\iota} = -e_{n,\iota}\mathrm{v}^-_{n,\iota}, \ \text{when } \mathrm{h}_{n,\iota} = 0, \ \dot{\mathrm{h}}_{n,\iota} < 0, \tag{2.6}$$

where $\mathrm{v}^-_{n,\iota}$ and $\mathrm{v}^+_{n,\iota}$ are the ante- and post-impact relative normal velocities, respectively, associated with contact point ι. In this work, the coefficient of restitution $e_{n,\iota}$ is assumed to be 0 for all ι, corresponding to a completely inelastic impact. For closed contacts, an impact law can be defined that relates the impulsive contact force $\Lambda_{n,\iota}$ to the post-impact normal velocity $\mathrm{v}_{n,\iota}$. Considering multi-contact systems, two situations can occur when a contact is closed:

1. $\Lambda_{n,\iota} > 0 \ \wedge \ \mathrm{v}_{n,\iota}^{+} = 0$ (ι participating in impact)
2. $\Lambda_{n,\iota} = 0 \ \wedge \ \mathrm{v}_{n,\iota}^{+} \geq 0$ (ι not participating in impact)

The situations described above are illustrated in Figure 2.2b, where again the orthogonality can be observed. The behavior can be summarized in the complementarity condition

$$0 \leq \mathrm{v}_{n,\iota}^{+} \perp \Lambda_{n,\iota} \geq 0, \qquad \forall \iota \in \mathcal{I}_{\mathrm{cl}}, \tag{2.7}$$

with $\mathcal{I}_{\mathrm{cl}}$ the set of closed contacts. The complementarity condition (2.7) is called Newton's impact law. Note that the impact law is defined on velocity level, whereas the contact law is defined on position level.

2.2.2 Coulomb's friction law

Coulomb's friction law is often used to model dry friction in mechanical systems. When considering isotropic friction in 3-dimensional environments, Coulomb's friction law states that the tangential reaction force vector at contact point ι satisfies the inclusion

$$-\boldsymbol{\lambda}_{t,\iota} \ \in \ \begin{cases} ||\mathbf{v}_{t,\iota}|| = 0 & \Rightarrow \quad ||\boldsymbol{\lambda}_{t,\iota}|| \leq \mu_\iota \lambda_{n,\iota} \\ ||\mathbf{v}_{t,\iota}|| > 0 & \Rightarrow \quad \boldsymbol{\lambda}_{t,\iota} = \mu_\iota \lambda_{n,\iota} \frac{\mathbf{v}_{t,\iota}}{||\mathbf{v}_{t,\iota}||} \end{cases} , \tag{2.8}$$

with μ_ι the friction coefficient at contact point ι. The behavior described in (2.8) can conveniently be described using the normal cone formulation [22, Section 5.3.2]. The set of admissible friction forces $C_{t,\iota} \subset \mathbb{R}^2$, which for isotropic friction is a disk given by

$$C_{t,\iota} = \{-\boldsymbol{\lambda}_{t,\iota} \mid ||\boldsymbol{\lambda}_{t,\iota}|| \leq \mu_\iota \lambda_{n,\iota}\} . \tag{2.9}$$

The spatial Coulomb's friction law can then given be formulated as

$$\mathbf{v}_{t,\iota} \in \mu \lambda_{n,\iota} N_{C_{t,\iota}}(-\boldsymbol{\lambda}_{t,\iota}), \tag{2.10}$$

where $N_{C_{t,\iota}}$ is the normal cone set of $C_{t,\iota}$. The normal cone set N_C of a convex set C is given by

$$N_C(\boldsymbol{x}) := \left\{ \boldsymbol{y} \mid \boldsymbol{y}^T(\boldsymbol{x}^* - \boldsymbol{x}) \leq 0, \quad \boldsymbol{x} \in C, \ \forall \boldsymbol{x}^* \in C \right\} . \tag{2.11}$$

The normal cone set $N_C(\boldsymbol{x}) = 0, \ \forall \boldsymbol{x} \in C \setminus \partial C$, where ∂C denotes the boundary of C. $N_C(\boldsymbol{x}) \neq 0, \ \forall \boldsymbol{x} \in \partial C$. For all $\boldsymbol{x}$ on the boundary of C, $N_C(\boldsymbol{x})$ consists of the normal cone to the boundary of C on the point $\boldsymbol{x}$. The normal cone set can be explained more intuitively using Figure 2.3. We consider two situations: situation one, where $||(\boldsymbol{\lambda}_{t,\iota})_1|| < \mu_\iota \lambda_{n,\iota}$, and situation two, where $||(\boldsymbol{\lambda}_{t,\iota})_2|| = \mu_\iota \lambda_{n,\iota}$. In situation one, $(\boldsymbol{\lambda}_{t,\iota})_1 \in C_{t,\iota} \setminus \partial C_{t,\iota}$, meaning that $(\mathbf{v}_{t,\iota})_1 = 0$ according to (2.10). In situation two, $(\boldsymbol{\lambda}_{t,\iota})_2 \in \partial C_{t,\iota}$, meaning that $(\mathbf{v}_{t,\iota})_2$ is somewhere in the normal cone of $\partial C_{t,\iota}$ at $-\boldsymbol{\lambda}_{t,\iota}$. When the boundary of $\partial C_{t,\iota}$ is smooth at $-\boldsymbol{\lambda}_{t,\iota}$, the normal cone $N_{C_{t,\iota}}(-\boldsymbol{\lambda}_{t,\iota})$ is actually a ray. While the normal cone N_C is also defined for nonsmooth boundaries of C, this situation is not considered as the boundary of the set of admissible friction forces $\partial C_{t,\iota}$ is smooth everywhere. The relative tangential velocity $\mathbf{v}_{t,\iota}$ is therefore somewhere in the direction of $-\boldsymbol{\lambda}_{t,\iota}$, which is equivalent to the desired behavior described in (2.8), i.e.,

$$\mathbf{v}_{t,\iota} \in \mu \lambda_{n,\iota} N_{C_{t,\iota}}(-\boldsymbol{\lambda}_{t,\iota}) \Leftrightarrow -\boldsymbol{\lambda}_{t,\iota} \in \begin{cases} ||\mathbf{v}_{t,\iota}|| = 0 & \Rightarrow \quad ||\boldsymbol{\lambda}_{t,\iota}|| \leq \mu_\iota \lambda_{n,\iota} \\ ||\mathbf{v}_{t,\iota}|| > 0 & \Rightarrow \quad \boldsymbol{\lambda}_{t,\iota} = \mu_\iota \lambda_{n,\iota} \frac{\mathbf{v}_{t,\iota}}{||\mathbf{v}_{t,\iota}||} \end{cases} . \tag{2.12}$$

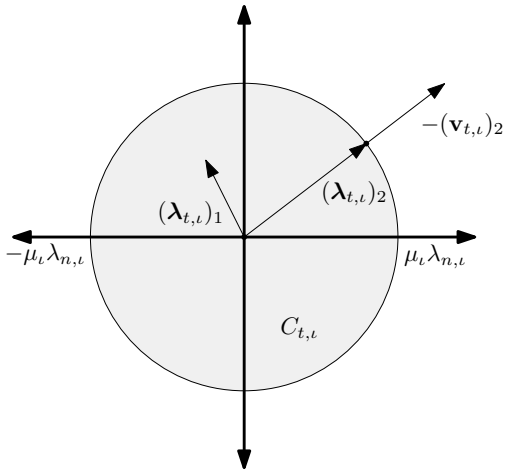

Figure 2.3: *The friction disk with two seperate friction forces* $\boldsymbol{\lambda}_{t,1}$ *and* $\boldsymbol{\lambda}_{t,2}$. $\boldsymbol{\lambda}_{t,1} = \mu\lambda_{n,1}$, *resulting in a tangential velocity* $\boldsymbol{\zeta}_{t,i} > 0$. $\boldsymbol{\lambda}_{t,2} < \mu\lambda_{n,2}$, *leading to a tangential velocity* $\boldsymbol{\zeta}_{t,i} = 0$.

The work in [63] shows a complementarity formulation that is algebraically equivalent to (2.10). This formulation is given by

$$\mathbf{v}_{t,\iota}||\boldsymbol{\lambda}_{t,\iota}|| = -\kappa_\iota\boldsymbol{\lambda}_{t,\iota}, \tag{2.13}$$
$$0 \leq \mu_\iota\lambda_{n,\iota} - ||\boldsymbol{\lambda}_{t,\iota}|| \perp \kappa_\iota \geq 0, \tag{2.14}$$

where κ_ι is a variable that determines the length of the velocity vector $\mathbf{v}_{t,\iota}$. Equations (2.13)-(2.14) will be used in this work to model spatial coulomb friction. We employ again Newton's impact law for modeling the impact behavior where now the tangential contact velocities before and after impact are related to each other using

$$\mathbf{v}_{t,\iota}^{+} = -e_{t,\iota}\mathbf{v}_{t,\iota}^{-}, \tag{2.15}$$

where $e_{t,\iota}$ is the tangential coefficient of restitution that we consider to be zero in this work. Then, similarly to the non-impulsive case, the impulsive Coulomb's friction law can be expressed as

$$\mathbf{v}_{t,\iota}^{+}||\boldsymbol{\Lambda}_{t,\iota}|| = \kappa_\iota\boldsymbol{\Lambda}_{t,\iota}, \qquad \forall\iota \in \mathcal{I}_{\mathrm{cl}}, \tag{2.16}$$
$$0 \leq \mu\Lambda_{n,\iota} - ||\boldsymbol{\Lambda}_{t,\iota}|| \perp \kappa_\iota \geq 0. \qquad \forall\iota \in \mathcal{I}_{\mathrm{cl}}. \tag{2.17}$$

Note that, just as the impulsive dynamics in the normal direction, the impulsive friction law only applies to closed contacts.

2.2.3 System dynamics with contact and friction law

When the contact and friction laws (2.5), (2.13) and (2.14) introduced in Sections 2.2.1 and 2.2.2 are incorporated in the flow dynamics (2.3) of the system, a complete model for the continuous dynamics is found, i.e.,

$$\boldsymbol{M}(\boldsymbol{q})\dot{\boldsymbol{\nu}} + \boldsymbol{C}(\boldsymbol{q},\boldsymbol{\nu}) = \boldsymbol{S}(\boldsymbol{q})\boldsymbol{u} + \sum_{\iota\in\mathcal{I}_{\mathrm{cl}}} \boldsymbol{w}_{n,\iota}(\boldsymbol{q})\lambda_{n,\iota} + \boldsymbol{W}_{t,\iota}(\boldsymbol{q})\boldsymbol{\lambda}_{t,\iota}, \tag{2.18}$$
$$0 \leq \mathrm{h}_{n,\iota} \perp \lambda_{n,\iota} \geq 0, \tag{2.19}$$
$$\mathbf{v}_{t,\iota}||\boldsymbol{\lambda}_{t,\iota}|| = -\kappa_\iota\boldsymbol{\lambda}_{t,\iota}, \tag{2.20}$$
$$0 \leq \mu\lambda_{n,\iota} - ||\boldsymbol{\lambda}_{t,\iota}|| \perp \kappa_\iota \geq 0, \tag{2.21}$$

with

$$\mathrm{h}_{n,\iota} := \mathrm{h}_{n,\iota}(\boldsymbol{q}), \tag{2.22}$$
$$\mathrm{v}_{n,\iota} := \boldsymbol{w}_{n,\iota}^T(\boldsymbol{q})\boldsymbol{\nu}, \tag{2.23}$$
$$\mathbf{v}_{t,\iota} := \boldsymbol{W}_{t,\iota}^T(\boldsymbol{q})\boldsymbol{\nu}. \tag{2.24}$$

Similarly, incorporating the impulsive contact and friction laws (2.7), (2.16), and (2.16) in the impact/discrete dynamics (2.4) gives a complete model for the impact behavior of the system. It follows that the discrete dynamics that are triggered by the occurrence of an impact event are given by

$$\boldsymbol{M}(\boldsymbol{q})(\boldsymbol{\nu}^+ - \boldsymbol{\nu}^-) = \sum_{\iota \in \mathcal{I}_{\mathrm{cl}}} \boldsymbol{w}_{n,\iota}(\boldsymbol{q})\Lambda_{n,\iota} + \boldsymbol{W}_{t,\iota}(\boldsymbol{q})\boldsymbol{\Lambda}_{t,\iota}, \tag{2.25}$$
$$0 \leq \mathrm{v}_{n,\iota}^+ \perp \Lambda_{n,\iota} \geq 0, \qquad \forall \iota \in \mathcal{I}_{\mathrm{cl}}, \tag{2.26}$$
$$\mathbf{v}_{t,\iota}^+ ||\boldsymbol{\Lambda}_{t,\iota}|| = \kappa_\iota \boldsymbol{\Lambda}_{t,\iota}, \qquad \forall \iota \in \mathcal{I}_{\mathrm{cl}}, \tag{2.27}$$
$$0 \leq \mu\Lambda_{n,\iota} - ||\boldsymbol{\Lambda}_{t,\iota}|| \perp \kappa_\iota \geq 0. \qquad \forall \iota \in \mathcal{I}_{\mathrm{cl}}, \tag{2.28}$$

with

$$\mathrm{v}_{n,\iota}^+ := \boldsymbol{w}_{n,\iota}^T(\boldsymbol{q})\boldsymbol{\nu}^+, \tag{2.29}$$
$$\mathbf{v}_{t,\iota}^+ := \boldsymbol{W}_{t,\iota}^T(\boldsymbol{q})\boldsymbol{\nu}^+. \tag{2.30}$$

2.3 Hybrid system formulation

In this section, the dynamics of the complementarity system defined in Section 2.2 is written to a hybrid formulation, resulting in a hybrid framework for mechanical systems with unilateral constraints and spatial friction. In [64, p. 222], event driven numerical methods are presented for mechanical systems with spatial friction. The model presented in this section is suitable for the simulation methods presented in [64].

2.3.1 Hybrid systems with impulsive effects

According to [65], an impulsive dynamical system can be described by a hybrid system with impulsive effects. This makes it a valid framework for mechanical systems with unilateral constraints and spatial friction. A hybrid system with impulsive effects consists of three elements:

1. Continuous dynamics, a continuous-time differential equation which defines the behavior of the system in between events
2. Discrete dynamics, a discrete map which defines the way the state of the system is reset during events
3. A criterion to decide when the state of the system is to be reset

The continuous dynamics of the hybrid system with impulsive effects are given by

$$\dot{\boldsymbol{x}}_j = \boldsymbol{f}_j(\boldsymbol{x}_j, \boldsymbol{u}_j, t), \qquad \boldsymbol{x}_j, \boldsymbol{u}_j \in \mathcal{C}_j, \tag{2.31}$$

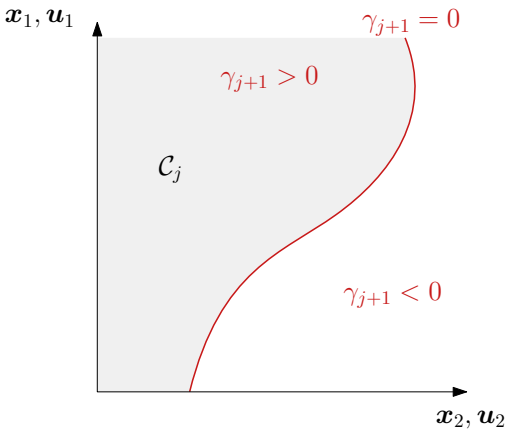

Figure 2.4: *A guard function defining the flow set $\mathcal{C}_j$ for a 2-dimensional system is illustrated in this figure.*

with the state $\boldsymbol{x}_j = \boldsymbol{x}(t,j) \in \mathbb{R}^{n(j)}$ and the input $\boldsymbol{u}_j = \boldsymbol{u}(t,j) \in \mathbb{R}^{m(j)}$. The nonlinear function $\boldsymbol{f}_j : \mathbb{R}^{n(j)} \times \mathbb{R}^{m(j)} \times \mathbb{R} \to \mathbb{R}^{n(j)}$ is a vector field which describes the flow of segment j. Here $j \in \{0, 1, \ldots, N\}$ is a counter that defines the flow set $\mathcal{C}_j$ in which the system resides, where N is the number of segments in a trajectory. When j is increased, and another flow set is entered, the vector field that defines the behavior of the system can change. We refer to (t, j) as the *hybrid time*. Note that the state dimension $n(j)$ and the input dimension $m(j)$ can vary in different segments j.

The discrete dynamics of the hybrid system with impulsive effects are given by

$$\boldsymbol{x}_{j+1} = \boldsymbol{g}_j(\boldsymbol{x}_j, \boldsymbol{u}_j, t), \qquad \boldsymbol{x}_j, \boldsymbol{u}_j \in \mathcal{D}_{j+1} \tag{2.32}$$

The discrete dynamics $\boldsymbol{g}_j : \mathbb{R}^{n(j-1)} \times \mathbb{R}^{m(j-1)} \times \mathbb{R} \to \mathbb{R}^{n(j)}$ is a mapping function, which maps the ante-event state to the post-event state. This map is evaluated when the system enters the set $\mathcal{D}_{j+1}(t) \subseteq \partial\mathcal{C}_j := \{\boldsymbol{x}(t,j) \in \mathbb{R}^{n(j)},\ \boldsymbol{u}(t,j) \in \mathbb{R}^{m(i)} \mid \gamma_{j+1}(\boldsymbol{x}^\wedge, \boldsymbol{u}^\wedge, t) = 0\}$, indicating that an event should occur. The set $\mathcal{D}_{j+1}$ is defined using some virtual state and input $\boldsymbol{x}^\wedge$, $\boldsymbol{u}^\wedge$ that are not necessarily physically realistic, and a *guard function* γ_{j+1}. A guard function is a state-and-input dependent differentiable function with the properties

$$\gamma_{j+1}(\boldsymbol{x}, \boldsymbol{u}, t) > 0, \qquad (\boldsymbol{x}, \boldsymbol{u}, t) \in \mathcal{C}_j \setminus \partial\mathcal{C}_j, \tag{2.33}$$
$$\gamma_{j+1}(\boldsymbol{x}, \boldsymbol{u}, t) = 0, \qquad (\boldsymbol{x}, \boldsymbol{u}, t) \in \mathcal{D}_{j+1} = \partial\mathcal{C}_j, \tag{2.34}$$
$$\gamma_{j+1}(\boldsymbol{x}, \boldsymbol{u}, t) < 0, \qquad (\boldsymbol{x}, \boldsymbol{u}, t) \in (\mathbb{R}^n \times \mathbb{R}^m \times \mathbb{R}) \setminus \mathcal{C}_j, \tag{2.35}$$

where $\partial\mathcal{C}_j$ is the boundary of flow set $\mathcal{C}_j$. Using a guard function, $\mathcal{C}_j$ and $\mathcal{D}_{j+1}$ can conveniently be described. This is illustrated in Figure 2.4. While the guard function is greater than zero, the continuous dynamics (2.31) should be evaluated, since the system is in the interior of flow set $\mathcal{C}_j$. When the guard function is activated, i.e., $\gamma_{j+1} = 0$, the ante-event state $\boldsymbol{x}_j(t_{j+1})$ is mapped to the post-event state $\boldsymbol{x}_{j+1}(t_{j+1})$ using the discrete dynamics (2.32). Here t_{j+1} denotes the time-instant where γ_{j+1} is activated. After this event, the system will continue flowing in $\mathcal{C}_{j+1}$ according to the vector field $\boldsymbol{f}_{j+1}$.

The hybrid dynamics (2.31),(2.32) will form the starting point in formulating the tracking problem for mechanical systems with unilateral constraints and spatial friction. In this, consider a nominal state-and-input trajectory $(\boldsymbol{\alpha}(t,j), \boldsymbol{\mu}(t,j))$ that is a solution to (2.31),(2.32) for initial condition $\boldsymbol{\alpha}(t_0, 0) = \boldsymbol{\alpha}_0 \in \mathcal{C}_0$ and consists of $N+1$ absolutely continuous segments discriminated by the event counter $j \in \{0, 1, \ldots, N\}$. The nominal event time of event j is denoted τ_j and regular time is denoted t. An example of a reference trajectory is illustrated in Figure 2.5.

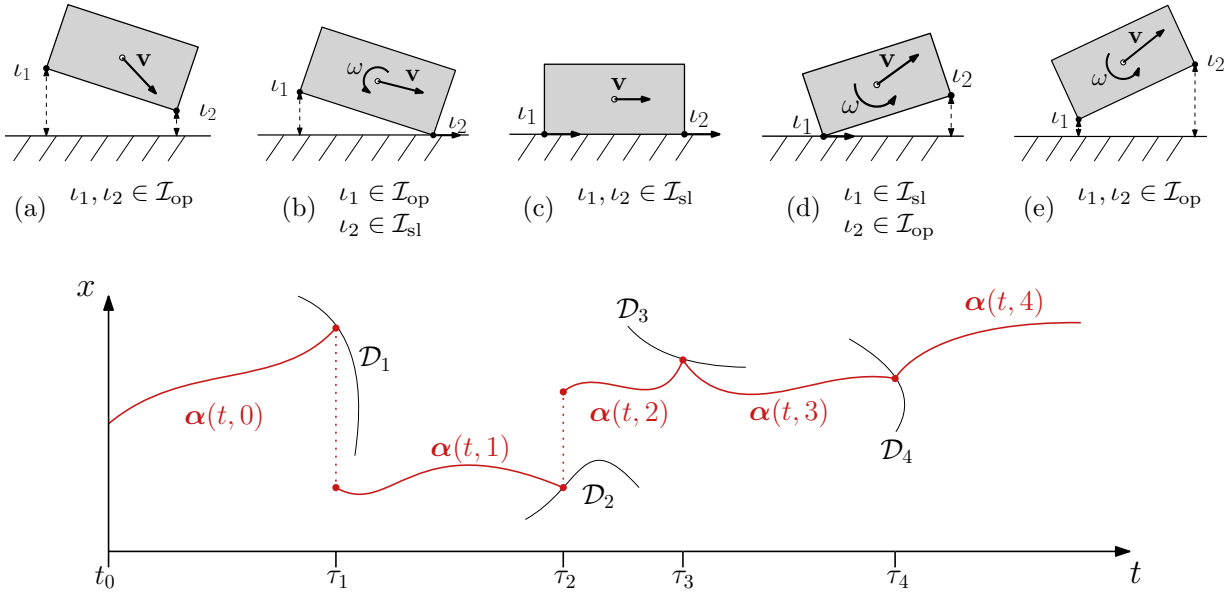

Figure 2.5: *An example trajectory, which satisfies the dynamics* (2.31)-(2.32)*, of a block pushing towards and withdrawing from a surface with velocity* $\mathbf{v}$*. Note that the sets* $\mathcal{D}$ *besides being dependent on* $\boldsymbol{x}$*, are also dependent on* $\boldsymbol{u}$*. Also, although not depicted in this image, the state space of the system varies with every event.*

The figure shows a block that impacts the ground, slides over the ground, and is subsequently lifted from the ground. The block has two contact points on its edges ι_1 and ι_2. The motion starts with both contact points open as can be seen in Figure 2.5a. The flow is described by $\dot{\boldsymbol{\alpha}}(t,0) = \boldsymbol{f}_0(\boldsymbol{\alpha}(t,0), \boldsymbol{\mu}(t,0), t)$ for $t \in [t_0, \tau_1]$. Then, contact is established at contact point ι_2 at the time τ_1, causing a jump in the state and a change in continuous dynamics to the vector field $\boldsymbol{f}_1(\boldsymbol{\alpha}(t,1), \boldsymbol{\mu}(t,1), t)$ for $t \in [\tau_1, \tau_2]$. This is illustrated in Figure 2.5b, where ι_2 is closed and slipping over the contact surface. At the time τ_2, another corner of the rectangle, i.e. contact point ι_1, impacts the ground as well causing another jump and another change in continuous dynamics. The block now has both contact points slipping over the contact surface. After this, both contact points release contact one by one. Since there are no impulsive forces present in this transition, the state does not jump when a contact point releases. However, due to frictional effects, a jump in the time-derivate of the state is possible, which makes these transitions continuous but nonsmooth.

Next, in Sections 2.3.3-2.3.4, the complementarity system defined in Section 2.2 will be fitted into the hybrid system (2.31),(2.32). In Section 2.3.2, the continuous dynamics $\boldsymbol{f}_j$ will be derived for mechanical systems with unilateral constraints and spatial friction. Then, in Section 2.3.3 the reset set $\mathcal{D}_j$ will be defined. Finally, in Section 2.3.4 the discrete dynamics $\boldsymbol{g}_j$ will be derived. This will fully define the hybrid system with impulsive effects for mechanical systems with unilateral constraints and spatial friction.

2.3.2 Continuous dynamics

Let us start by considering the state $\boldsymbol{x}$ to be composed as

$$\boldsymbol{x} = \begin{bmatrix} \boldsymbol{q} \\ \dot{\boldsymbol{q}} \end{bmatrix}. \tag{2.36}$$

As described in Section 2.2, for mechanical systems a set of contact points $\mathcal{I} = \{\iota_1, \iota_2, \ldots, \iota_c\}$ is defined, with c is the number of considered contact points. A set $\mathcal{I}_{\text{cl}}$ is defined as the set of closed contact points, such that a contact $\iota \in \mathcal{I}_{\text{cl}}$ has closed a unilateral constraint. The set of contact points in open contact is defined as $\mathcal{I}_{\text{op}} := \{\iota \mid \iota \notin \mathcal{I}_{\text{cl}}\}$. The set $\mathcal{I}_{\text{cl}}$ is divided in the subsets $\mathcal{I}_{\text{sl}}$ and $\mathcal{I}_{\text{st}}$, where $\mathcal{I}_{\text{sl}}$ is the set of closed contact points in slip and $\mathcal{I}_{\text{st}}$ the set of closed contact points in stick. The division implies that $\mathcal{I}_{\text{cl}} = \mathcal{I}_{\text{sl}} \cup \mathcal{I}_{\text{st}}$ and that $\mathcal{I}_{\text{sl}} \cap \mathcal{I}_{\text{st}} = \emptyset$.

The equations of motion, given in (2.3), can be rewritten to

$$\dot{\boldsymbol{\nu}} = \boldsymbol{M}^{-1}(\boldsymbol{q}) \left[\boldsymbol{S}(\boldsymbol{q})\boldsymbol{u} - \boldsymbol{C}(\boldsymbol{q}, \boldsymbol{\nu}) + \boldsymbol{W}_n(\boldsymbol{q})\boldsymbol{\lambda}_n + \boldsymbol{W}_t(\boldsymbol{q})\boldsymbol{\lambda}_t\right], \tag{2.37}$$

with

$$\begin{aligned}
\boldsymbol{W}_n &= \left[\boldsymbol{w}_{n,i_1}, \boldsymbol{w}_{n,i_2}, \ldots, \boldsymbol{w}_{n,\iota}\right] \in \mathbb{R}^{n \times c}, \\
\boldsymbol{W}_t &= \left[\boldsymbol{W}_{t,i_1}, \boldsymbol{W}_{t,i_2}, \ldots, \boldsymbol{W}_{t,\iota}\right] \in \mathbb{R}^{n \times 2c}, \\
\boldsymbol{\lambda}_n &= \left[\lambda_{n,\iota_1}; \lambda_{n,\iota_2}; ...; \lambda_{n,\iota_c}\right] \in \mathbb{R}^{c}, \\
\boldsymbol{\lambda}_t &= \left[\boldsymbol{\lambda}_{t,\iota_1}; \boldsymbol{\lambda}_{t,\iota_2}; ...; \boldsymbol{\lambda}_{t,\iota_c}\right] \in \mathbb{R}^{2c}.
\end{aligned}$$

Note that since $\boldsymbol{f}_j$ is only defined on $\boldsymbol{x}(t,j), \boldsymbol{u}(t,j) \notin \mathcal{D}_{j+1}$, it is not necessary to use $\boldsymbol{\nu}$ to define the equations of motion as done in (2.3). It follows that $\boldsymbol{f}_j$ can be written as

$$\dot{\boldsymbol{x}}_j(t) = \begin{bmatrix} \dot{\boldsymbol{q}} \\ \boldsymbol{M}^{-1}(\boldsymbol{q}) \left[\boldsymbol{S}(\boldsymbol{q})\boldsymbol{u} - \boldsymbol{C}(\boldsymbol{q}, \dot{\boldsymbol{q}}) + \boldsymbol{W}_n(\boldsymbol{q})\boldsymbol{\lambda}_n + \boldsymbol{W}_t(\boldsymbol{q})\boldsymbol{\lambda}_t\right] \end{bmatrix}. \tag{2.38}$$

The closed contact points in $\mathcal{I}_{\text{cl}}$ experience reaction forces $\lambda_{n,\iota}$ and $\boldsymbol{\lambda}_{t,\iota}$, as can be seen in (2.37). Therefore, for all closed contact points $\iota \in \mathcal{I}_{\text{cl}}$, constraints are included which restrict these reaction forces. These constraints are given by

$$\boldsymbol{w}_{n,\iota}^T(\boldsymbol{q})\ddot{\boldsymbol{q}} + \dot{\boldsymbol{w}}_{n,\iota}^T(\boldsymbol{q})\dot{\boldsymbol{q}} = 0, \qquad \forall \iota \in \mathcal{I}_{\text{cl}}, \tag{2.39}$$

$$\boldsymbol{\lambda}_{t,\iota} ||\boldsymbol{W}_{t,\iota}^T \dot{\boldsymbol{q}}|| + \mu_\iota \lambda_{n,\iota} \boldsymbol{W}_{t,\iota}^T \dot{\boldsymbol{q}} = 0, \qquad \forall \iota \in \mathcal{I}_{\text{sl}}, \tag{2.40}$$

$$\boldsymbol{W}_{t,\iota}^T(\boldsymbol{q})\ddot{\boldsymbol{q}} + \dot{\boldsymbol{W}}_{t,\iota}^T(\boldsymbol{q})\dot{\boldsymbol{q}} = 0, \qquad \forall \iota \in \mathcal{I}_{\text{st}}, \tag{2.41}$$

where again $\mathcal{I}_{\text{sl}}$ and $\mathcal{I}_{\text{st}}$ are the sets of closed contacts in slip and closed contacts in stick, respectively. With (2.38) and (2.39)-(2.41), the continuous dynamics of the hybrid system are correctly defined.

System mode descriptor

A system will have different flow dynamics as the system mode changes, as can be seen in (2.39)-(2.41). Also the jump sets $\mathcal{D}_j$ change with the mode, as will be shown in Section 2.3.3. Therefore it is necessary to keep track of the mode the system is in. The system mode descriptor σ_j is introduced to conveniently describe the current system mode. Each contact point can either be in open-contact, closed-contact slip or closed-contact stick. The system mode descriptor is therefore defined as the ordered set

$$\sigma = (\sigma_1, \sigma_2, \ldots, \sigma_\iota), \tag{2.42}$$

where σ_ι is the mode of contact point ι. σ_ι can either have the value 'op' for a contact point in open-contact, 'sl' for a contact point in closed-contact slip, or 'st' for a contact point in closed-contact stick. For example, the system mode descriptor of the mode in Figure 2.5b is $\sigma = (\text{op}, \text{sl})$.

2.3.3 Discrete event sets

When the system state enters an event set $\mathcal{D}$, an event will take place. The current mode for the different contact points is in that case altered and a corresponding state reset is applied. In this section the sets $\mathcal{D}$ are defined for each mode of a contact point. The derivation of the discrete event sets can be found in Appendix A.1. The discrete event sets are defined using guard functions as presented in Section 2.3.1. Furthermore, in this section the superscript $(\cdot)^{\sigma_\iota^- \to \sigma_\iota^+}$ is introduced to indicate that the guard function $\gamma^{\sigma_\iota^- \to \sigma_\iota^+}$, or event set $\mathcal{D}^{\sigma_\iota^- \to \sigma_\iota^+}$ is related to the transition from ante-event mode σ_ι^- to post-event mode σ_ι^+.

Discrete events sets in open contact
For all contact points $\iota \in \mathcal{I}_{\text{op}}$, the discrete event sets are defined as

$$\mathcal{D}_\iota^{\text{op}\to\text{cl}} = \{\boldsymbol{x} \mid \gamma_\iota^{\text{op}\to\text{cl}} = 0\}, \tag{2.43}$$

with

$$\gamma_\iota^{\text{op}\to\text{cl}} = \text{h}_{n,\iota}(\boldsymbol{q}). \tag{2.44}$$

Discrete events sets in closed contact slip
For all contact points $\iota \in \mathcal{I}_{\text{sl}}$, the discrete event sets are defined as

$$\mathcal{D}_\iota^{\text{sl}\to\text{st}} = \{\boldsymbol{q} \mid \gamma_\iota^{\text{sl}\to\text{st}} = 0\}, \tag{2.45}$$
$$\mathcal{D}_\iota^{\text{cl}\to\text{op}} = \{\boldsymbol{q}, \boldsymbol{u} \mid \gamma_\iota^{\text{cl}\to\text{op}} = 0\}, \tag{2.46}$$

with

$$\gamma_\iota^{\text{sl}\to\text{st}} = \sqrt{\mathbf{v}_{t,\iota}^T \mathbf{v}_{t,\iota}}, \tag{2.47}$$
$$\gamma_\iota^{\text{cl}\to\text{op}} = \lambda_{n,\iota}. \tag{2.48}$$

Discrete events sets in closed contact stick
For all contact points $\iota \in \mathcal{I}_{\text{st}}$, the discrete event sets are defined as

$$\mathcal{D}_\iota^{\text{st}\to\text{sl}} = \{\boldsymbol{q}, \boldsymbol{u} \mid \gamma_\iota^{\text{st}\to\text{sl}} = 0\}, \tag{2.49}$$
$$\mathcal{D}_\iota^{\text{cl}\to\text{op}} = \{\boldsymbol{q}, \boldsymbol{u} \mid \gamma_\iota^{\text{cl}\to\text{op}} = 0\}, \tag{2.50}$$

with

$$\gamma_\iota^{\text{st}\to\text{sl}} = \mu^2 \lambda_{n,\iota}^2 - \boldsymbol{\lambda}_{t,\iota} \boldsymbol{\lambda}_{t,\iota}^T, \tag{2.51}$$
$$\gamma_\iota^{\text{cl}\to\text{op}} = \lambda_{n,\iota}. \tag{2.52}$$

2.3.4 Discrete dynamics

Whenever the state $\boldsymbol{x}$ reaches the discrete event set $\mathcal{D}$, continuous evolution in its current mode is generally not feasible. The system should therefore go through a discrete event, in which the state is reinitialized and the mode is changed. One contact point entering a discrete event set can lead to other contact points experiencing infeasible reaction forces, making it difficult to determine in what mode each contact point should be. The reinitialization of the state and selection of a post-event mode is described by the discrete dynamics in this section. First a *nonlinear complementarity problem* (NCP) is solved to reinitialize the state. The NCP generates a unique feasible solution [66],

which for simple systems can be found by iterating over all possible modes until the feasible solution is found. Then, a mode selection algorithm is presented to find a feasible post-event mode, which defines the continuous dynamics to be integrated after the event.

State reinitialization

From the impulsive dynamics (2.25)-(2.28), the discrete dynamics for an impulsive event which determine the post-event joint velocity $\dot{\boldsymbol{q}}^+$ can be derived as

$$\dot{\boldsymbol{q}}^+ = \boldsymbol{M}^{-1}\left[\boldsymbol{W}_n\boldsymbol{\Lambda}_n + \boldsymbol{W}_t\boldsymbol{\Lambda}_t\right] + \dot{\boldsymbol{q}}^-, \tag{2.53}$$

$$\boldsymbol{w}_{n,\iota}^T\dot{\boldsymbol{q}}^+ = 0, \qquad \forall \iota \in \mathcal{I}_{\mathrm{cl}}, \tag{2.54}$$

$$\boldsymbol{\Lambda}_{t,\iota}||\boldsymbol{W}_{t,\iota}^T\dot{\boldsymbol{q}}^+|| + \mu\Lambda_{n,\iota}\boldsymbol{W}_{t,\iota}^T\dot{\boldsymbol{q}}^+ = 0, \qquad \forall \iota \in \mathcal{I}_{\mathrm{sl}}, \tag{2.55}$$

$$\boldsymbol{W}_{t,\iota}^T\dot{\boldsymbol{q}}^+ = 0, \qquad \forall \iota \in \mathcal{I}_{\mathrm{st}}. \tag{2.56}$$

Here the unknown variables are $\dot{\boldsymbol{q}}^+ \in \mathbb{R}^n$, $\boldsymbol{\Lambda}_n \in \mathbb{R}^{c_{\mathrm{cl}}}$ and $\boldsymbol{\Lambda}_t \in \mathbb{R}^{2c_{\mathrm{cl}}}$, which means that there are $n + 3c_{\mathrm{cl}}$ unknown variables. From (2.53) we get n equations, from (2.54) we get c_{cl} equations and since $\mathcal{I}_{\mathrm{sl}} \cup \mathcal{I}_{\mathrm{st}} = \mathcal{I}_{\mathrm{cl}}$, $\boldsymbol{\Lambda}_{t,\iota} \in \mathbb{R}^2$, and $\dot{\boldsymbol{W}}_{t,\iota}^T\dot{\boldsymbol{q}}^+ \in \mathbb{R}^2$ we get $2c_{\mathrm{cl}}$ equations from (2.55)-(2.56). Since we have $n + 3c_{\mathrm{cl}}$ unknown variables and $n + 3c_{\mathrm{cl}}$ equations, the system is solvable.

The problem that remains is that it is not straightforward to identify what the correct mode and therewith what the sets $\mathcal{I}_{\mathrm{op}}$, $\mathcal{I}_{\mathrm{sl}}$, and $\mathcal{I}_{\mathrm{st}}$ should be after an event. The set of equations that should be solved is the set of equations that corresponds to the system-mode which generates a feasible post-event state. When a contact point enters a discrete event set, and thus generates an infeasible state, it can be concluded that the system will go through an event because in it's current mode the system is infeasible. However, it is not guaranteed that the contact point which entered the event set will change their mode. Actually any contact point, or even several contact points, can change their mode. Therefore the dynamics should be solved for several modes, until a feasible post-event state is found. A feasible post-event state is a post-event state solved for a certain system-mode σ, such that the all corresponding guard functions are inactive, i.e., all $\Gamma_\iota > 0$. As mentioned earlier, there will exist a unique system-mode where the system has a feasible post-impact state. Similar to the non-impulsive guard functions defined in Section 2.3.3, the impulsive guard functions are given by

$$\Gamma_\iota^{\mathrm{cl}\to\mathrm{op}} = \Lambda_{n,\iota}, \tag{2.57}$$

$$\Gamma_\iota^{\mathrm{sl}\to\mathrm{st}} = (\mathbf{v}_{t,\iota}^+)^T\mathbf{v}_{t,\iota}^+, \tag{2.58}$$

$$\Gamma_\iota^{\mathrm{st}\to\mathrm{sl}} = \mu^2\Lambda_{n,\iota}^2 - \boldsymbol{\Lambda}_{t,\iota}\boldsymbol{\Lambda}_{t,\iota}^T. \tag{2.59}$$

Note that all guard functions are defined at velocity level during the state reinitialization. The NCP (2.53)-(2.56) is defined at velocity level, meaning that only guard functions on velocity level need to be considered. For example, it is impossible for the state reinitialization to generate an infeasible position because the position of the system is not updated during the state reinitialization. When $\Lambda_{n,\iota} = 0$ and $\boldsymbol{\Lambda}_{t,\iota} = 0$ during an event, one speaks of a non-impulsive event. In this case, the state is not reinitialized during the event. However, the system will enter a different mode. For both impulsive and non-impulsive events, the post-event mode is determined during the mode selection, which is described below.

Mode selection

The mode σ of a system is determined by the guard functions defined in Section 2.3.3. All guard functions γ_ι should be greater than zero for the system to be in a feasible mode. Because some of these guard functions are defined on acceleration level and the post-event acceleration is not constrained by the NCP, we should first find a post-event mode σ^+ where the accelerations $\ddot{\boldsymbol{q}}$ and reaction forces $\boldsymbol{\lambda}_n, \boldsymbol{\lambda}_t$ are feasible before we know which vector field is suitable to define the next flow

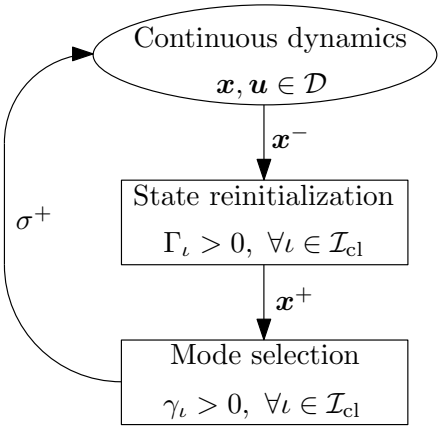

Figure 2.6: *The algorithm used to solve a hybrid system with impulsive effects depicted in a flowchart.*

phase. From the continuous dynamics (2.18)-(2.21), post-event accelerations and reaction forces can be computed from

$$\ddot{\boldsymbol{q}}^+ = \boldsymbol{M}^{-1}\left[\boldsymbol{S}\boldsymbol{u}^+ - \boldsymbol{C} + \boldsymbol{W}_n\boldsymbol{\lambda}_n^+ + \boldsymbol{W}_t\boldsymbol{\lambda}_t^+\right], \tag{2.60}$$

$$\boldsymbol{w}_{n,\iota}^T\ddot{\boldsymbol{q}}^+ + \dot{\boldsymbol{w}}_{n,\iota}^T\dot{\boldsymbol{q}}^+ = 0, \qquad \forall \iota \in \mathcal{I}_{\mathrm{cl}}, \tag{2.61}$$

$$\boldsymbol{\lambda}_{t,\iota}^+||\boldsymbol{W}_{t,\iota}^T\dot{\boldsymbol{q}}^+|| + \mu\lambda_{n,\iota}^+\boldsymbol{W}_{t,\iota}^T\dot{\boldsymbol{q}}^+ = 0, \qquad \forall \iota \in \mathcal{I}_{\mathrm{sl}}, \tag{2.62}$$

$$\boldsymbol{W}_{t,\iota}^T\ddot{\boldsymbol{q}}^+ + \dot{\boldsymbol{W}}_{t,\iota}^T\dot{\boldsymbol{q}}^+ = 0, \qquad \forall \iota \in \mathcal{I}_{\mathrm{st}}, \tag{2.63}$$

where $\boldsymbol{M}$, $\boldsymbol{S}$, $\boldsymbol{C}$, $\boldsymbol{w}_{n,\iota}$ and $\boldsymbol{W}_{t,\iota}$ are evaluated at the post-event joint configuration $\boldsymbol{q}^+$ and velocity $\dot{\boldsymbol{q}}^+$. Because we are interested in whether the accelerations and reaction forces are feasible, the guard functions defined on acceleration level are evaluated. The guard functions that determine the feasibility of a post-event mode are given by

$$\gamma_\iota^{\mathrm{cl}\to\mathrm{op}} = \lambda_{n,\iota}, \qquad \forall \iota \in \mathcal{I}_{\mathrm{cl}}, \tag{2.64}$$

$$\gamma_\iota^{\mathrm{st}\to\mathrm{sl}} = \mu_\iota^2\lambda_{n,\iota}^2 - \boldsymbol{\lambda}_{t,\iota}\boldsymbol{\lambda}_{t,\iota}^T, \qquad \forall \iota \in \mathcal{I}_{\mathrm{st}}, \tag{2.65}$$

with $\mathcal{I}_{\mathrm{sl}} \cup \mathcal{I}_{\mathrm{st}} = \mathcal{I}_{\mathrm{cl}}$. Note that the guard functions $\gamma_\iota^{\mathrm{op}\to\mathrm{cl}}$ and $\gamma_\iota^{\mathrm{sl}\to\mathrm{st}}$ are not evaluated. This is unnecessary, because open contact points can only trigger guard functions defined at position level. Since the non-impulsive dynamics only update the acceleration, it is impossible for a contact point in open contact to change mode during an impulsive event. This also holds for the guard function from slip to stick, which is defined on velocity level.

The process of solving a hybrid system with impulsive effects is illustrated in Figure 2.6. The system first flows according to a vector field $\boldsymbol{f}$. When the event set $\mathcal{D}$ is reached, a jump in the system state $\boldsymbol{x}$ is applied. This jump is the result of solving an NCP to find the post-event state $\boldsymbol{x}^+$. Finally, the mode selection is performed to find a feasible post-event mode σ^+ for that post-event state $\boldsymbol{x}^+$. The continuous dynamics for the next flow segment is defined by σ^+ with $\boldsymbol{x}^+$ as initial condition.

2.4 Summary

The modeling of mechanical systems with unilateral constraints and spatial friction is presented in this chapter. First, a complementarity problem formulation for such systems is presented using Signorini's contact law, Newton's impact law, and Coulomb's friction law. This system fully defines

the dynamics of mechanical systems with unilateral constraints and spatial friction. From the complementarity problem formulation a hybrid system with impulsive effects is derived. This system is constructed with a control point-of-view in mind, and its compatibility with the control strategy that will be presented in the following chapters. The hybrid system is defined in three parts. First the continuous dynamics are presented. Then the discrete event sets are given, which are state-input sets that trigger a discrete event when the state and input enters such a set. Finally, the dynamics of such an event are presented, which consist of a state reinitialization and a mode selection.

Chapter 3

Sensitivity Analysis with Isolated State-and-Input-Triggered Events

The behavior of trajectories tracking a nominal reference trajectory is analyzed in this chapter. More specifically, an analysis of tracking trajectories with state-and-input-triggered jumps of hybrid systems is presented. We will refer to the considered class of systems as *nonlinear state-and-input-triggered hybrid systems* (NSITHS). In this chapter, isolated events are considered, indicating that guard functions are activated separately, such that there is always flow between the activations. The work in this chapter is an extension on [49, 55, 59], where a sensitivity analysis for *nonlinear state-triggered hybrid systems* (NSTHS) has been presented. In this work, We will analyze the behavior of the system in the neighborhood of a nominal trajectory assuming that atleast locally these isolated events also occur in the same sequence. However, the timing of the events will differ from the nominal event times for nearby trajectories. The mismatch in event time between the nominal trajectory and state trajectory can result in *peaking behavior* of the tracking error [41, 42]. Peaking behavior is known to result in undesirable large actuation forces. First, we introduce a different notion of error to avoid peaking behavior. After that, an approximation of the NSITHS will be presented in the form of a *linear time-triggered hybrid system* (LTTHS), which we expect to be first order. There is no proof yet available that the LTTHS is a first-order approximation of the NSITHS, but it is strongly presumed. This chapter partially extends the work in [55], in the sense that the sensitivity analysis in this chapter is suitable for input-dependent guard functions, which are introduced by frictional effects and releasing motions. In [55] there is also a proof which infers stability properties of an NSTHS about a reference trajectory from its corresponding LTTHS. Our claim is that a similar result will hold for the stability of the LTTHS implying local asymptotic stability of the NSITHS. This proof is however left for future work. Under the presumption that stability of the LTTHS implies local asymptotic stability of the NSITHS, conventional stability analysis tools for LTTHS can be used to asses the local stability of the NSITHS. Finally, a short summary of the findings in this chapter is given.

3.1 Trajectories with state-and-input-triggered jumps

This section presents *reference spreading* (RS) for trajectories with isolated events. Reference spreading is presented for isolated events in [49], which is extended to be suitable for input-dependent guards in this section. When the hybrid system starts from a different initial condition than that of the reference trajectory for example, the resulting state trajectory and reference trajectory will likely have non-coinciding event-times. The notion of error defined in reference spreading eliminates

the peaking behavior that results from the mismatch in event-time. In order to explain this notion of error better, we will first elaborate on the class of systems we consider, on the type of reference trajectories we allow, and we will introduce notation.

3.1.1 Nonlinear state-and-input-triggered hybrid systems

The framework of hybrid systems with impulsive effects is now used to formally define the NSITHS, which is the class of systems that is considered in this work.

Definition 1 (NSITHS)**.** *A nonlinear state-and-input-triggered hybrid system is a system with dynamics of the form*

$$\dot{\boldsymbol{x}}_j = \boldsymbol{f}_j(\boldsymbol{x}_j, \boldsymbol{u}_j, t), \qquad \boldsymbol{x}_j, \boldsymbol{u}_j \in \mathcal{C}_j \tag{3.1}$$

$$\boldsymbol{x}_{j+1} = \boldsymbol{g}_{j+1}(\boldsymbol{x}_j, \boldsymbol{u}_j, t), \qquad \boldsymbol{x}_j, \boldsymbol{u}_j \in \mathcal{D}_{j+1} \tag{3.2}$$

with the state $\boldsymbol{x}_j := \boldsymbol{x}(t, j)$, the input $\boldsymbol{u}_j := \boldsymbol{u}(t, j)$, nonlinear vector field $\boldsymbol{f}_j$, flow set $\mathcal{C}_j$ after event j, and a jump set $\mathcal{D}_{j+1} \subseteq \partial\mathcal{C}_j$, where when $(\boldsymbol{x}_j, \boldsymbol{u}_j) \in \mathcal{D}_{j+1}$ a state reinitialization is triggered according to the jump map $\boldsymbol{g}_{j+1}$ in (3.2)*. Note that in $\boldsymbol{x}_j$ and $\boldsymbol{u}_j$, the time-dependency is implicit.*

Consider a nominal trajectory of an NSITHS, as illustrated in Figure 3.1 in red. We denote this nominal trajectory $\boldsymbol{\alpha}_j := \boldsymbol{\alpha}(t, j)$ and assume it is the solution to (3.1)-(3.2) for input signal $\boldsymbol{\mu}_j := \boldsymbol{\mu}(t, j)$ starting from initial condition $\boldsymbol{\alpha}(t_0, 0) = \boldsymbol{\alpha}_0 \in \mathcal{C}_0$. The following assumption on the nominal trajectory is imposed, to exclude that nominal jump times accumulate in time. Note that also for $\boldsymbol{\alpha}_j$ and $\boldsymbol{\mu}_j$, the time-dependency is left implicit.

Assumption 1 (t-completeness and non-Zeno behavior of $\boldsymbol{\alpha}$)**.** *The reference trajectory $\boldsymbol{\alpha}$ is defined for all $t > t_0$. Also, each segment $\boldsymbol{\alpha}_j$ has non-vanishing time-domains $I_j^{\boldsymbol{\alpha}} = [\tau_j, \tau_{j+1}]$, i.e., $\tau_{j+1} - \tau_j \geq c > 0$, where τ_j is the j^{th} event time and c is a positive constant.*

Remark. *The non-vanishing time-domains assumption posed in Assumption 1 is guaranteed if $\boldsymbol{g}_{j+1}(\boldsymbol{\alpha}_j(\tau_{j+1}), \boldsymbol{\mu}_j(\tau_{j+1})) \notin \mathcal{D}_{j+1}$ for all $j \in \{0, 1, \ldots, N\}$. This indicates that there is flow necessary, and therefore time, to reach the subsequent event set $\mathcal{D}_{j+1}$.*

Consider now a state trajectory $\boldsymbol{x}$ starting from initial condition $\boldsymbol{x}(t_0, 0, \epsilon) = \boldsymbol{x}_0(\epsilon) = \boldsymbol{\alpha}_0 + \epsilon \boldsymbol{z}_0$ with input $\boldsymbol{u}_j(\epsilon) = \boldsymbol{\mu}_j + \epsilon \boldsymbol{v}_j$, where ϵ is an initial state and input perturbation. In this $\boldsymbol{z}_0 = \partial \boldsymbol{x}_0 / \partial \epsilon$, $\boldsymbol{\mu}_j = \boldsymbol{\mu}(t, j)$ the feedforward corresponding to $\boldsymbol{\alpha}_j$, and $\boldsymbol{v}_j = \boldsymbol{v}(t, j)$ the feedback. An example of a perturbed trajectory $\boldsymbol{x}(\epsilon)$ is shown in Figure 3.1.

For the nominal trajectory, the state and input curves are known over the entire time-domain, meaning that the event-times are also known. For the perturbed trajectory this is not the case. Referring to Figure 3.1, there will be a mismatch between the nominal event times τ_1 and τ_2 and the perturbed event times t_1 and t_2. Taking a closer look at the first event of Figure 3.2, the peaking behavior can be illustrated as the result of a jump mismatch. In Figure 3.2, the state evolution $\boldsymbol{x}$ of the first event is depicted besides the conventional tracking error $||\boldsymbol{x} - \boldsymbol{\alpha}||$ (assuming that $\boldsymbol{\alpha}_j, \boldsymbol{x}_j$ and $\boldsymbol{\alpha}_{j+1}, \boldsymbol{x}_{j+1}$ are of the same dimension), where both trajectories are considered a function of conventional time t alone. One can clearly see that a peak arises in the tracking error when the jump times do not coincide. At time equal to t_1, the state trajectory jumps, while the reference trajectory does not. At time equal to τ_1, the reference trajectory jumps as well. This means that in $[t_1, \tau_1]$, a post-event state trajectory is compared to a ante-event reference trajectory, resulting in a large peak in the tracking error. This is undesirable in stability analysis and may for example lead to large and unnecessary actuation forces when considered in feedback control.

In the next section, a different notion of error will be introduced that does not illustrate peaking behavior.

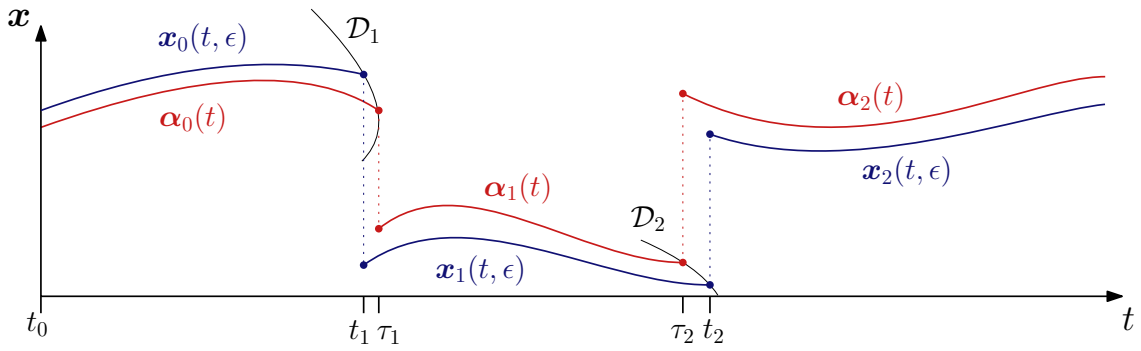

Figure 3.1: *A nominal (red) and a perturbed (blue) trajectory of a hybrid system with impulsive effects are depicted in this figure. The nominal and the state trajectory enter the jump sets D at mismatching time instants, as a result from the perturbation in the state trajectory.*

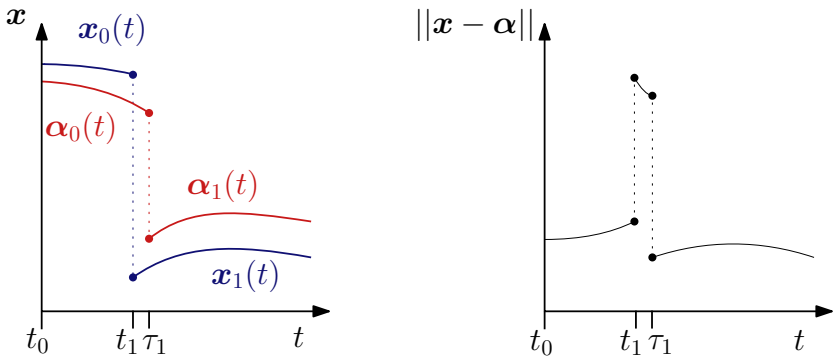

Figure 3.2: *A closer look at the first event of the trajectory in Figure 3.1. On the left the state-evolution $\boldsymbol{x}$ is depicted and on the right the tracking error $||\boldsymbol{x}-\boldsymbol{\alpha}||$. A clear peak can be noticed in the tracking error as a result from the event-time mismatch.*

3.1.2 Reference-spreading

To avoid peaking behavior in the tracking error, in [49] a methodology is presented which is named reference spreading in [53]. In reference spreading a novel notion of error is introduced, called the *reference spreading error* (RS error). The methodology uses reference trajectories which are extended beyond event-times, such that an ante-event state trajectory can always be compared to an ante-event reference trajectory and a post-event state trajectory can always be compared to a post-event reference trajectory. This is illustrated in Figure 3.3, where the reference trajectory $\boldsymbol{\alpha}_j$ is extended resulting in $\bar{\boldsymbol{\alpha}}_j$. The extension is made by forward integrating the vector field $\boldsymbol{f}_j$ beyond τ_{j+1} and backward integrating $\boldsymbol{f}_j$ before τ_j, for all $j \in \{0, 1, \ldots, N\}$. Adopting the notation of [16], the hybrid domain of $\boldsymbol{\alpha}$ is defined by segments $I_j^{\boldsymbol{\alpha}} = [\tau_j, \tau_{j+1}]$, which together form the entire domain of $\boldsymbol{\alpha}$ as

$$\operatorname{dom} \boldsymbol{\alpha} = \bigcup_{j=0}^{N} I_j^{\boldsymbol{\alpha}} \times \{j\}. \tag{3.3}$$

Similarly the state segments $\boldsymbol{x}_j$ are defined on the time intervals $I_j^{\boldsymbol{x}} = [t_j, t_{j+1}]$ with the entire domain defined as

$$\operatorname{dom} \boldsymbol{x} = \bigcup_{j=0}^{N} I_j^{\boldsymbol{x}} \times \{j\}. \tag{3.4}$$

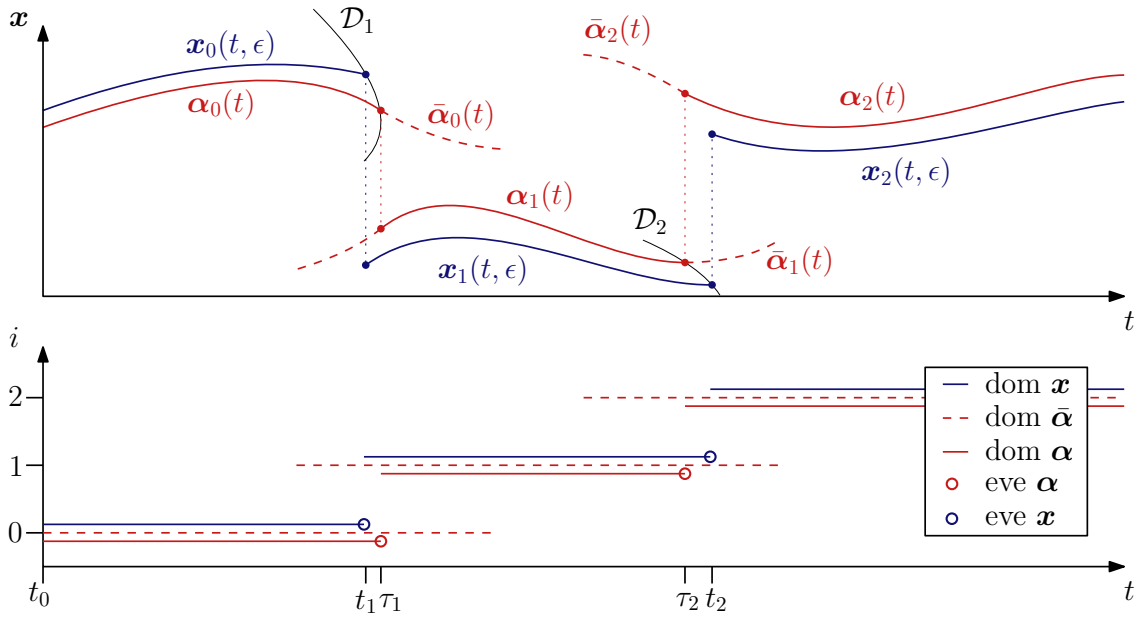

Figure 3.3: *An illustration of the nominal reference trajectory (red) and the perturbed trajectory (blue), where the nominal reference trajectory is extended such that* $\operatorname{dom} \boldsymbol{x} \subseteq \operatorname{dom} \bar{\boldsymbol{\alpha}}$.

The domain of the extended reference trajectory segments is extended such that $I_j^{\boldsymbol{x}} \subseteq I_j^{\bar{\boldsymbol{\alpha}}}$. The set of jump times of $\boldsymbol{\alpha}_j$ and $\boldsymbol{x}_j(\epsilon)$ are denoted as

$$\operatorname{eve} \boldsymbol{\alpha} = \bigcup_{j=1}^{N} \{\tau_j\} \times \{j-1\}, \tag{3.5}$$

$$\operatorname{eve} \boldsymbol{x} = \bigcup_{j=1}^{N} \{t_j\} \times \{j-1\}, \tag{3.6}$$

respectively.

Let us now pose a continuity based assumption on the vector field $\boldsymbol{f}_j$. This assumption (along with other assumptions) is instrumental to making sure that the ante-event state of the perturbed trajectory $\boldsymbol{x}_j(t_{j+1},\epsilon)$ lies close to the ante-event state of the nominal trajectory $\boldsymbol{\alpha}_j(\tau_{j+1})$, which is necessary to define an approximation of the perturbed trajectory.

Assumption 2 (Lipschitz continuity of $\boldsymbol{f}_j$)**.** *We assume that in a neighborhood of the reference trajectory* $\boldsymbol{\alpha}_j$*,* $\boldsymbol{f}_j$ *is Lipschitz with respect to* $\boldsymbol{x}$ *uniformly in* t *and* j*. That is,* $\exists \varepsilon_{\boldsymbol{f}} > 0$ *and* $\exists L$*, independent of* t, j*, such that* $\forall j$*,* $||\boldsymbol{f}_j(\boldsymbol{a},t) - \boldsymbol{f}_j(\boldsymbol{b},t)|| < L||\boldsymbol{a}-\boldsymbol{b}||$*,* $\forall t \in (\tau_j - \varepsilon_{\boldsymbol{f}}, \tau_{j+1} + \varepsilon_{\boldsymbol{f}})$ *and* $\forall \boldsymbol{a}, \boldsymbol{b} \in B_{\varepsilon_{\boldsymbol{f}}}(\bar{\boldsymbol{\alpha}}_j)$*, where* $B_{\varepsilon_{\boldsymbol{f}}}(\bar{\boldsymbol{\alpha}}_j)$ *is a ball with radius* $\epsilon_{\boldsymbol{f}}$ *around* $\bar{\boldsymbol{\alpha}}_j$*.*

In the lower plot of Figure 3.3, the hybrid time domains of $\boldsymbol{x}$, $\boldsymbol{\alpha}$ and $\bar{\boldsymbol{\alpha}}$ are illustrated. Note that for every j, it holds that $I_j^{\boldsymbol{x}} \subseteq I_j^{\bar{\boldsymbol{\alpha}}}$. This means that the reference spreading error $||\boldsymbol{x} - \bar{\boldsymbol{\alpha}}||$ can be evaluated until $t = t_j$ is reached. The reference spreading error $||\boldsymbol{x} - \bar{\boldsymbol{\alpha}}||$ is therefore continuous for fixed j, even in the case where $t_j \neq \tau_j$, since the state $\boldsymbol{x}_j$ will be compared to $\boldsymbol{\alpha}_j$ until $t = t_j$ is reached. Once $t = t_j$, the counter j is increased, and $\boldsymbol{x}_{j+1}$ is compared to $\boldsymbol{\alpha}_{j+1}$. Using this notion of error leaves only one jump at t_j in the tracking error, even under the presence of event-time mismatches. More importantly, the peak in the tracking error is avoided, and an ante-event state trajectory will not be compared to a post-event reference trajectory (and vice versa) anymore.

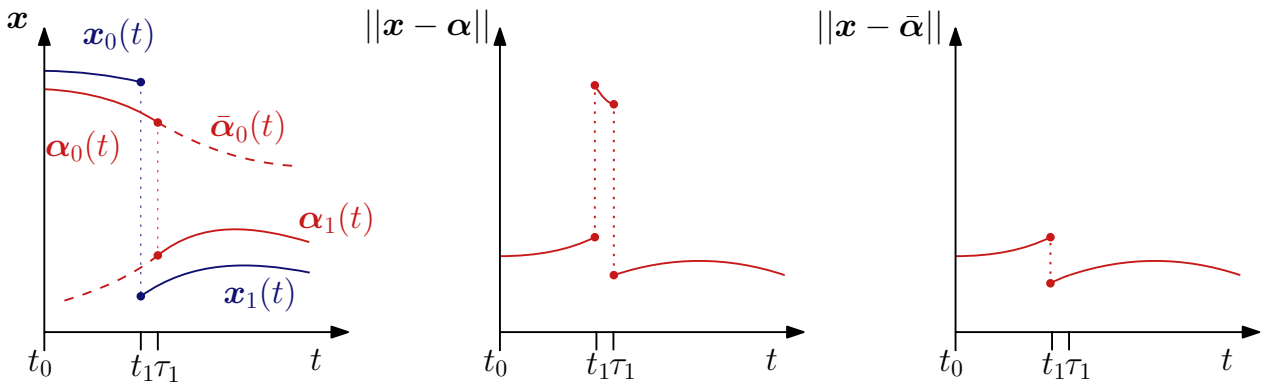

Figure 3.4: *A close up of the first event of the reference trajectory, with the conventional error* $||\boldsymbol{x} - \boldsymbol{\alpha}||$ *illustrated in the middle figure, and the reference spreading error* $||\boldsymbol{x} - \bar{\boldsymbol{\alpha}}||$ *in the right figure. Since* $\bar{\boldsymbol{\alpha}}$ *is evaluated in the same mode as* $\boldsymbol{x}$*, i.e., the reference spreading error is* $||\boldsymbol{x}_0 - \bar{\boldsymbol{\alpha}}_0||$ *for* $t \leq t_1$ *and* $||\boldsymbol{x}_1 - \bar{\boldsymbol{\alpha}}_1||$ *for* $t \geq t_1$*, the peaking behavior is not observed in the reference spreading error.*

This is illustrated in Figure 3.4, where the tracking errors with and without reference spreading are compared. Also, note that $\boldsymbol{\alpha}_j$ and $\boldsymbol{\alpha}_{j+1}$, for $j \in \{0, 1, \ldots, N\}$, do not need the be of the same dimension when the tracking error is defined as $||\boldsymbol{x} - \bar{\boldsymbol{\alpha}}||$.

In the next section, the reference spreading error will be used to analyze the behavior of perturbed trajectories with isolated events.

3.2 Approximating perturbed trajectories with isolated events

In [51] a sensitivity analysis is presented, where so-called sensitivity functions are used to provide first-order approximations of the effects of parameter variations on solutions. These sensitivity functions can also be used to approximate the solution under sufficiently small parameter variations. For the class of systems we consider here, the sensitivity equations describe the response of the system to perturbations in initial condition and input. This perturbation dynamics can be used to formulate an approximation of the perturbed state of the system, which we expect to be first-order. To find an approximation of state reinitializations in nonsmooth trajectories, an extension to this sensitivity analysis is necessary in the form of a linearized jump gain. The linearized jump gain and the linearized perturbation dynamics together define the LTTHS. In [55] stability properties of an NSTHS are associated with the stability the corresponding LTTHS. In this section, the LTTHS is derived for an NSITHS, which we expect can be used to assess the stability of the NSITHS under the presumption that a similar relation between the LTTHS and NSITHS exists. As mentioned in the intro to this chapter, the proof for this relation is left as future work. For a more thorough derivation of the following analysis, Appendix C should be consulted. We will first pose few assumptions on the reference events and jump maps that are required for the sensitivity analysis. First, we assume transversality of the reference events for which we assume the existence of a guard function that locally describes the flow and jump sets about each reference event.

Assumption 3 (Existence of a guard function)**.** *We assume that there exist constants* ε_γ*, and real valued guard function* $\gamma(\boldsymbol{x}, \boldsymbol{u}, t, j)$ *which is continuously differentiable with respect to* $\boldsymbol{x}$*,* $\boldsymbol{u}$*, and* t*,*

for each $j \in \{1, 2, \ldots, N\}$, where N is potentially infinite, such that

$$\begin{aligned} &\gamma_{j+1}(\boldsymbol{x}_j, \boldsymbol{u}_j, t) > 0 \qquad (\boldsymbol{x}, \boldsymbol{u}) \in B_{\varepsilon_\gamma}(\boldsymbol{\alpha}_j(\tau), \boldsymbol{\mu}_j(\tau)) \cap \mathcal{C}_j \setminus \partial\mathcal{C}_j \\ &\gamma_{j+1}(\boldsymbol{x}_j, \boldsymbol{u}_j, t) = 0 \qquad (\boldsymbol{x}, \boldsymbol{u}) \in B_{\varepsilon_\gamma}(\boldsymbol{\alpha}_j(\tau), \boldsymbol{\mu}_j(\tau)) \cap \mathcal{D}_{j+1} \\ &\gamma_{j+1}(\boldsymbol{x}_j, \boldsymbol{u}_j, t) < 0 \qquad (\boldsymbol{x}, \boldsymbol{u}) \in B_{\varepsilon_\gamma}(\boldsymbol{\alpha}_j(\tau), \boldsymbol{\mu}_j(\tau)) \cap (\mathbb{R}^n \times \mathbb{R}^m \times \mathbb{R}) \setminus \mathcal{C}_j \end{aligned} \tag{3.7}$$

where $B_{\varepsilon_\gamma}(\boldsymbol{\alpha}_j(\tau), \boldsymbol{\mu}_j(\tau))$ is a ball with radius ε_γ around $\boldsymbol{\alpha}_j(\tau), \boldsymbol{\mu}_j(\tau)$ with $\tau = \tau_{j+1}$. The set $\mathcal{C}_j$ is the flow set of a trajectory after event j and $\mathcal{D}_{j+1} \subseteq \partial\mathcal{C}_j$ is the event set which triggers event $j+1$, where $\partial\mathcal{C}_j$ represents the boundary of flow set $\mathcal{C}_j$. Note that $B_{\varepsilon_\gamma}(\boldsymbol{\alpha}_j(\tau), \boldsymbol{\mu}_j(\tau)) \cap (\mathbb{R}^n \times \mathbb{R}^m \times \mathbb{R}) \setminus \mathcal{C}_j$ only exists if $\mathcal{C}_j$ is not closed.

Assumption 4 (Transversal guard activations)**.** *Under Assumption 3, we assume there exists a constant $c > 0$, such that*

$$D_1\gamma_j(\boldsymbol{\alpha}_j, \boldsymbol{\mu}_j, t) \cdot \boldsymbol{f}_j(\boldsymbol{\alpha}_j, \boldsymbol{\mu}_j, t) + D_2\gamma_j(\boldsymbol{\alpha}_j, \boldsymbol{\mu}_j, t) \cdot \boldsymbol{f}_j(\boldsymbol{\alpha}_j, \boldsymbol{\mu}_j, t) + D_3\gamma_j(\boldsymbol{\alpha}_j, \boldsymbol{\mu}_j, t) \leq -c, \tag{3.8}$$

for every event time $(t, j) \in \operatorname{eve} \boldsymbol{\alpha}$.

Remark. *As can be seen in Assumption 4, the time derivative of the guard function at $\gamma_j(\boldsymbol{\alpha}_j, \boldsymbol{\mu}_j, t) = 0$ is needed to check for transversality. For $\gamma^{sl\to st} = \sqrt{\mathbf{v}_t^T \mathbf{v}_t}$, the time derivative is undefined when $\gamma^{sl\to st} = 0$. Therefore, a Taylor expansion is used to find the left limit of $\dot{\gamma}^{sl\to st}$ at $t = \tau_j$, to check whether the guard is activated transversally. More information on this can be found in Appendix A.1.*

The state, input and time where $\gamma_j(\boldsymbol{x}_j, \boldsymbol{u}_j, t) = 0$ represents the set where an event will happen, which together with Assumption 4 guarantees that an event will happen, even under perturbations. If the vector field is continuous with respect to ϵ, Assumption 4 assumes that the vector field pushes the reference trajectory out of the flow set $\mathcal{C}_j$, and that grazing incidents are avoided. The combination of the existence of a guard function in an area around the nominal ante-event state and the transversal guard activation guarantees that there exists a range of perturbations where the guard is activated as well. Let us now pose an assumption on the jump map $\boldsymbol{g}$.

Assumption 5 (Locally differentiable jump maps)**.** *We assume that for all $j \in \{0, 1, 2, \ldots, N\}$ the jump map $\boldsymbol{g}_{j+1}(\boldsymbol{x}_j, \boldsymbol{u}_j)$ is locally differentiable, in the sense that $D_1\boldsymbol{g}_{j+1}(\boldsymbol{x}_j, \boldsymbol{u}_j)$ and $D_2\boldsymbol{g}_{j+1}(\boldsymbol{x}_j, \boldsymbol{u}_j)$ exist in the ball $B_{\varepsilon_\gamma}(\boldsymbol{\alpha}_j(\tau), \boldsymbol{\mu}_j(\tau), \tau) \subseteq \mathbb{R}^n \times \mathbb{R}^m \times \mathbb{R}$, where $\tau = \tau_{j+1}$.*

The differentiability of the jump map is necessary to construct an approximation of the perturbed state trajectory. This will be explained in more detail in the next section.

3.2.1 Sensitivity analysis

The sensitivity analysis for the continuous segments of a perturbed trajectory gives a set of equations which describe the reaction of the system to an initial state-and-input perturbation. Introducing the initial state-and-input perturbation enables us to analyze the solution of a system under parameter variations. Writing (3.1) in integral form, a perturbed solution $\boldsymbol{x}_j(t, \epsilon)$ to (3.1) satisfies

$$\boldsymbol{x}_j(t, \epsilon) = \boldsymbol{x}_j(t_j, \epsilon) + \int_{t_j}^{t} \boldsymbol{f}_j(\boldsymbol{x}_j(s, \epsilon), \boldsymbol{u}_j(s, \epsilon), s) ds. \tag{3.9}$$

To find an approximation of the perturbed state, the perturbed state direction $\boldsymbol{z}(t)$ and the perturbed input direction $\boldsymbol{v}(t)$ are defined as

$$\boldsymbol{z}_j := \left.\frac{\partial \boldsymbol{x}_j(\epsilon)}{\partial \epsilon}\right|_{\epsilon=0}, \text{ and } \boldsymbol{v}_j := \left.\frac{\partial \boldsymbol{u}_j(\epsilon)}{\partial \epsilon}\right|_{\epsilon=0}, \tag{3.10}$$

where we use the abbreviations $\boldsymbol{z}_j = \boldsymbol{z}(t, j)$, and $\boldsymbol{v}_j = \boldsymbol{v}(t, j)$. Conforming to the sensitivity analysis presented in [51], a Taylor expansion is performed on $\boldsymbol{x}_j(t, \epsilon)$ with respect to ϵ. This results in

$$\boldsymbol{x}_j(t, \epsilon) = \boldsymbol{x}_j(t, 0) + \epsilon \left.\frac{\partial \boldsymbol{x}_j(t, \epsilon)}{\partial \epsilon}\right|_{\epsilon=0} + o(\epsilon). \tag{3.11}$$

Since $\boldsymbol{x}_j$ evaluated at $\epsilon = 0$ is $\bar{\boldsymbol{\alpha}}_j$, and using (3.10), we find

$$\boldsymbol{x}_j(t, \epsilon) = \bar{\boldsymbol{\alpha}}_j + \epsilon \bar{\boldsymbol{z}}_j + o(\epsilon), \tag{3.12}$$

with $o(\epsilon)$ indicating the Landau symbol little-o, which represents higher order terms ϵ. The state perturbation $\boldsymbol{z}_j$ in (3.12) is also extended, such that the approximation for $\boldsymbol{x}_j$ can be extended beyond $I_j^{\boldsymbol{\alpha}}$. To find an approximation of $\dot{\boldsymbol{x}}_j(\epsilon)$, an expression for $\dot{\boldsymbol{z}}_j$ should be found. By first taking the partial derivative of (3.9) with respect to ϵ, and then with respect to t, the perturbation dynamics are found to be

$$\dot{\boldsymbol{z}}_j = \boldsymbol{A}_j(t)\boldsymbol{z}_j + \boldsymbol{B}_j(t)\boldsymbol{v}_j, \tag{3.13}$$

with

$$\boldsymbol{A}_j(t) = D_1 \boldsymbol{f}_j(\boldsymbol{\alpha}_j, \boldsymbol{\mu}_j, t), \tag{3.14}$$
$$\boldsymbol{B}_j(t) = D_2 \boldsymbol{f}_j(\boldsymbol{\alpha}_j, \boldsymbol{\mu}_j, t), \tag{3.15}$$

where D_a represents the partial derivative with respect to the a-th argument. By extending the perturbed input direction $\boldsymbol{v}_j$, $\bar{\boldsymbol{v}}_j$ is obtained. Using $\boldsymbol{z}_0 = \boldsymbol{z}(0, \epsilon)$ and $\bar{\boldsymbol{v}}_j$, $\dot{\boldsymbol{z}}_j$ can be integrated past the nominal event-time τ_j, which results in the extension of the perturbed state direction $\bar{\boldsymbol{z}}_j$. With $\bar{\boldsymbol{\alpha}}_j$ and $\bar{\boldsymbol{z}}_j$, the first-order approximation of the perturbed state dynamics in continuous time can be defined as

$$\dot{\boldsymbol{x}}_j(\epsilon) = \dot{\bar{\boldsymbol{\alpha}}}_j + \epsilon \dot{\bar{\boldsymbol{z}}}_j + o(\epsilon). \tag{3.16}$$

Equation (3.16) defines the first-order approximation for the continuous segments of a trajectory. What remains is that the state reinitializations should be linearized as well. The reinitialization of the nominal trajectory satisfies

$$\boldsymbol{\alpha}_j(\tau_j) = \boldsymbol{g}_j(\boldsymbol{\alpha}_{j-1}(\tau_j), \boldsymbol{\mu}_{j-1}(\tau_j), \tau_j), \tag{3.17}$$

and the reinitialization of the perturbed state is described by

$$\boldsymbol{x}_j(t_j, \epsilon) = \boldsymbol{g}_j(\boldsymbol{x}_{j-1}(t_j, \epsilon), \boldsymbol{u}_{j-1}(t_j, \epsilon), t_j). \tag{3.18}$$

Similar to the Taylor expansion used in (3.11), the state and input of the next segment evaluated at the perturbed event time t_j can be expanded to

$$\boldsymbol{x}_j(t_j, \epsilon) = \bar{\boldsymbol{\alpha}}_j(t_j) + \epsilon \bar{\boldsymbol{z}}_j(t_j) + o(\epsilon), \tag{3.19}$$
$$\boldsymbol{u}_j(t_j, \epsilon) = \bar{\boldsymbol{\mu}}_j(t_j) + \epsilon \bar{\boldsymbol{v}}_j(t_j) + o(\epsilon). \tag{3.20}$$

The same can be done for $\boldsymbol{\alpha}_j(t_j)$, $\boldsymbol{\mu}_j(t_j)$, $\boldsymbol{z}_j(t_j)$, and $\boldsymbol{v}_j(t_j)$, which also depend on ϵ since they are evaluated at the perturbed event time $t_j(\epsilon)$. Substituting these expansions in (3.19) and (3.20) results in

$$\boldsymbol{x}_j(t_j, \epsilon) = \boldsymbol{\alpha}_j(\tau_j) + \epsilon \dot{\boldsymbol{\alpha}}_j(\tau_j)\Delta + \epsilon \boldsymbol{z}_j(\tau_j) + o(\epsilon), \tag{3.21}$$
$$\boldsymbol{u}_j(t_j, \epsilon) = \boldsymbol{\mu}_j(\tau_j) + \epsilon \dot{\boldsymbol{\mu}}_j(\tau_j)\Delta + \epsilon \boldsymbol{v}_j(\tau_j) + o(\epsilon), \tag{3.22}$$

with

$$\Delta = \left.\frac{\mathrm{d}t_j}{\mathrm{d}\epsilon}\right|_{\epsilon=0}. \tag{3.23}$$

To find Δ, we observe that

$$\gamma_j(\boldsymbol{x}_{j-1}(t_j,\epsilon),\boldsymbol{u}_{j-1}(t_j,\epsilon),t_j) = 0. \tag{3.24}$$

Note that γ_j is dependent on the input $\boldsymbol{u}_j$, whereas in [58] the sensitivity analysis is performed for guard functions which solely depend on state $\boldsymbol{x}_j$ and time t. From (3.24) the expression for Δ is found to be

$$\Delta = -\frac{D_1\gamma^- \cdot \boldsymbol{z}^- + D_2\gamma^- \cdot \boldsymbol{v}^-}{\dot{\gamma}^-}, \tag{3.25}$$

with

$$\begin{aligned}
\gamma^- &:= \gamma_j(\boldsymbol{\alpha}_{j-1}(\tau_j),\boldsymbol{\mu}_{j-1}(\tau_j),\tau_j),\\
\dot{\gamma}^- &:= D_1\gamma^- \cdot \dot{\boldsymbol{\alpha}}_{j-1}(\tau_j) + D_2\gamma^- \cdot \dot{\boldsymbol{\mu}}_{j-1}(\tau_j) + D_3\gamma^-,\\
\boldsymbol{z}^- &:= \boldsymbol{z}_{j-1}(\tau_j),\\
\boldsymbol{v}^- &:= \boldsymbol{v}_{j-1}(\tau_j),
\end{aligned}$$

where the $(\cdot)^-$ superscript indicates a left limit of event j. Expanding the right-hand side of (3.18) gives

$$\boldsymbol{x}^+ = \boldsymbol{g}^- + \epsilon\left[\frac{\partial \boldsymbol{g}_j}{\partial \epsilon}\right]_{\epsilon=0} + o(\epsilon), \tag{3.26}$$

$$= \boldsymbol{\alpha}^+ + \epsilon\left[\frac{\partial \boldsymbol{g}_j}{\partial \boldsymbol{x}}\left(\frac{\partial \boldsymbol{x}^-}{\partial \epsilon} + \frac{\partial \boldsymbol{x}^-}{\partial t}\frac{\mathrm{d}t_j}{\mathrm{d}\epsilon}\right) + \frac{\partial \boldsymbol{g}_j}{\partial \boldsymbol{u}}\left(\frac{\partial \boldsymbol{u}^-}{\partial \epsilon} + \frac{\partial \boldsymbol{u}^-}{\partial t}\frac{\mathrm{d}t_j}{\mathrm{d}\epsilon}\right) + \frac{\partial \boldsymbol{g}_j}{\partial t}\frac{\mathrm{d}t_j}{\mathrm{d}\epsilon}\right]_{\epsilon=0} + o(\epsilon), \tag{3.27}$$

$$= \boldsymbol{\alpha}^+ + \epsilon\left[D_1\boldsymbol{g}^- \cdot \left(\boldsymbol{z}^- + \dot{\boldsymbol{\alpha}}^-\Delta\right) + D_2\boldsymbol{g}^- \cdot \left(\boldsymbol{v}^- + \dot{\boldsymbol{\mu}}^-\Delta\right) + D_3\boldsymbol{g}^- \cdot \Delta\right] + o(\epsilon), \tag{3.28}$$

with

$$\begin{aligned}
\boldsymbol{x}^- &:= \boldsymbol{x}_{j-1}(t_j,\epsilon),\\
\boldsymbol{x}^+ &:= \boldsymbol{x}_j(t_j,\epsilon),\\
\boldsymbol{u}^- &:= \boldsymbol{u}_{j-1}(t_j,\epsilon),\\
\boldsymbol{g}^- &:= \boldsymbol{g}_j(\boldsymbol{\alpha}^-,\boldsymbol{\mu}^-,\tau_j),\\
\boldsymbol{g}_j &:= \boldsymbol{g}_j(\boldsymbol{x}^-,\boldsymbol{u}^-,t_j),\\
\boldsymbol{\alpha}^- &:= \boldsymbol{\alpha}_{j-1}(\tau_j),\\
\boldsymbol{\alpha}^+ &:= \boldsymbol{\alpha}_j(\tau_j),\\
\boldsymbol{\mu}^- &:= \boldsymbol{\mu}_{j-1}(\tau_j).
\end{aligned}$$

Here, the $(\cdot)^+$ superscript indicates the right limit of event j. Rewriting (3.21) into

$$\boldsymbol{z}^+ = \frac{1}{\epsilon}\left(\boldsymbol{x}^+ - \boldsymbol{\alpha}^+\right) - \dot{\boldsymbol{\alpha}}^+\Delta, \tag{3.29}$$

with $\boldsymbol{z}^+ := \boldsymbol{z}_j(\tau_j)$ and substituting (3.28) into (3.29), finally results in

$$\boldsymbol{z}^+ = D_1\boldsymbol{g}^- \cdot \left(\boldsymbol{z}^- + \dot{\boldsymbol{\alpha}}^-\Delta\right) + D_2\boldsymbol{g}^- \cdot \left(\boldsymbol{v}^- + \dot{\boldsymbol{\mu}}^-\Delta\right) + D_3\boldsymbol{g}^- \cdot \Delta - \dot{\boldsymbol{\alpha}}^+\Delta, \tag{3.30}$$

By substituting (3.23) into (3.30), we find

$$\boldsymbol{z}^+ = D_1\boldsymbol{g}^- \cdot \boldsymbol{z}^- + D_2\boldsymbol{g}^- \cdot \boldsymbol{v}^- - \left(D_1\boldsymbol{g}^- \cdot \boldsymbol{f}^- + D_2\boldsymbol{g}^- \cdot \dot{\boldsymbol{\mu}}^- + D_3\boldsymbol{g}^- \cdot 1 - \boldsymbol{f}^+\right) \frac{D_1\gamma^- \cdot \boldsymbol{z}^- + D_2\gamma^- \cdot \boldsymbol{v}^-}{\dot{\gamma}^-}, \tag{3.31}$$

which can be rewritten in compact form as

$$\boldsymbol{z}^+ = \boldsymbol{G}_j(\tau_j)\boldsymbol{z}^- + \boldsymbol{J}_j(\tau_j)\boldsymbol{v}^-, \tag{3.32}$$

with

$$\boldsymbol{G}_j(\tau_j) = D_1\boldsymbol{g}^- - \left(\dot{\boldsymbol{g}}^- - \boldsymbol{f}^+\right) \frac{D_1\gamma^-}{\dot{\gamma}^-}, \tag{3.33}$$

$$\boldsymbol{J}_j(\tau_j) = D_2\boldsymbol{g}^- - \left(\dot{\boldsymbol{g}}^- - \boldsymbol{f}^+\right) \frac{D_2\gamma^-}{\dot{\gamma}^-}, \tag{3.34}$$

where

$$\begin{aligned}
\boldsymbol{f}^- &:= \boldsymbol{f}_{j-1}(\boldsymbol{\alpha}_{j-1}(\tau_j), \boldsymbol{\mu}_{j-1}(\tau_j), \tau_j),\\
\boldsymbol{f}^+ &:= \boldsymbol{f}_j(\boldsymbol{\alpha}_j(\tau_j), \boldsymbol{\mu}_j(\tau_j), \tau_j),\\
\dot{\boldsymbol{g}}^- &:= D_1\boldsymbol{g}^- \cdot \boldsymbol{f}^- + D_2\boldsymbol{g}^- \cdot \dot{\boldsymbol{\mu}}^- + D_3\boldsymbol{g}^-.
\end{aligned}$$

The jump gains in (3.33) and (3.34) consist of two terms. The first term in (3.33), $D_1\boldsymbol{g}^-$, represents the effect of the ante-event state perturbation on the post-event perturbation. The perturbation does not only change the ante-event state, but also the time-instant the event takes place. The second term in (3.33), $-\left(\dot{\boldsymbol{g}}^- - \boldsymbol{f}^+\right)\frac{D_1\gamma^-}{\dot{\gamma}^-}$, represents the effect of the difference in time, in comparison to the nominal event. Obviously, the same can be said for (3.34).

Equation (3.32) describes the relation between the post-event state perturbation $\boldsymbol{z}^+$ and the ante-event state and input perturbations $\boldsymbol{z}^-$ and $\boldsymbol{v}^-$. The relation given in (3.32) is an extension on the results that have been obtained in [67]. The jump gain in [67] is derived with state-dependent guard functions γ and jump gains $\boldsymbol{g}$, whereas the jump gain $\boldsymbol{G}_j$ in (3.32) is derived using state-and-input-dependent guard functions γ and jump gains $\boldsymbol{g}$. The second term in (3.32) describes the effect of the ante-event input perturbation $\boldsymbol{v}^-$ on the post-event state perturbation $\boldsymbol{z}^+$, which is a contribution of this work. This term is a result of the jump gains $\boldsymbol{g}$ being state-and-input-dependent, where in previous work the jump gains were considered state-dependent.

3.2.2 Linear time-triggered hybrid system

The sensitivity analysis performed in the previous section will be used next to define the LTTHS associated to reference trajectory $\boldsymbol{\alpha}$ and the NSITHS defined in Definition 1. The LTTHS converts the state-triggered behavior of the NSITHS to a time-triggered behavior using an approximation of the state jumps, which we expect to be first order. Where the jump times of the NSITHS are unknown, the LTTHS jumps at the same event-times as the nominal trajectory $\boldsymbol{\alpha}$. Since the stability assessment of LTTHS is well established in literature, the LTTHS can then be used to conveniently assess the local asymptotic stability of the NSITHS. Let us now formally define the LTTHS.

Definition 2 (LTTHS)**.** *The linear time-triggered hybrid system associated with the reference trajectory* $\boldsymbol{\alpha}$ *and the NSITHS* (3.1)-(3.2) *is given by*

$$\dot{\boldsymbol{z}}_j = \boldsymbol{A}_j(t)\boldsymbol{z}_j + \boldsymbol{B}_j(t)\boldsymbol{v}_j, \qquad (t,j) \in \operatorname{dom}\boldsymbol{\alpha}, \tag{3.35}$$

$$\boldsymbol{z}^+ = \boldsymbol{G}_{j+1}(t)\boldsymbol{z}^- + \boldsymbol{J}_{j+1}(t)\boldsymbol{v}^-, \qquad (t,j) \in \operatorname{eve}\boldsymbol{\alpha}, \tag{3.36}$$

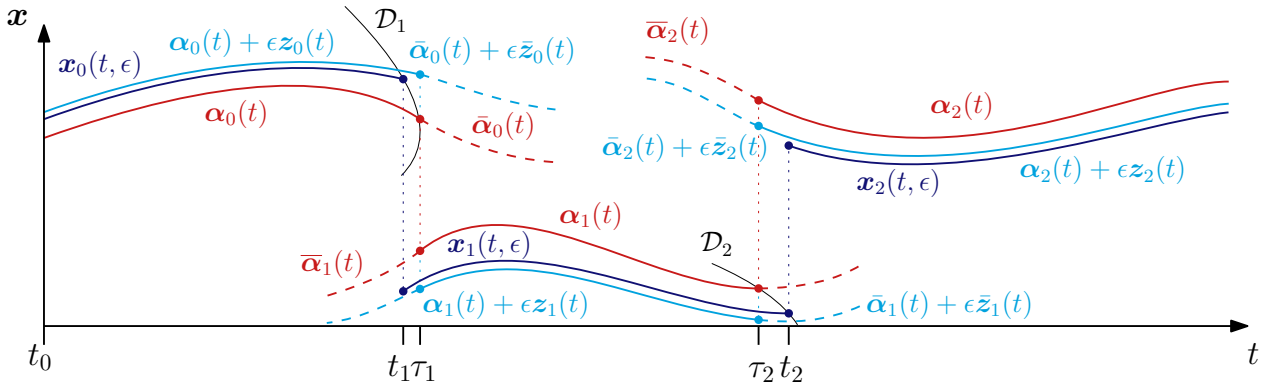

Figure 3.5: *The approximation of the perturbed trajectory $\boldsymbol{\alpha}+\epsilon\boldsymbol{z}$ (cyan) generated by the LTTHS is illustrated besides the perturbed trajectory $\boldsymbol{x}$ (blue) and the nominal trajectory $\boldsymbol{\alpha}$ (red). Note that the event times of the approximation are the same as those of the nominal trajectory.*

with initial condition $\boldsymbol{z}(t_0,0)=\boldsymbol{z}_0$, $\boldsymbol{z}^+=\boldsymbol{z}(t,j+1)$, $\boldsymbol{z}^-=\boldsymbol{z}(t,j)$,

$$
\begin{aligned}
\boldsymbol{A}_j(t) &= D_1\boldsymbol{f}_j(\boldsymbol{\alpha}_j(t),\boldsymbol{\mu}_j(t),t),\\
\boldsymbol{B}_j(t) &= D_2\boldsymbol{f}_j(\boldsymbol{\alpha}_j(t),\boldsymbol{\mu}_j(t),t),\\
\boldsymbol{G}_j &= D_1\boldsymbol{g}^- - \left(\dot{\boldsymbol{g}}^- - \boldsymbol{f}^+\right)\frac{D_1\gamma^-}{\dot{\gamma}^-},\\
\boldsymbol{J}_j &= D_2\boldsymbol{g}^- - \left(\dot{\boldsymbol{g}}^- - \boldsymbol{f}^+\right)\frac{D_2\gamma^-}{\dot{\gamma}^-},
\end{aligned}
$$

and

$$
\begin{aligned}
\dot{\boldsymbol{\mu}}^- &:= \dot{\boldsymbol{\mu}}_{j-1}(\tau_j),\\
\boldsymbol{f}^- &:= \boldsymbol{f}_{j-1}(\boldsymbol{\alpha}_{j-1}(\tau_j),\boldsymbol{\mu}_{j-1}(\tau_j),\tau_j),\\
\boldsymbol{f}^+ &:= \boldsymbol{f}_j(\boldsymbol{\alpha}_j(\tau_j),\boldsymbol{\mu}_j(\tau_j),\tau_j),\\
\boldsymbol{g}^- &:= \boldsymbol{g}_j(\boldsymbol{\alpha}_{j-1}(\tau_j),\boldsymbol{\mu}_{j-1}(\tau_j),\tau_j),\\
\dot{\boldsymbol{g}}^- &:= D_1\boldsymbol{g}^-\cdot\boldsymbol{f}^- + D_2\boldsymbol{g}^-\cdot\dot{\boldsymbol{\mu}}^- + D_3\boldsymbol{g}^-,\\
\gamma^- &:= \gamma_j(\boldsymbol{\alpha}_{j-1}(\tau_j),\boldsymbol{\mu}_{j-1}(\tau_j),\tau_j),\\
\dot{\gamma}^- &:= D_1\gamma^-\cdot\boldsymbol{f}^- + D_2\gamma^-\cdot\dot{\boldsymbol{\mu}}^- + D_3\gamma^-.
\end{aligned}
$$

The LTTHS of Definition 2 gives an approximation of the NSITHS about the state-input reference trajectory $(\boldsymbol{\alpha},\boldsymbol{\mu})$. With a nominal trajectory $\boldsymbol{\alpha}$ with input $\boldsymbol{\mu}$, the perturbed trajectory $\boldsymbol{x}_j(\epsilon)$ is the trajectory starting from initial condition $\boldsymbol{x}_0(\epsilon)=\boldsymbol{\alpha}_0+\epsilon\boldsymbol{z}_0$ and with input $\boldsymbol{u}_j(\epsilon)=\boldsymbol{\mu}_j+\epsilon\boldsymbol{v}_j$. The approximation is then defined as $\boldsymbol{x}_j(\epsilon)=\bar{\boldsymbol{\alpha}}_j+\epsilon\bar{\boldsymbol{z}}_j+o(\epsilon)$, with $\boldsymbol{z}$ defined by the LTTHS. The reader should be aware that the term $\boldsymbol{v}^-$ is not an input that can be freely chosen. The ante-event input perturbation $\boldsymbol{v}^-$ is directly related to $\boldsymbol{v}_j$, as it is a result of the input law implemented during the continuous segment before the event. Also, note that the approximation jumps at the same time instants as the nominal trajectory, with $(t,j)\in\operatorname{eve}\boldsymbol{\alpha}$. This results in a trajectory which is generally infeasible around the jump times. However, due to the short timescales of the events, we are more interested in finding a good approximation of the continuous segments between the events, which is what the LTTHS achieves. In [55] a proof is given, which shows that stability of the LTTHS implies tracking of a NSTHS. The presumption is made that a similar proof exists, saying that stability of the LTTHS implies local stability of the NSITHS.

3.3 Summary

In this chapter, a linear approximation of the NSITHS is presented. The NSITHS is formally defined, which is a framework suitable for the dynamics defined in Chapter 2. Perturbations in the initial condition and input curve are introduced into this system, resulting in perturbed trajectories of which the event times differ from the nominal event times, and are not known beforehand. This mismatch in event time leads to a behavior called peaking. Reference spreading is then presented to eliminate peaking behavior. After posing assumptions on continuity of the vector fields, transversality of the guard activations, and differentiability of the jump maps, a sensitivity analysis is performed. The sensitivity analysis leads to an LTTHS describing the tracking error dynamics, which is used to generate an approximation of the perturbed state. While there is no proof available that the approximation generated by the LTTHS is first order, our claim is that such a proof exists. In addition, under the presumption that a proof exists that uniform asymptotic stability of the LTTHS implies local asymptotic stability of the NSITHS, conventional stability analysis tools can be used to evaluate tracking of the nominal reference trajectory.

Chapter 4

Sensitivity Analysis with Simultaneous State-and-Input-Triggered Events

In this chapter, the analysis presented in Chapter 3 will be extended to be suitable for trajectories with simultaneous guard activations. Simultaneous guard activations are activations where a trajectory triggers two or more guard functions at the same time-instant. Take for example a box with two contact points, where both contacts are closed at the same time. When perturbations are introduced in these trajectories, the simultaneity of the event can be lost. Also, the order of activations can change depending on the perturbation. The box can first impact one contact point and then at the other, or the other way around. This complicates the definition of the approximation of the perturbed trajectory.

In this chapter, a novel notation introduced in [67] will be presented to describe trajectories with simultaneous guard functions. Reference spreading is applied to trajectories with simultaneous events, which is used as a basis to define a positively homogeneous jump gain which approximates the jump behavior of the perturbed trajectory. The positively homogeneous jump gain defines the *positively homogeneous time-triggered hybrid system* (PTTHS). This chapter extends the work presented in [59,67], making the approximation suitable for trajectories with input-dependent guard functions, and therefore mechanical systems experiencing dry friction and releasing motions.

4.1 Simultaneous guard-activation

To be able to perform a sensitivity analysis in the spirit of the one presented in Chapter 3 for trajectories with simultaneous guard activations, some adjustments need to be made to the notation of the system definition. In this section, a notation similar to the notation in [67] is presented, namely: the event character, micro and macro events, multiscale hybrid time, guard function index, mode descriptor, phantom segments, and historical notation. After this, reference spreading for simultaneous guard-activations is discussed. Note that the notation that will be presented in this section is not a contribution, but merely presented for completeness.

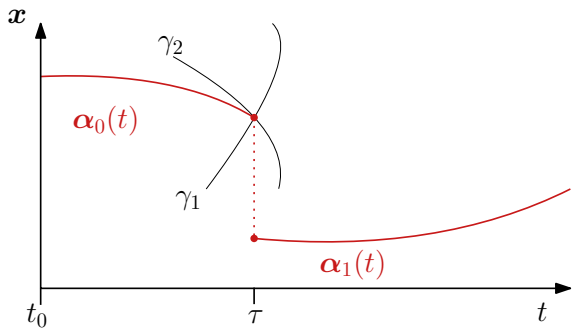

Figure 4.1: *An illustration of a trajectory with a simultaneous event. At $t = \tau$, the trajectory activates two guard functions, γ_1 and γ_2.*

4.1.1 Adopted notation

In a simultaneous event, multiple guard functions are activated at the same time instant. In Figure 4.1, an example of a simultaneous activation of two guards is illustrated. The ante-event reference trajectory, $\boldsymbol{\alpha}_0(t)$, activates two guard functions, γ_1 and γ_2. The number of guard functions that are activated in a single nominal event is called the *event character*, and indicated with the letter c. In the example in Figure 4.1, the event character is two ($c = 2$).

When perturbations are introduced in an event with simultaneous activations, the number of events the system undergoes can change. Instead of a simultaneous activation of c guards, the guards can be activated in rapid succession. These events that are the result of loss of simultaneity are called *micro events*, where several micro events are associated to the same transition. Such a transition is called a *macro event*. When a macro event consists of simultaneous activations, one jump will be observed. Loss of simultaneity will generate micro events, resulting in that more jumps and flow segments can be observed in the state trajectory in comparison to the reference trajectory. To keep track of these segments, *multiscale hybrid time* is introduced. Multiscale hybrid time is denoted by (t, i, k), where t is regular time, i the macro event counter, and k the micro event counter. The micro event counter k is incremented every time an event occurs, except when a macro event is completed by reaching the nominal post-event mode. The micro event counter k is then reset to zero, and the macro event counter i is incremented. One can now write $\boldsymbol{x}(t, i, k)$ to make a distinction between all the segments that are generated as a result of loss of simultaneity. Multiscale hybrid time is directly related to the standard hybrid time as defined in Section 2.3.1, according to

$$j(i, k) = k + \sum_{\kappa=1}^{i} l_\kappa, \tag{4.1}$$

with l_κ the number of micro events in macro event κ. The perturbed event times of micro events are denoted by t_i^k, i.e., the event time of the k-th micro event of macro event i. A set of guard function indexes η is introduced to identify the several guard functions that are involved with an event. A guard function that is inactive is a guard function that is associated to a transition, but not yet activated. With c_i the event character of the i-th event, the index set of inactive guard functions is defined as

$$\left\{\eta = 2^\nu \mid \nu \in \{0, 1, \ldots, c_i\}\right\}. \tag{4.2}$$

The index set of inactive guard functions η is written in the binary numeral system for a more intuitive notation of the different guard functions. The inactive guard functions can then be denoted

as γ^{η}. While the micro counter i and macro counter k are left out for readability, note that

$$\gamma^{\eta} = \gamma^{\eta}(\cdot, i, k), \tag{4.3}$$

meaning that the guard functions not only change with macro events, but also with micro events. Now an example is given to illustrate the relation between the set of guard functions γ^{η} and the guard functions defined in Section 2.3.3. Let us consider a block with two contact points not in contact, i.e., $\iota_1, \iota_2 \in \mathcal{I}_{\text{op}}$. We consider a nominal trajectory with a character-2 event ($c = 2$), where both contact points simultaneously close contact with a surface. The index set of inactive guards η before the event is, in this example, $\eta = \{01, 10\}$. The associated guard functions are then defined as

$$\gamma^{01} = \gamma_{\iota_1}^{\text{op}\to\text{cl}} = \mathrm{h}_{n,\iota_1}(\boldsymbol{q}), \tag{4.4}$$

$$\gamma^{10} = \gamma_{\iota_2}^{\text{op}\to\text{cl}} = \mathrm{h}_{n,\iota_2}(\boldsymbol{q}). \tag{4.5}$$

The mode of the system is indicated using the *mode descriptor* s_i^k. The mode descriptor s_i^k is associated to event i, similar to τ_i[1]. The micro segments associated to macro event i will be described using

$${}^{s_i^k}\boldsymbol{x}(t) := \boldsymbol{x}(t, i-1, k), \tag{4.6}$$

with s_i^k the mode of the k-th micro event associated to macro event i. Note that s_i^k is a mode descriptor to describe the micro segments associated to macro event i. The macro segments, where $k = 0$, are still written as

$$\boldsymbol{x}_i(t) = \boldsymbol{x}(t, i, 0). \tag{4.7}$$

When the considered macro event is known from context, the macro counter i can be dropped to simplify the notation. From here on, we will also write the mode descriptor as s^k if the macro counter i is known. Similar to the inactive guard index set η, the mode descriptor is written in the binary numeral system. This binary numeral system is used as follows. When there is an event with character $c = 4$, four guard functions can be activated. When the mode of the system is described by $s^k = 1010$, this means that two guard functions are already activated, and two are still inactive. Namely, the guard functions that are still to be activated are those with index $\eta = \{0100, 0001\}$. The mode descriptor now intuitively shows which guard functions are inactive, as the zeros in the mode descriptor denote the inactive guard function indexes. The index of the guard function that is activated during event k is denoted by η_k. The superscript $(\cdot)^{\epsilon}$ is introduced for the state $\boldsymbol{x}$, to indicate that the state trajectory is perturbed, i.e.,

$${}^{s_i^k}\boldsymbol{x}^{\epsilon}(t) = \boldsymbol{x}(t, i-1, k, \epsilon). \tag{4.8}$$

We will illustrate the adopted notation in an example. Let us consider a transition, depicted in Figure 4.2, with event character $c = 2$ and guard functions γ^{10} and γ^{01}. The state evolution of the system begins in the mode described by $s^0 = 00$, where $\gamma^{10} > 0$ and $\gamma^{01} > 0$. When the state activates one of the guard functions, in the example of Figure 4.2 $\gamma^{01} = 0$, the next mode is described by $s^1 = 01$. When the other guard function γ^{10} is activated as well, then the system completes its macro event with $s^2 = 11$. Note that the guard function can change when the system is in another mode, i.e., the guard function γ^{10} defined in s^0 is different from the guard function γ^{10} defined in s^1.

[1]The reader should be aware of the distinction between the event i and the hybrid time i. The hybrid time i indicates a segment of flow, whereas the event i indicates a point.

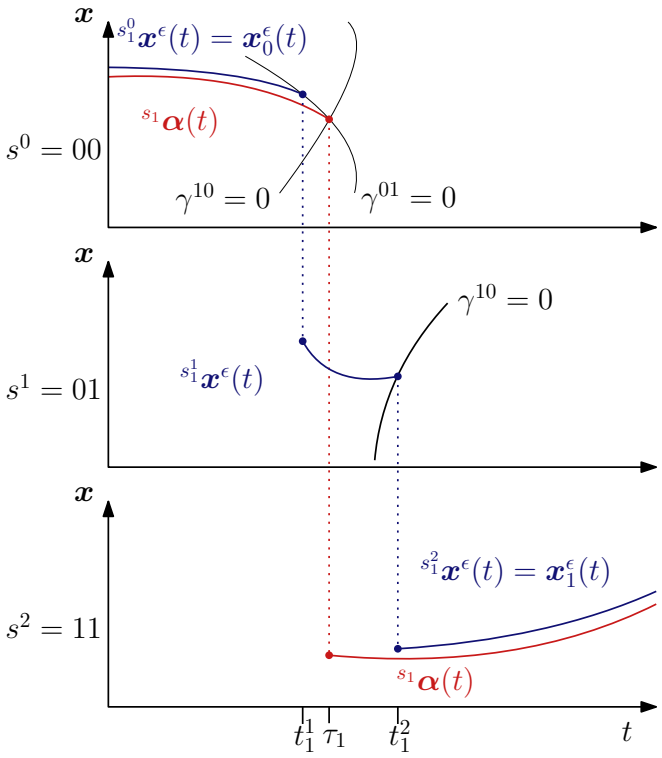

Figure 4.2: *A reference trajectory going through a simultaneous event and a state trajectory experiencing loss of simultaneity. Where the reference trajectory activates γ^{10} and γ^{01} simultaneously, the state trajectory first activates γ^{01} at $t = t^1$, flows for $t \in [t^1_1, t^2_1]$, and then activates γ^{10} at $t = t^2$.*

Depending on the perturbation, several mode sequences can achieve the expected nominal end mode when simultaneity is lost. The different mode sequences can generate a different post-event state, because of the flow phases in between the micro events. Therefore, it is useful to be able to indicate an entire mode sequence with one symbol. We call this notation the *historical notation*. We define the sequence for macro event i as

$$S^k_i = s^k_i \leftarrow s^{k-1}_i \leftarrow \cdots \leftarrow s^0_i, \tag{4.9}$$

where $s^0_i = 00\ldots0$ with length c_i. Again, the macro counter i can be left out for convenience. A growing mode sequence is a sequence of micro events, where at eacht micro event another guard function is activated and no guard functions deactivated. We can now define ${}^{S^k}\boldsymbol{x}(t)$ as ${}^{s^k}\boldsymbol{x}(t)$ that is a result of the growing sequence S^k. The jump maps that are applied during such a sequence are given by

$${}^{p}\boldsymbol{x} = {}^{p\leftarrow a}\boldsymbol{g}({}^{a}\boldsymbol{x}, {}^{a}\boldsymbol{u}, t), \tag{4.10}$$

where p represents the post-event mode descriptor, and a the ante-event mode descriptor. For example, the state jump from s^k to s^{k+1} is given by ${}^{s^{k+1}}\boldsymbol{x} = {}^{s^{k+1}\leftarrow s^k}\boldsymbol{g}({}^{s^k}\boldsymbol{x}, {}^{s^k}\boldsymbol{u}, t)$. Sequences with a particular order of events can also be expressed as

$${}^{\nu_k\nu_{k-1}\ldots\nu_1}S^k = s^k \leftarrow s^{k-1} \leftarrow \cdots \leftarrow s^0, \tag{4.11}$$

where all mode descriptor entries are defined as $s^\kappa = s^{\kappa-1} + \eta_\kappa$, with $\eta_\kappa = 2^{\nu_\kappa - 1}$ and $\kappa = \{1, 2, \ldots, k\}$. For a simultaneous activation during a micro event, the participating guard functions are placed within brackets. For example, for a character-4 ($c = 4$) growing sequence, we

write

$$^{23(14)}S^3 = 1111 \leftarrow 1101 \leftarrow 1001 \leftarrow 0000. \tag{4.12}$$

With the notation for trajectories experiencing simultaneous guard activations in place, reference spreading for such activations is presented in the next section.

4.1.2 Reference-spreading for simultaneous events

For trajectories with simultaneous activations, the perturbed state can experience more events than the reference trajectory. The perturbed state will enter intermediate modes and segments that are not entered by the reference trajectory. To be able to define a physically realistic comparison between the reference and state trajectories, the concept of reference trajectory has to be revised. This is achieved by means of introducing *nominal phantom modes* and *nominal phantom segments*. Phantom modes are modes defined in the reference trajectory that do not physically exist, but they allow for an approximation of the perturbed state to be defined during micro segments. Definition of these modes requires a property of the state jumps that we term associativity.

Assumption 6 (Jump map associativity)**.** *We assume that the jump map* $^{p}\boldsymbol{x} = {}^{p\leftarrow a}\boldsymbol{g}({}^{a}\boldsymbol{x}, {}^{a}\boldsymbol{u}, t)$ *is associative, meaning that taking an arbitrary growing sequence* $s^k \leftarrow s^{k-1} \leftarrow \cdots \leftarrow s^0$*, finished by* $p = s^k$ *and entered by* $a = s^0$*, it holds that*

$$^{p\leftarrow a}\boldsymbol{g}({}^{a}\boldsymbol{x}, {}^{a}\boldsymbol{u}, t) = {}^{p\leftarrow s^{k-1}}\boldsymbol{g}(\cdot, {}^{s^{k-1}}\boldsymbol{u}, t) \circ {}^{s^{k-1}\leftarrow s^{k-2}}\boldsymbol{g}(\cdot, {}^{s^{k-2}}\boldsymbol{u}, t) \circ \cdots \circ {}^{s^{1}\leftarrow a}\boldsymbol{g}({}^{a}\boldsymbol{x}, {}^{a}\boldsymbol{u}, t), \tag{4.13}$$

where $\circ$ *indicates the composition operator. Intuitively, this means that the simultaneous jump gain from* a *to* p *can be described with a sequence of jumps evaluated at the same time instant.*

Using Assumption 6, the phantom modes can be defined. All micro modes, which the state can enter as a result of loss of simultaneity, are defined in the nominal trajectory. These modes are called the phantom modes in the nominal trajectory. The initial states associated to these modes are found by applying the corresponding jump maps $^{p\leftarrow a}\boldsymbol{g}$ to the nominal ante-event state,

$$\begin{aligned} {}^{s_i^1}\boldsymbol{\alpha} &= {}^{s_i^1\leftarrow s_i^0}\boldsymbol{g}({}^{s_i^0}\boldsymbol{\alpha}, {}^{s_i^0}\boldsymbol{\mu}, \tau_i) \\ {}^{s_i^2}\boldsymbol{\alpha} &= {}^{s_i^2\leftarrow s_i^1}\boldsymbol{g}({}^{s_i^1}\boldsymbol{\alpha}, {}^{s_i^1}\boldsymbol{\mu}, \tau_i) \\ &\vdots \\ {}^{s_i^k}\boldsymbol{\alpha} &= {}^{s_i^k\leftarrow s_i^{k-1}}\boldsymbol{g}({}^{s_i^{k-1}}\boldsymbol{\alpha}, {}^{s_i^{k-1}}\boldsymbol{\mu}, \tau_i), \end{aligned} \tag{4.14}$$

resulting in the reference trajectory being defined in all modes that exist in the state trajectory. The analysis presented in [55] uses guard functions and jump maps that depend on the state $\boldsymbol{x}$ and time t. As mentioned in Section 3.2.1, the sensitivity analysis in [55] is extended to be suitable for input-dependent guards. In (4.14), another contribution is made, in the sense that also the jump maps $\boldsymbol{g}$ are input-dependent. The sensitivity analysis in this work is therefore suitable for both input-dependent guards and input-dependent jump maps.

Based on physical realization of the input, we limit ourselves to two options of the feedforward term $^{S_i^k}\bar{\boldsymbol{\mu}}(t)$. We define *withdrawing phantom modes* and *pushing phantom modes*, which are defined by the feedforwards

$$^{S_i^k}_{\nearrow}\bar{\boldsymbol{\mu}}(t) := \begin{cases} \bar{\boldsymbol{\mu}}_{i-1}(t), & k = 0 \\ \bar{\boldsymbol{\mu}}_i(t), & k \neq 0 \end{cases}, \tag{4.15}$$

and

$$^{S_i^k}_{\searrow}\bar{\boldsymbol{\mu}}(t) := \begin{cases} \bar{\boldsymbol{\mu}}_{i-1}(t), & k \neq l_i \\ \bar{\boldsymbol{\mu}}_i(t), & k = l_i \end{cases}, \tag{4.16}$$

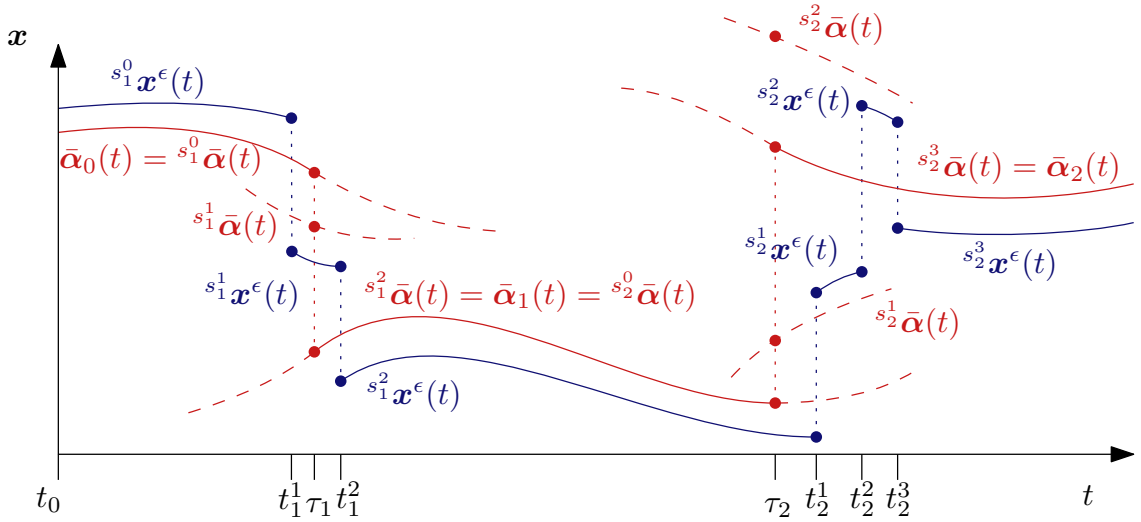

Figure 4.3: *The state evolution of the reference trajectory and state trajectory. The reference trajectory is enriched with phantom segments, to which the micro segments of the state trajectory can be compared.*

where $\nearrow$ indicates a withdrawing feedforward and $\searrow$ indicates a pushing feedforward, and l_i is the number of micro events associated with macro event i. For each event it should be specified whether a withdrawing or pushing phantom mode is used.

Since the micro segments of the state trajectory are defined over a time-interval rather than a time instant, the points in (4.14) should be integrated forwards and backwards to define the phantom segments over a time-interval. Using the initial states ${}^{S_i^k}\boldsymbol{\alpha}$ defined in (4.14) and inputs ${}^{S_i^k}\bar{\boldsymbol{\mu}}$ defined in (4.16), the vector field ${}^{s_i^k}\boldsymbol{f}$ can be integrated forward and backward to find the (pushing or withdrawing) phantom segments corresponding to the phantom modes. These phantom modes and segments are illustrated in Figure 4.3, where ${}^{s_0^1}\bar{\boldsymbol{\alpha}}(t), {}^{s_1^1}\bar{\boldsymbol{\alpha}}(t), {}^{s_1^2}\bar{\boldsymbol{\alpha}}(t)$ are examples of phantom segments.

4.2 Approximating perturbed trajectories with simultaneous events

Using the notation presented in Section 4.1.1, an approximation of the NSITHS will be derived for trajectories with simultaneous activations. First, a sensitivity analysis is presented for a simultaneous event with character 2. The result is used to define a jump gain that approximates the behavior of a simultaneous event with an arbitrary event-character, which holds for a particular sequence of events. Since multiple sequences of events are feasible in a simultaneous event, multiple jump gains can be associated with such an event. These jump gains are used to define a positively homogeneous jump gain, which is a state- and input-dependent jump gain that describes the jumping behavior of the state near $(\boldsymbol{\alpha}, \boldsymbol{\mu})$. Finally, the PTTHS is formally defined, which is a approximation of the NSITHS near the reference trajectory. Similar to the LTTHS presented in Section 3.2, we presume that the PTTHS is a first-order approximation of the NSITHS. The proof that the approximation is first order is not yet available, however.

4.2.1 Sensitivity analysis for simultaneous guard-activation

Similar to the sensitivity analysis for trajectories with isolated events presented in Section 3.2.1, the continuous macro segments ($k = 0$) of the state trajectory can be approximated as

$$\boldsymbol{x}_i^\epsilon(t) = \bar{\boldsymbol{\alpha}}_i + \epsilon \bar{\boldsymbol{z}}_i + o(\epsilon), \tag{4.17}$$

where the subscript $(\cdot)^\epsilon$ indicates that the variable is dependent on ϵ and $\boldsymbol{z}_i$ satisfies

$$\dot{\boldsymbol{z}}_i = \boldsymbol{A}_i(t)\boldsymbol{z}_i + \boldsymbol{B}_i(t)\boldsymbol{v}_i, \quad i \in \operatorname{dom} \boldsymbol{\alpha} \tag{4.18}$$

with

$$\begin{aligned}\boldsymbol{A}_i(t) &= D_1 \boldsymbol{f}_i(\boldsymbol{\alpha}_i, \boldsymbol{\mu}_i, t),\\ \boldsymbol{B}_i(t) &= D_2 \boldsymbol{f}_i(\boldsymbol{\alpha}_i, \boldsymbol{\mu}_i, t).\end{aligned}$$

We will now derive an approximation of the jump map of a simultaneous event with character $c_i = 2$. A more thorough derivation can be found in Appendix C.2. In this chapter, the macro counter i is dropped for the sake of readability. By posing ${}^{s^{k+1}}\boldsymbol{g} := {}^{s^{k+1}\leftarrow s^k}\boldsymbol{g}$, the perturbed post-event state associated with micro event $k+1$ is given by

$${}^{s^{k+1}}\boldsymbol{x}^\epsilon(t^{k+1}) = {}^{s^{k+1}}\boldsymbol{g}({}^{s^k}\boldsymbol{x}^\epsilon(t^{k+1}), {}^{s^k}\boldsymbol{u}^\epsilon(t^{k+1}), t^{k+1}), \tag{4.19}$$

with

$${}^{s^k}\boldsymbol{x}^\epsilon(t^{k+1}) = \int_{t^k}^{t^{k+1}} \left[{}^{s^k}\boldsymbol{f}\left({}^{s^k}\boldsymbol{x}^\epsilon(t), {}^{s^k}\boldsymbol{u}^\epsilon(t), t\right)\right] dt + {}^{s^k}\boldsymbol{g}\left({}^{s^{k-1}}\boldsymbol{x}^\epsilon(t^k), {}^{s^{k-1}}\boldsymbol{u}^\epsilon(t^k), t^k\right). \tag{4.20}$$

Here the left superscript ${}^{s^k}(\cdot)$ indicates that the variable is in micro segment k and t^k represents the event-time of micro event k. Similar to (3.23), we define the micro event time as

$$\Delta^k := \left.\frac{\mathrm{d}t^k}{\mathrm{d}\epsilon}\right|_{\epsilon=0} = -\frac{D_1 {}^{s^k}\gamma \cdot {}^{s^{k-1}}\bar{\boldsymbol{z}}(\tau) + D_2 {}^{s^k}\gamma \cdot {}^{s^{k-1}}\bar{\boldsymbol{v}}(\tau)}{{}^{s^k}\dot{\gamma}}, \tag{4.21}$$

with

$$\begin{aligned}{}^{s^k}\gamma &:= {}^{s^k}\gamma({}^{s^{k-1}}\boldsymbol{\alpha}(\tau), {}^{s^{k-1}}\boldsymbol{\mu}(\tau), \tau),\\ {}^{s^k}\dot{\gamma} &:= D_1 {}^{s^k}\gamma \cdot {}^{s^{k-1}}\boldsymbol{f} + D_2 {}^{s^k}\gamma \cdot {}^{s^{k-1}}\dot{\boldsymbol{\mu}} + D_3\gamma^-.\end{aligned}$$

The right-hand side of (4.19) is expanded with respect to ϵ, to find

$${}^{s^{k+1}}\boldsymbol{x}^\epsilon(t^{k+1}) = {}^{s^{k+1}}\boldsymbol{\alpha}(\tau) + \epsilon \left.\frac{\partial}{\partial \epsilon} {}^{s^{k+1}}\boldsymbol{g}\right|_{\epsilon=0} + o(\epsilon), \tag{4.22}$$

where, similar to the expansion of $\boldsymbol{g}_j(\boldsymbol{x}^-, \boldsymbol{u}^-, t_j)$ in (3.28),

$$\begin{aligned}\left.\frac{\partial^{s^{k+1}}\boldsymbol{g}}{\partial\epsilon}\right|_{\epsilon=0} = D_1 {}^{s^{k+1}}\boldsymbol{g} \cdot \Big({}^{s^k}\dot{\boldsymbol{\alpha}}(\Delta^{k+1} - \Delta^k) + D_1 {}^{s^k}\boldsymbol{g} \cdot \left({}^{s^{k-1}}\boldsymbol{z} + {}^{s^{k-1}}\dot{\boldsymbol{\alpha}}\Delta^k\right) + D_2 {}^{s^k}\boldsymbol{g} \cdot \left({}^{s^{k-1}}\boldsymbol{v} + {}^{s^{k-1}}\dot{\boldsymbol{\mu}}\Delta^k\right)\\ + D_3 {}^{s^k}\boldsymbol{g} \cdot \Delta^k \Big) + D_2 {}^{s^{k+1}}\boldsymbol{g} \cdot \left({}^{s^k}\boldsymbol{v} + {}^{s^k}\dot{\boldsymbol{\mu}}\Delta^{k+1}\right) + D_3 {}^{s^{k+1}}\boldsymbol{g} \cdot \Delta^{k+1},\end{aligned} \tag{4.23}$$

with

$$
\begin{aligned}
{}^{s^k}\boldsymbol{f} &:= {}^{s^k}\boldsymbol{f}({}^{s^k}\boldsymbol{\alpha}(\tau), {}^{s^k}\boldsymbol{\mu}(\tau), \tau),\\
{}^{s^k}\boldsymbol{g} &:= {}^{s^k}\boldsymbol{g}({}^{s^{k-1}}\boldsymbol{\alpha}(\tau), {}^{s^{k-1}}\boldsymbol{\mu}(\tau), \tau),\\
{}^{s^k}\dot{\boldsymbol{g}} &:= D_1{}^{s^k}\boldsymbol{g} \cdot {}^{s^{k-1}}\boldsymbol{f} + D_2{}^{s^k}\boldsymbol{g} \cdot {}^{s^{k-1}}\dot{\boldsymbol{\mu}} + D_3{}^{s^k}\boldsymbol{g}.
\end{aligned}
$$

In (4.23), the expansion of the post-event state ${}^{s^{k+1}}\boldsymbol{x}^\epsilon(t^{k+1})$ is expressed in terms of ${}^{s^k}$ and ${}^{s^{k-1}}$. This is done to find a relation between the ante-event state and input perturbation and the post-event state perturbation. By expanding the left-hand side of (4.19) with respect to ϵ, we find

$$
\begin{aligned}
{}^{s^{k+1}}\boldsymbol{x}^\epsilon(t^{k+1}) &= {}^{s^{k+1}}\bar{\boldsymbol{\alpha}}(t^{k+1}) + \epsilon\,{}^{s^{k+1}}\bar{\boldsymbol{z}}(t^{k+1}) + o(\epsilon), &(4.24)\\
&= {}^{s^{k+1}}\boldsymbol{\alpha}(\tau) + \epsilon\,{}^{s^{k+1}}\dot{\boldsymbol{\alpha}}(\tau)\Delta^{k+1} + \epsilon\,{}^{s^{k+1}}\boldsymbol{z}(\tau) + o(\epsilon). &(4.25)
\end{aligned}
$$

From the work in Section 3.2.1, the jump gains $\boldsymbol{G}$ and $\boldsymbol{J}$ are derived for single events. With ${}^{s^k}\boldsymbol{G}(t) := {}^{s^k \leftarrow s^{k-1}}\boldsymbol{G}(t)$ and ${}^{s^k}\boldsymbol{J}(t) := {}^{s^k \leftarrow s^{k-1}}\boldsymbol{J}(t)$, these jump gains translate to the micro-event case as

$$
{}^{s^k}\boldsymbol{G}(\tau) = D_1{}^{s^k}\boldsymbol{g} - \left({}^{s^k}\dot{\boldsymbol{g}} - {}^{s^k}\boldsymbol{f}\right)\frac{D_1{}^{s^k}\gamma}{{}^{s^k}\dot{\gamma}}, \tag{4.26}
$$

$$
{}^{s^k}\boldsymbol{J}(\tau) = D_2{}^{s^k}\boldsymbol{g} - \left({}^{s^k}\dot{\boldsymbol{g}} - {}^{s^k}\boldsymbol{f}\right)\frac{D_2{}^{s^k}\gamma}{{}^{s^k}\dot{\gamma}}. \tag{4.27}
$$

Using (4.22) and (4.25), an expression for ${}^{s^{k+1}}\boldsymbol{z}(\tau)$ is found, which is

$$
\begin{aligned}
{}^{s^{k+1}}\boldsymbol{z}(\tau) = {}&D_1{}^{s^{k+1}}\boldsymbol{g} \cdot {}^{s^k}\boldsymbol{f}\Delta^{k+1} - D_1{}^{s^{k+1}}\boldsymbol{g} \cdot {}^{s^k}\boldsymbol{f}\Delta^k + D_1{}^{s^{k+1}}\boldsymbol{g} \cdot \Big(D_1{}^{s^k}\boldsymbol{g} \cdot \left({}^{s^{k-1}}\boldsymbol{z} + {}^{s^{k-1}}\boldsymbol{f}\Delta^k\right)\\
&+D_2{}^{s^k}\boldsymbol{g}\cdot\left({}^{s^{k-1}}\boldsymbol{v} + {}^{s^{k-1}}\dot{\boldsymbol{\mu}}\Delta^k\right)+D_3{}^{s^k}\boldsymbol{g}\cdot\Delta^k\Big)+D_2{}^{s^{k+1}}\boldsymbol{g}\cdot\left({}^{s^k}\boldsymbol{v} + {}^{s^k}\dot{\boldsymbol{\mu}}\Delta^{k+1}\right)+\left(D_3{}^{s^{k+1}}\boldsymbol{g} - {}^{s^{k+1}}\boldsymbol{f}\right)\Delta^{k+1}.
\end{aligned} \tag{4.28}
$$

which can be rewritten to

$$
\begin{aligned}
{}^{s^{k+1}}\boldsymbol{z}(\tau) = {}&\left(D_1{}^{s^{k+1}}\boldsymbol{g} - \left(D_1{}^{s^{k+1}}\boldsymbol{g} \cdot {}^{s^k}\boldsymbol{f} + D_2{}^{s^{k+1}}\boldsymbol{g} \cdot {}^{s^k}\dot{\boldsymbol{\mu}} + D_3{}^{s^{k+1}}\boldsymbol{g} - {}^{s^{k+1}}\boldsymbol{f}\right)\frac{D_1{}^{s^{k+1}}\gamma}{{}^{s^{k+1}}\dot{\gamma}}\right){}^{s^k}\boldsymbol{G}^{s^{k-1}}\boldsymbol{z}\\
&+\left(D_1{}^{s^{k+1}}\boldsymbol{g} - \left(D_1{}^{s^{k+1}}\boldsymbol{g} \cdot {}^{s^k}\boldsymbol{f} + D_2{}^{s^{k+1}}\boldsymbol{g} \cdot {}^{s^k}\dot{\boldsymbol{\mu}} + D_3{}^{s^{k+1}}\boldsymbol{g} - {}^{s^{k+1}}\boldsymbol{f}\right)\frac{D_1{}^{s^{k+1}}\gamma}{{}^{s^{k+1}}\dot{\gamma}}\right){}^{s^k}\boldsymbol{J}^{s^{k-1}}\boldsymbol{v}\\
&+\left(D_2{}^{s^{k+1}}\boldsymbol{g} - \left(D_1{}^{s^{k+1}}\boldsymbol{g} \cdot {}^{s^k}\boldsymbol{f} + D_2{}^{s^{k+1}}\boldsymbol{g} \cdot {}^{s^k}\dot{\boldsymbol{\mu}} + D_3{}^{s^{k+1}}\boldsymbol{g} - {}^{s^{k+1}}\boldsymbol{f}\right)\frac{D_2{}^{s^{k+1}}\gamma}{{}^{s^{k+1}}\dot{\gamma}}\right){}^{s^k}\boldsymbol{v},
\end{aligned} \tag{4.29}
$$

which is equal to

$$
{}^{s^{k+1}}\boldsymbol{z}(\tau) = {}^{s^{k+1}}\boldsymbol{G}\,{}^{s^k}\boldsymbol{G}\,{}^{s^{k-1}}\boldsymbol{z} + {}^{s^{k+1}}\boldsymbol{G}\,{}^{s^k}\boldsymbol{J}\,{}^{s^{k-1}}\boldsymbol{v} + {}^{s^{k+1}}\boldsymbol{J}\,{}^{s^k}\boldsymbol{v}. \tag{4.30}
$$

An important realization is that (4.30) is also found by evaluating two single jumps at τ, and taking the post-event state of the first jump as the ante-event state of the second jump. These two jumps are given by

$$
{}^{s^k}\boldsymbol{z}(\tau) = {}^{s^k}\boldsymbol{G}\,{}^{s^{k-1}}\boldsymbol{z} + {}^{s^k}\boldsymbol{J}\,{}^{s^{k-1}}\boldsymbol{v}, \tag{4.31}
$$

$$
{}^{s^{k+1}}\boldsymbol{z}(\tau) = {}^{s^{k+1}}\boldsymbol{G}\,{}^{s^k}\boldsymbol{z} + {}^{s^{k+1}}\boldsymbol{J}\,{}^{s^k}\boldsymbol{v}, \tag{4.32}
$$

respectively. This implies that the approximation of the post-impact state of two simultaneous jumps at τ can be found by evaluating the two jumps separately. For an arbitrary number of micro events k, the approximation of the post-event state can be found to be

$$ {}^{S^k}\boldsymbol{z}(\tau) = {}^{s^k\leftarrow s^0}\boldsymbol{G}\ {}^{s^0}\boldsymbol{z}(\tau) + \sum_{\iota=0}^{k-1} {}^{s^k\leftarrow s^{\iota+1}}\boldsymbol{G}\ \ {}^{s^{\iota+1}\leftarrow s^{\iota}}\boldsymbol{J}\ {}^{s^{\iota}}\boldsymbol{v}(\tau), \tag{4.33} $$

where ${}^{p\leftarrow a}\boldsymbol{G}$ and ${}^{p\leftarrow a}\boldsymbol{J}$ are defined as

$$ {}^{p\leftarrow a}\boldsymbol{G} := {}^{p}\boldsymbol{G}\ {}^{p-1}\boldsymbol{G}\cdots{}^{a}\boldsymbol{G}, \tag{4.34} $$

$$ {}^{p\leftarrow a}\boldsymbol{J} := {}^{p}\boldsymbol{J}\ {}^{p-1}\boldsymbol{J}\cdots{}^{a}\boldsymbol{J}, \tag{4.35} $$

for a sequence $p \leftarrow p-1 \leftarrow \cdots \leftarrow a$, with slight abuse of notation, in the sense that $p-1$ indicates the mode descriptor associated to the mode before p.

Remark. *While it is not proven that* (4.33) *is true, it is strongly suggested by the relation found in* (4.30)*. Whereas* (4.30) *only holds for a simultaneous event with character-2 ($c = 2$), an induction-like proof can extend the derivation presented in this section to be true for an event with an arbitrary character, resulting in the relation given in* (4.33)*. This proof, however, is left for future work.*

The relation between the post-event state perturbation ${}^{s^{k+1}}\boldsymbol{z}(\tau)$ and the ante-event state and input perturbation ${}^{s^{k-1}}\boldsymbol{z}$ and $\boldsymbol{v}$ in (4.33) is the main result of this section. Using that result, the effect of a perturbation on the jumping behavior of the system can be approximated. For a more complete derivation, consult Appendix C.2. The first term in (4.33) represents the effect of the perturbed ante-event state on the perturbed post-event state. This term is already found in [67], where a sensitivity analysis is presented without input-dependent guards and jump maps. The summation in (4.33) is a contribution of this work, which represents the effects of the chosen feedback during micro-segments.

Note that the approximation of the post-event state (4.33) shares an algebraic similarity with the impulse response of linear discrete time systems. With $\boldsymbol{x}_d(t)$ the state, $\boldsymbol{u}_d(t)$ the input, and $\boldsymbol{y}_d(t)$ the output of a discrete system, the discrete impulse response is in the form of

$$ \boldsymbol{y}_d(t) = \boldsymbol{C}\boldsymbol{x}_d(0) + \sum_{j=0}^{t} \boldsymbol{D}(j)\boldsymbol{u}_d(t-j), \tag{4.36} $$

where $\boldsymbol{y}_d(t) := \boldsymbol{y}_d(\boldsymbol{x}_d(0), \boldsymbol{u}(t), t)$, and $\boldsymbol{C}$ and $\boldsymbol{D}$ some matrices defined by the discrete systems dynamics [68]. Note that, similar to the discrete impulse response $\boldsymbol{y}_d$, the post-event perturbation ${}^{S^k}\boldsymbol{z}$ is also dependent on the ante-event state perturbation ${}^{s^0}\boldsymbol{z}$, the entire evolution of the input $\boldsymbol{u}$, and the time t, i.e., ${}^{S^k}\boldsymbol{z}(\tau) := {}^{S^k}\boldsymbol{z}({}^{s^0}\boldsymbol{z}, \boldsymbol{v}, \tau)$.

When $\boldsymbol{v}$ is considered a feedback term that is turned off when the first micro event is detected, then the approximation of the post-event state perturbation can be simplified to

$$ {}^{S^k}\boldsymbol{z}(\tau) = {}^{S^k}\boldsymbol{L}\begin{bmatrix} {}^{s^0}\boldsymbol{z}(\tau) \\ {}^{s^0}\boldsymbol{v}(\tau) \end{bmatrix}, \text{ with } {}^{S^k}\boldsymbol{L} = \begin{bmatrix} {}^{S^k}\boldsymbol{G} & {}^{S^{k\leftarrow 1}}\boldsymbol{G}\ {}^{S^{1\leftarrow 0}}\boldsymbol{J} \end{bmatrix}, \tag{4.37} $$

since only the ante-event feedback term will be non-zero. The jump gain ${}^{S^k}\boldsymbol{L}$ defined in (4.37) is defined for a particular order of guard activations. When considering a simultaneous event, different trajectories close to $(\boldsymbol{\alpha}, \boldsymbol{\mu})$ can be associated to different sequences of guard-activations. Since the sensitivity analysis considers all trajectories close to $(\boldsymbol{\alpha}, \boldsymbol{\mu})$, several sequences of guard-activations,

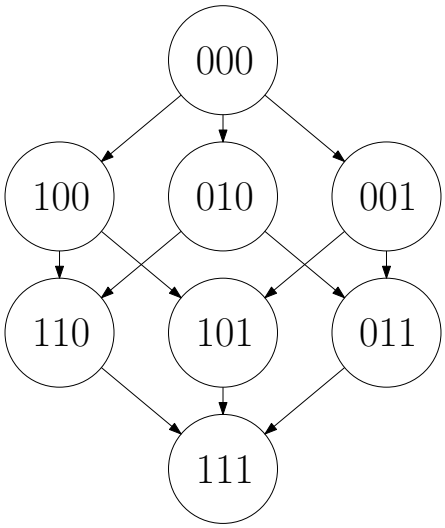

Figure 4.4: *An example of the possible modes in a character-3 event ($c = 3$) illustrated with a graph. When the mode sequences are growing, the edges between the modes are unidirectional, resulting in a finite amount of paths to the post-event mode described by $s = 111$.*

and therefore several jumps gains as in (4.37), can be associated with a simultaneous event. In the next section, the jump gain (4.37) associated to an a priori known mode sequence is used to define a state-dependent jump gain, which covers all possible mode sequences.

Note that the description of the jump gain given in (4.37) is less complicated than jump gain (4.33) for a micro event where feedback is nonzero. Since the micro events usually happen too rapidly to control on, feedback is often turned off when micro events are taking place. Therefore, only situations with zero feedback during micro events are considered in this work. Under these considerations the jump gain in (4.37) is used from here on to define ${}^{S^k}\boldsymbol{L}$.

4.2.2 The positively homogeneous jump map

As mentioned in Section 4.1, an event with simultaneous guard activation will experience loss of simultaneity when perturbations are introduced. Due to the loss of simultaneity, the order of events is unknown. For that reason, one simultaneous event has several feasible event sequences associated with it. For there to be a finite amount of possibilities of event sequences, all sequences should be growing. A graph of growing mode sequences is illustrated for a character-3 event ($c = 3$) in Figure 4.4, where the nodes represent the possible system modes and the edges represent the possible transitions. When the mode sequences are growing, the edges are unidirectional. Therefore a finite number of paths can be found from the ante-event mode described by $s = 000$ to the post-event mode described by $s = 111$. When the mode sequences are not growing, the edges are bidirectional. One can then travel both ways over each edge, resulting in an infinite number of possible mode sequences.

To be able to define a jump map, only a finite number of sequences can be considered. Therefore, an assumption is posed that the mode sequences should be growing.

Assumption 7 (Growing mode sequences)**.** *We assume, locally at each macro event, that all considered mode sequences are growing. Namely, at each micro event, all activated guards will remain active. In other words, considering one macro event, we assume that $s^0 < s^1 < \cdots < s^l$, where $s^0 = 00\ldots0$ and $s^l = 11\ldots1$, and l is the number of micro events in the considered macro*

event.

For example, when we consider a block with two contact points ι_1 and ι_2 executing a pushing motion towards a surface, with $s^0 = 00$ is both contact points open and $s^l = 11$ is both contact points in closed contact stick. Let us say we are in mode $s^1 = 10$, i.e., ι_1 is in closed contact stick and ι_2 is still open. The system goes through the second micro event by activating γ_2^{01}. Under Assumption 7, the event can not cause ι_1 to release contact, i.e., $\Gamma_{\iota_1}^{\text{cl}\to\text{op}} > 0$, $\Gamma_{\iota_1}^{\text{st}\to\text{sl}} > 0$, $\gamma_{\iota_1}^{\text{cl}\to\text{op}} > 0$ and $\gamma_{\iota_1}^{\text{st}\to\text{sl}} > 0$ when solving the state reinitialization and mode selection presented in Section 2.3.4. Under Assumption 7, all mode sequences in a neighborhood of $\boldsymbol{\alpha}, \boldsymbol{\mu}$ will be growing and a finite number of jump gains are possible for a range of perturbations. Let us now pose an assumption on the association between guard functions and transitions.

Assumption 8 (Guard-transition association)**.** *We assume that activation of a guard will result in a transition associated with that guard, i.e., the guard function γ^{η_k} activated in mode s^{k-1}, will result in a post-event mode of which the mode descriptor satisfies $s^k = s^{k-1} + \eta_k$. Here η_k is the index of the guard function that is activated during micro event k.*

Remark. *Considering mechanical systems, Assumption 8 is easily verified for most guard functions. Because $\gamma_\iota^{op\to cl} = \text{h}_{n,\iota}(\boldsymbol{q})$ is defined on position level, under Assumption 7 it will always be contact point ι that will change mode when $\gamma_\iota^{op\to cl}$ is activated. For guard functions defined on acceleration level, i.e.,*

$$\begin{aligned}\gamma^{\text{st}\to\text{sl}} &= \mu_\iota^2 \lambda_{n,\iota} - \boldsymbol{\lambda}_{t,\iota}^T \boldsymbol{\lambda}_{t,\iota},\\ \gamma^{\text{cl}\to\text{op}} &= \lambda_{n,\iota},\end{aligned}$$

the situation is different. The feasible post-event mode is determined by the post-event acceleration for these guard functions. It is therefore possible that a guard function is activated in mode s^{k-1}, but is inactive in mode s^k. Under Assumption 8 this is not possible. Therefore a constraint is introduced on the post-event acceleration, which can be determined by the set of equations, called the mode selection in Section 2.3.4,

$$\begin{aligned}\ddot{\boldsymbol{q}}^+ &= \boldsymbol{M}^{-1}\left[\boldsymbol{S}\boldsymbol{u}^+ - \boldsymbol{C} + \boldsymbol{W}_n\boldsymbol{\lambda}_n^+ + \boldsymbol{W}_t\boldsymbol{\lambda}_t^+\right],\\ \boldsymbol{w}_{n,\iota}^T\ddot{\boldsymbol{q}}^+ + \dot{\boldsymbol{w}}_{n,\iota}^T\dot{\boldsymbol{q}}^+ &= 0, && \forall \iota \in \mathcal{I}_{cl},\\ \boldsymbol{\lambda}_{t,\iota}^+ ||\boldsymbol{W}_{t,\iota}^T\dot{\boldsymbol{q}}^+|| + \mu\lambda_{n,\iota}^+\boldsymbol{W}_{t,\iota}^T\dot{\boldsymbol{q}}^+ &= 0, && \forall \iota \in \mathcal{I}_{sl},\\ \boldsymbol{W}_{t,\iota}^T\ddot{\boldsymbol{q}}^+ + \dot{\boldsymbol{W}}_{t,\iota}^T\dot{\boldsymbol{q}}^+ &= 0. && \forall \iota \in \mathcal{I}_{st},\end{aligned}$$

From the mode selection we can conclude that the post-event acceleration $\ddot{\boldsymbol{q}}$ is directly dependent on the post-event input $\boldsymbol{u}^+$. Therefore, the post-event input $\boldsymbol{u}^+$ should be chosen in such a way that Assumption 8 is met. Appendix B.2 gives an example of an event for which the guard is not necessarily associated with the transition the system goes through.

A state-dependent jump gain for all possible mode sequences associated to a simultaneous event will be defined in the following. This jump gain should consider all growing sequences that can take place for that range of perturbations. Therefore, a state-dependent matrix gain is defined, in the form of

$${}^{p\leftarrow a}\boldsymbol{H}({}^a\boldsymbol{z}(\tau), {}^a\boldsymbol{v}(\tau), \tau) = \begin{cases} \boldsymbol{H}^1({}^{s^0}\boldsymbol{z}, {}^{s^0}\boldsymbol{v}, \tau), & \text{if condition 1 is true,}\\ \boldsymbol{H}^2({}^{s^0}\boldsymbol{z}, {}^{s^0}\boldsymbol{v}, \tau), & \text{if condition 2 is true,}\\ \vdots & \vdots\\ \boldsymbol{H}^r({}^{s^0}\boldsymbol{z}, {}^{s^0}\boldsymbol{v}, \tau), & \text{if condition } r \text{ is true,}\end{cases} \tag{4.38}$$

where r the number of possible mode sequences in a macro event. The jump map $\boldsymbol{H}$ is presented later in this section for a character-2 event ($c = 2$). While it is possible to construct a straightforward algorithm that defines $\boldsymbol{H}$ for any character c, this is left as future work. We will now derive the jump maps and associated conditions in (4.38) to obtain an explicit expression. Note that the several jump gains $\boldsymbol{H}$ in (4.38) all coincide with a particular sequence of events.

For a certain perturbation, only a specific order of micro events is feasible. This order can be found by determining the perturbed jump time of all possible micro events, and selecting the micro event with the earliest event time as the next event. The perturbed event-time of the next micro event ${}^{s^{k+1}\leftarrow S^k}t^\epsilon$ can be approximated at first order as

$$t^{k+1} = \tau + \epsilon\Delta^{k+1} + o(\epsilon), \tag{4.39}$$

$$= \tau + \epsilon\left({}^{S^{k+1}}\boldsymbol{a}^T\ {}^{S^k}\boldsymbol{z} + {}^{S^{k+1}}\boldsymbol{b}^T\ {}^{S^k}\boldsymbol{v}\right) + o(\epsilon), \tag{4.40}$$

with

$${}^{S^k}\boldsymbol{a} := -\frac{1}{\dot{\gamma}^{\eta_k}} D_1\gamma^{\eta_k}({}^{s^{k-1}}\boldsymbol{\alpha}, {}^{s^{k-1}}\boldsymbol{\mu}, \tau),$$

$${}^{S^k}\boldsymbol{b} := -\frac{1}{\dot{\gamma}^{\eta_k}} D_2\gamma^{\eta_k}({}^{s^{k-1}}\boldsymbol{\alpha}, {}^{s^{k-1}}\boldsymbol{\mu}, \tau).$$

Defining the set mode descriptors related to all possible post-event modes

$$\mathcal{S} := \left\{ s^+ = s^- + \eta_+ \mid \eta_+ \in \eta \right\}, \tag{4.41}$$

the mode descriptor of the next mode can be written as

$$s^{k+1} = \underset{s^*}{\arg\min} \left\{ t^{k+1} \mid s^* \in \mathcal{S} \right\}. \tag{4.42}$$

Since the minimization of the impact-time does not depend on τ and ϵ, we can rewrite (4.42) to

$$s^{k+1} = \underset{s^*}{\arg\min} \left\{ {}^{S^{k+1}}\boldsymbol{a}^T\ {}^{S^k}\boldsymbol{z} + {}^{S^{k+1}}\boldsymbol{b}^T\ {}^{S^k}\boldsymbol{v} \mid s^* \in \mathcal{S} \right\}, \tag{4.43}$$

which can be written as

$$s^{k+1} = s^k + \eta_{k+1}, \tag{4.44}$$

with

$$\eta_{k+1} = \underset{\eta^*}{\arg\min} \left\{ -\frac{D_1\gamma^{\eta^*}({}^{s^k}\boldsymbol{\alpha}, {}^{s^k}\boldsymbol{\mu}, \tau) \cdot {}^{S^k}\boldsymbol{z} + D_2\gamma^{\eta^*}({}^{s^k}\boldsymbol{\alpha}, {}^{s^k}\boldsymbol{\mu}, \tau) \cdot {}^{S^k}\boldsymbol{v}}{\dot{\gamma}^{\eta^*}} \mid \eta^* \in \eta \right\}. \tag{4.45}$$

Here η is the index set of inactive guard functions as defined in (4.2) and η_{k+1} is the identifier of the guard that is activated during micro event $k+1$. Finally, (4.45) can be rewritten as

$$\eta_{k+1} = \underset{\eta^*}{\arg\min} \left({}^{S^*}\boldsymbol{a}^T\ {}^{S^k}\boldsymbol{z} + {}^{S^*}\boldsymbol{b}^T\ {}^{S^k}\boldsymbol{v} \right), \tag{4.46}$$

with

$${}^{S^*}\boldsymbol{a} := -\frac{1}{\dot{\gamma}^{\eta^*}} D_1\gamma^{\eta^*}({}^{s^k}\boldsymbol{\alpha}, {}^{s^k}\boldsymbol{\mu}, \tau),$$

$${}^{S^*}\boldsymbol{b} := -\frac{1}{\dot{\gamma}^{\eta^*}} D_2\gamma^{\eta^*}({}^{s^k}\boldsymbol{\alpha}, {}^{s^k}\boldsymbol{\mu}, \tau).$$

By checking (4.45) for every micro event, we can determine what the post-event mode of each micro-event will be. With that knowledge, we can decide which jump gains we should apply in (4.33) to find the correct jump gain.

We now pose an example to illustrate the positively homogeneous jump gain. Let us consider a system with $c_i = 2$, ${}^{s^1}\boldsymbol{v} = {}^{s^2}\boldsymbol{v} = \cdots = {}^{s^l}\boldsymbol{v} = 0$, and with a macro event starting in $s^0 = 00$ and ending in $s^l = 11$, this gives

$$ {}^{11\leftarrow 00}\boldsymbol{H}({}^{s^0}\boldsymbol{z}(\tau), {}^{s^0}\boldsymbol{v}(\tau), \tau) = \begin{cases} \begin{bmatrix} {}^{11\leftarrow 00}_{(12)S^1}\boldsymbol{G}, & {}^{11\leftarrow 00}_{(12)S^1}\boldsymbol{J} \end{bmatrix}, & \text{if (I)}, \\ \begin{bmatrix} {}^{11\leftarrow 01}_{12S^2}\boldsymbol{G}\,{}^{01\leftarrow 00}_{2S^1}\boldsymbol{G}, & {}^{11\leftarrow 01}_{12S^2}\boldsymbol{G}\,{}^{01\leftarrow 00}_{2S^1}\boldsymbol{J} \end{bmatrix}, & \text{if (II)}, \\ \begin{bmatrix} {}^{11\leftarrow 10}_{12S^2}\boldsymbol{G}\,{}^{10\leftarrow 00}_{2S^1}\boldsymbol{G}, & {}^{11\leftarrow 10}_{12S^2}\boldsymbol{G}\,{}^{10\leftarrow 00}_{2S^1}\boldsymbol{J} \end{bmatrix}, & \text{if (III)}, \end{cases} \tag{4.47} $$

with

$$ \begin{aligned} \text{(I)} &: {}^{2S^1}\boldsymbol{a}^T\ {}^{s^0}\boldsymbol{z} + {}^{2S^1}\boldsymbol{b}^T\ {}^{s^0}\boldsymbol{v} = {}^{1S^1}\boldsymbol{a}^T\ {}^{s^0}\boldsymbol{z} + {}^{1S^1}\boldsymbol{b}^T\ {}^{s^0}\boldsymbol{v}, \\ \text{(II)} &: {}^{2S^1}\boldsymbol{a}^T\ {}^{s^0}\boldsymbol{z} + {}^{2S^1}\boldsymbol{b}^T\ {}^{s^0}\boldsymbol{v} > {}^{1S^1}\boldsymbol{a}^T\ {}^{s^0}\boldsymbol{z} + {}^{1S^1}\boldsymbol{b}^T\ {}^{s^0}\boldsymbol{v}, \\ \text{(III)} &: {}^{2S^1}\boldsymbol{a}^T\ {}^{s^0}\boldsymbol{z} + {}^{2S^1}\boldsymbol{b}^T\ {}^{s^0}\boldsymbol{v} < {}^{1S^1}\boldsymbol{a}^T\ {}^{s^0}\boldsymbol{z} + {}^{1S^1}\boldsymbol{b}^T\ {}^{s^0}\boldsymbol{v}. \end{aligned} \tag{4.48} $$

Remark. *Note that the jump map* (4.47) *only applies to simultaneous activations in the same manifold. The situation where a single guard activation generates a post-event state that immediately activates another guard in the post-event mode is not what we name a simultaneous event. However, an example that might be worth exploring can be found in the application of this theory to mechanical systems. When a contact point impacts a surface, the post-event state of that event could immediately activate a stick/slip-transition related guard function. We believe that this situation might be worth exploring, because of its association with high performance. Let us consider a running robot. When it places one of his feet, it will want to push that foot as hard as possible while staying in stick. In this situation the reference trajectory might be chosen in such a way, that the post-event state of the impact is at the border of a stick-to-slip transition. We believe that a state-dependent matrix gain can be found, similar to* (4.47)*, which approximates the behavior of such events. This would be a useful addition to the RS control approach, and is therefore a suggestion for future research.*

The jump gain in (4.47) is called a positively homogeneous jump gain for character-2 events ($c = 2$). Due to the behavior of the simultaneous events, the linearity property of the jump gain is lost. This is shown in Appendix C.3. Instead, the jump gain is positively homogeneous, which is now formally defined.

Definition 3 (Positive homogeneity)**.** *Suppose that $\boldsymbol{f}(\boldsymbol{x}, \boldsymbol{u}, t)$ is a continuously differentiable function. The function $\boldsymbol{f}$ is positively homogeneous of degree k in $\boldsymbol{x}$ and $\boldsymbol{u}$, and uniform in t, if*

$$ \boldsymbol{f}(a\boldsymbol{x}, a\boldsymbol{u}, t) = a^k \boldsymbol{f}(\boldsymbol{x}, \boldsymbol{u}, t), \tag{4.49} $$

for all $a > 0$ [69].

The reader should be aware that the positively homogeneous jump gain (4.47) is non-unique. Due to the simultaneous activation of two guards γ^{01} and γ^{10}, the term $\begin{bmatrix} {}^{11\leftarrow 00}_{(12)S^1}\boldsymbol{G}, & {}^{11\leftarrow 00}_{(12)S^1}\boldsymbol{J} \end{bmatrix}$ can be defined using either γ^{01} or γ^{10}. However, this gain is only applied under the condition that

$$ {}^{2S^1}\boldsymbol{a}^T\ {}^{s^0}\boldsymbol{z} + {}^{2S^1}\boldsymbol{b}^T\ {}^{s^0}\boldsymbol{v} = {}^{1S^1}\boldsymbol{a}^T\ {}^{s^0}\boldsymbol{z} + {}^{1S^1}\boldsymbol{b}^T\ {}^{s^0}\boldsymbol{v}, \tag{4.50} $$

which means that the positively homogeneous jump map ${}^{11\leftarrow 00}\boldsymbol{H}\begin{bmatrix} {}^{s^0}\boldsymbol{z} & {}^{s^0}\boldsymbol{v} \end{bmatrix}^T$ is unique. For this reason, despite the jump gain ${}^{11\leftarrow 00}\boldsymbol{H}$ being non-unique, the post-event state perturbation ${}^{s^k}\boldsymbol{z}$ resulting from the positively homogeneous jump gain is unique.

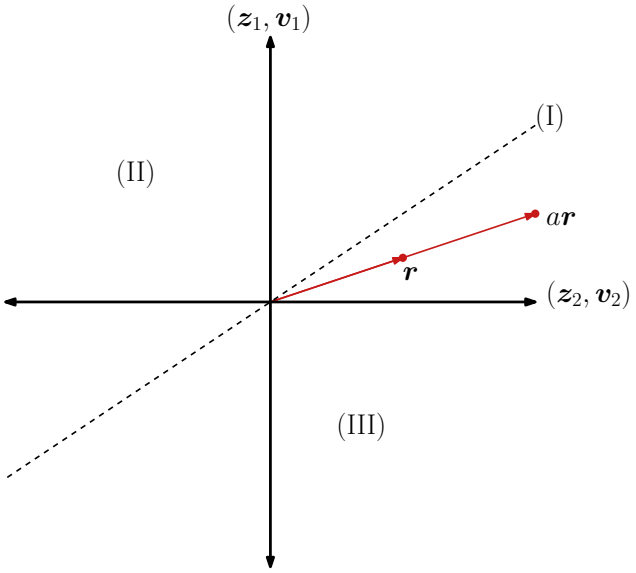

Figure 4.5: *An illustration of the conditions in* (4.48)*, and how they result in a order zero positively homogeneous jump gain. The areas* (I)*,* (II)*, and* (III) *coincide with the conditions* (I)*,* (II)*, and* (III) *in* (4.48)*.*

The conditions that decide which jump gain to use are illustrated in Figure 4.5. Since the conditions are linear in $\boldsymbol{z}$ and $\boldsymbol{v}$, they appear as lines in the state space of $\boldsymbol{z}$ and $\boldsymbol{v}$. When we introduce more conditions, we will find several cones that relate a certain jump gain to a $\boldsymbol{z}, \boldsymbol{v}$ pair. When we look at the vector $\boldsymbol{r}(\boldsymbol{z}, \boldsymbol{v})$ in Figure 4.5, it can be noticed that when $\boldsymbol{r}$ is multiplied with a positive constant a, the same jump gain is applied. Therefore, the positively homogeneous jump gain (4.47) is positively homogeneous of order zero. The non-uniqueness of ${}^{11\leftarrow 00}\boldsymbol{H}$ appears on the dashed line associated with condition (I), depicted in Figure 4.5.

4.2.3 The positively homogeneous time-triggered hybrid system

With the positively homogeneous jump gain presented in the previous section, the PTTHS can be defined. The PTTHS forms an approximation of the NSITHS defined in Definition 1. We presume this approximation to be first order. The PTTHS will jump at the same time as the nominal trajectory $\boldsymbol{\alpha}$, and will also experience the same number of jumps. This means that a controller designed on the PTTHS will only switch once during a macro event, and not on every micro event. This is desired behavior, as the micro events will likely happen too rapidly to control on. We now define the PTTHS formally, with the positively homogeneous jump gain being defined for a character-2 event ($c = 2$, with $a = 00$ and $p = 11$) for brevity reasons.

Definition 4 (PTTHS)**.** *The positively homogeneous time-triggered hybrid system associated with the NSITHS and the associative and transversal reference trajectory* $(\boldsymbol{\alpha}(t,i), \boldsymbol{\mu}(t,i))$ *is given by*

$$\dot{\boldsymbol{z}} = \boldsymbol{A}_i(t)\boldsymbol{z} + \boldsymbol{B}_i(t)\boldsymbol{v}, \qquad (t,i) \in \text{dom } \boldsymbol{\alpha}, \tag{4.51}$$

$$\boldsymbol{z}^+ = \boldsymbol{H}_{i+1}\begin{bmatrix}\boldsymbol{z}^- \\ \boldsymbol{v}^-\end{bmatrix}, \qquad (t,i) \in \text{eve } \boldsymbol{\alpha}, \tag{4.52}$$

where $\boldsymbol{H}_{i+1} := {}^{p\leftarrow a}\boldsymbol{H}(\boldsymbol{z}^-, \boldsymbol{v}^-, t)$ *is a positively homogeneous jump gain of order zero,*

$$\begin{aligned}
\boldsymbol{A}_i(t) &:= D_1\boldsymbol{f}(\boldsymbol{\alpha}(t,i), \boldsymbol{\mu}(t,i), t, i),\\
\boldsymbol{B}_i(t) &:= D_2\boldsymbol{f}(\boldsymbol{\alpha}(t,i), \boldsymbol{\mu}(t,i), t, i),\\
\boldsymbol{v}^- &:= {}^a\boldsymbol{v} = \boldsymbol{v}(t,i),\\
\boldsymbol{z}^- &:= {}^a\boldsymbol{z} = \boldsymbol{z}(t,i),\\
\boldsymbol{z}^+ &:= {}^p\boldsymbol{z} = \boldsymbol{z}(t,i+1),
\end{aligned}$$

with $a = s_i^0 = 00\ldots0$ *and* $p = s_i^l = 11\ldots1$ *where* l *is the amount of micro events in the growing sequence* $p \leftarrow \cdots \leftarrow a$*. The domain* dom $\boldsymbol{\alpha}$ *and event set* eve $\boldsymbol{\alpha}$ *are defined as*

$$\text{dom }\boldsymbol{\alpha} := \bigcup_{i=0}^{N}[\tau_i, \tau_{i+1}] \times \{i\}, \tag{4.53}$$

$$\text{eve }\boldsymbol{\alpha} := \bigcup_{i=1}^{N}\{\tau_i\} \times \{i-1\}, \tag{4.54}$$

with $\tau_0 = t_0$*. The positively homogeneous jump gain* ${}^{p\leftarrow a}\boldsymbol{H}$ *for a character-2 event* ($c = 2$)*, with the macro counter* i *omitted for readability, is given by*

$${}^{11\leftarrow00}\boldsymbol{H}({}^{s^0}\boldsymbol{z}(\tau), {}^{s^0}\boldsymbol{v}(\tau), \tau) = \begin{cases} \begin{bmatrix} {}^{11\leftarrow00}_{(12)S^1}\boldsymbol{G}, & {}^{11\leftarrow00}_{(12)S^1}\boldsymbol{J}\end{bmatrix}, & \text{if (I)},\\ \begin{bmatrix} {}^{11\leftarrow01}_{12S^2}\boldsymbol{G}\,{}^{01\leftarrow00}_{2S^1}\boldsymbol{G}, & {}^{11\leftarrow01}_{12S^2}\boldsymbol{G}\,{}^{01\leftarrow00}_{2S^1}\boldsymbol{J}\end{bmatrix}, & \text{if (II)},\\ \begin{bmatrix} {}^{11\leftarrow10}_{12S^2}\boldsymbol{G}\,{}^{10\leftarrow00}_{2S^1}\boldsymbol{G}, & {}^{11\leftarrow10}_{12S^2}\boldsymbol{G}\,{}^{10\leftarrow00}_{2S^1}\boldsymbol{J}\end{bmatrix}, & \text{if (III)}, \end{cases} \tag{4.55}$$

with

$$\begin{aligned}
(I) &: {}^{2S^1}\boldsymbol{a}^T\ {}^{s^0}\boldsymbol{z} + {}^{2S^1}\boldsymbol{b}^T\ {}^{s^0}\boldsymbol{v} = {}^{1S^1}\boldsymbol{a}^T\ {}^{s^0}\boldsymbol{z} + {}^{1S^1}\boldsymbol{b}^T\ {}^{s^0}\boldsymbol{v},\\
(II) &: {}^{2S^1}\boldsymbol{a}^T\ {}^{s^0}\boldsymbol{z} + {}^{2S^1}\boldsymbol{b}^T\ {}^{s^0}\boldsymbol{v} > {}^{1S^1}\boldsymbol{a}^T\ {}^{s^0}\boldsymbol{z} + {}^{1S^1}\boldsymbol{b}^T\ {}^{s^0}\boldsymbol{v},\\
(III) &: {}^{2S^1}\boldsymbol{a}^T\ {}^{s^0}\boldsymbol{z} + {}^{2S^1}\boldsymbol{b}^T\ {}^{s^0}\boldsymbol{v} < {}^{1S^1}\boldsymbol{a}^T\ {}^{s^0}\boldsymbol{z} + {}^{1S^1}\boldsymbol{b}^T\ {}^{s^0}\boldsymbol{v}.
\end{aligned} \tag{4.56}$$

The jump gains ${}^{s^+\leftarrow s^-}_{S^k}\boldsymbol{G}$ *and* ${}^{s^+\leftarrow s^-}_{S^k}\boldsymbol{J}$ *in* (4.55)*, with* $s^+ = s^k$ *and* $s^- = s^0$ *and* $S^k = s^k \leftarrow s^{k-1} \leftarrow \cdots \leftarrow s^0$*, are given by*

$${}^{s^+\leftarrow s^-}_{S^k}\boldsymbol{G} := D_1\boldsymbol{g}^- - \left(\dot{\boldsymbol{g}}^- - \boldsymbol{f}^+\right)\frac{D_1\gamma^-}{\dot{\gamma}^-}, \tag{4.57}$$

$${}^{s^+\leftarrow s^-}_{S^k}\boldsymbol{J} := D_2\boldsymbol{g}^- - \left(\dot{\boldsymbol{g}}^- - \boldsymbol{f}^+\right)\frac{D_2\gamma^-}{\dot{\gamma}^-}, \tag{4.58}$$

and

$$\begin{aligned}
\boldsymbol{f}^- &:= {}^{s^-}\boldsymbol{f}\left({}^{S^-}\boldsymbol{\alpha}(\tau), {}^{S^-}_{\rightarrow}\boldsymbol{\mu}(\tau), \tau\right),\\
\boldsymbol{f}^+ &:= {}^{s^+}\boldsymbol{f}\left({}^{S^+}\boldsymbol{\alpha}(\tau), {}^{S^+}_{\rightarrow}\boldsymbol{\mu}(\tau), \tau\right),\\
\boldsymbol{g}^- &:= {}^{s^+\leftarrow s^-}\boldsymbol{g}\left({}^{S^-}\boldsymbol{\alpha}(\tau), {}^{S^-}_{\rightarrow}\boldsymbol{\mu}(\tau), \tau\right),\\
\gamma^- &:= \gamma^{\eta(s^+\leftarrow s^-)}\left({}^{S^-}\boldsymbol{\alpha}(\tau), {}^{S^-}_{\rightarrow}\boldsymbol{\mu}(\tau), \tau\right),\\
\dot{\boldsymbol{g}}^- &:= D_1\boldsymbol{g}^- \cdot \boldsymbol{f}^- + D_2\boldsymbol{g}^- \cdot \dot{\boldsymbol{\mu}}^- + D_3\boldsymbol{g}^-,\\
\dot{\gamma}^- &:= D_1\gamma^- \cdot \boldsymbol{f}^- + D_2\gamma^- \cdot \dot{\boldsymbol{\mu}}^- + D_3\gamma^-,
\end{aligned}$$

where the $\rightarrow$ *left subscript should be interpreted as* $\searrow$ *or* $\nearrow$ *to indicate whether the feedforward is pushing or withdrawing, respectively.* $\gamma^{\eta(s^+\leftarrow s^-)}$ *is the guard function that is activated during the transition* $s^+ \leftarrow s^-$*. If the transition* $s^+ \leftarrow s^-$ *is associated with multiple guard functions, one of the guard functions can be chosen, as it will have no effect on the jump gain. For example, during the transition* $11 \leftarrow 00$*,* γ^{01} *or* γ^{10} *should be used for defined the jump gain. Finally, the vectors* ${}^{S^k}\boldsymbol{a}$ *and* ${}^{S^k}\boldsymbol{b}$ *in* (4.56) *are given by*

$$
\begin{aligned}
{}^{S^k}\boldsymbol{a} &= -\frac{1}{\dot{\gamma}^-} D_1 \gamma^-, \\
{}^{S^k}\boldsymbol{b} &= -\frac{1}{\dot{\gamma}^-} D_2 \gamma^-.
\end{aligned}
$$

4.3 Summary

An approximation for nonlinear state-and-input-triggered systems with input-dependent guard experiencing simultaneous impacts is presented. Simultaneous guard activations are introduced and the adopted notation required to deal with such activations is presented and elaborated. Assumptions on the reference trajectory are presented, which reduce the complexity of the problem while maintaining practical usability. Then, reference spreading is extended to transitions with simultaneous events. After that, a sensitivity analysis is presented, to find an approximation of the behavior of the NSITHS near $(\boldsymbol{\alpha}, \boldsymbol{\mu})$, where so-called loss of simultaneity occurs. Similar to the result presented in Chapter 3, we presume the approximation being first order, despite the proof not yet being available. A state-and-input dependent jump gain, called the positively homogeneous jump gain, is used to define the positively homogeneous time-triggered hybrid system (PTTHS). The PTTHS is expected to be suitable for assessing the local asymptotic stability of a nonlinear state-and-input triggered hybrid system with simultaneous guard activations.

Chapter 5

Numerical Validation

To take the first steps towards numerically validating the theory presented in this work, a trajectory tracking simulation for mechanical systems with unilateral constraints and spatial friction is presented in this chapter. While progress is made in creating the numerical validation, the reader should be aware that it is not yet complete. More work is required to validate the LTTHS and PTTHS, presented in Chapter 3 and Chapter 4 respectively, in the sense that the example discussed in this chapter does not yet contain state-and-input-dependent guards but merely state-dependent guards, and is modeled without friction. First an example system is given in Section 5.1, which describes the kinematics and dynamics of an RRR-robot opening a door. Then, the tracking behavior of that system is simulated and presented, where in particular the design of a feasible reference trajectory is discussed. The chapter is concluded by a summary.

5.1 A planar 4-DOF system: RRR-robot opening a door

In this section, an example of a mechanical system with unilateral constraints is presented, which will be simulated to validate the theory presented in this work. The system is a robot arm with three revolute joints opening a door, in a planar setting. The forward kinematics and equations of motion for that system will be presented in a concise manner. For a more thorough derivation of the equations of motion, the reader is referred to [70].

5.1.1 Forward kinematics

Let us now consider the system in Figure 5.1. The robot consists of four links, where link 0 is connected to the fixed world and link 3 is a foot-shaped end effector. Link 4 is a door connected to the fixed world with a torsional spring and damper. Coordinate frames are attached to each link, which are referred to as Ψ_0 to Ψ_4. The centers of mass of the links are assumed to be halfway the link, except for the center of mass of link 3. A closer look at link 3 can be seen in Figure 5.2, where the parameters $c_{3,x}$ and $c_{3,y}$ position the center of mass of link 3. Also, two additional coordinate frames Ψ_{3a} and Ψ_{3b} are depicted, which are attached to the contact points defined in the end effector for contact modeling. The set of contact points is given by $\mathcal{I} = \{1, 2\}$, where contact point 1 and 2 are related to coordinate frames Ψ_{3a} and Ψ_{3b} respectively. The set of guard identifiers, which is written in binary form, is given by $\eta = \{01, 10\}$, where γ_{01} is related to contact point 1 and γ^{10} to contact point 2. in The system is modeled without friction and trajectories with releasing motions are not considered. Therefore, the system does not contain input-dependent guard functions.

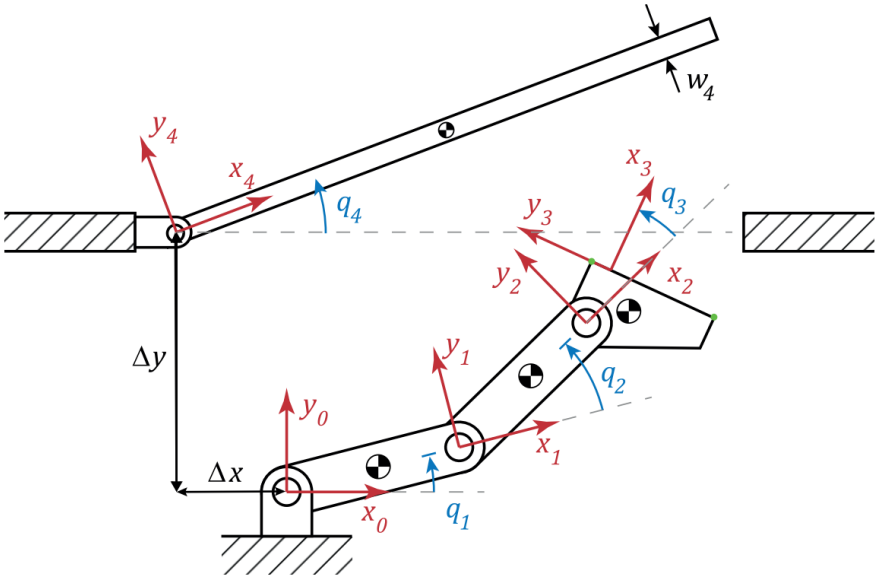

Figure 5.1: *An RRR-robot and a door in top-down view. This 4-DOF planar system is used to numerically validate the theory presented in this work.*

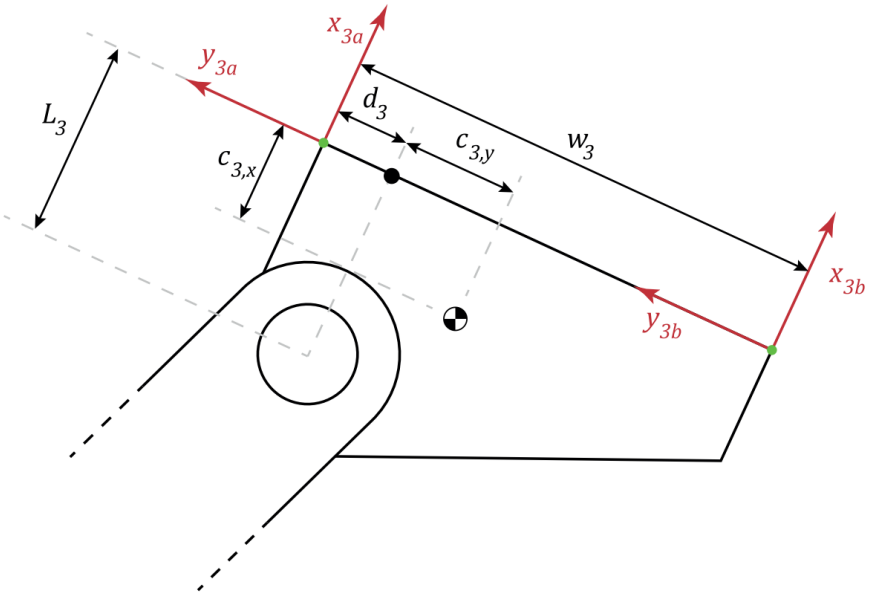

Figure 5.2: *A closer look at the foot of the RRR-robot.*

The generalized coordinates are defined as

$$\boldsymbol{q} := \begin{bmatrix} q_1 \\ q_2 \\ q_3 \\ q_4 \end{bmatrix}, \tag{5.1}$$

where $\boldsymbol{q}_i$ is the angular displacement related to the i-th link, as illustrated in Figure 5.1. The state of the system is then defined as

$$\boldsymbol{x} := \begin{bmatrix} \boldsymbol{q} \\ \dot{\boldsymbol{q}} \end{bmatrix}. \tag{5.2}$$

The forward kinematics of the system are now described using homogeneous transformation matrices $\boldsymbol{H}_b^a$, where $\boldsymbol{H}_b^a$ relates coordinate frame Ψ_b to coordinate frame Ψ_a. Since the system is in a planar setting, the transformation matrices are in the Special Euclidean group SE(2), i.e., $\boldsymbol{H}_b^a \in \mathrm{SE}(2)$. The transformation matrices that relate all coordinate frames to coordinate frame Ψ_0 are given by

$$\boldsymbol{H}_1^0 = \begin{bmatrix} \cos(q_1) & -\sin(q_1) & L_1\cos(q_1) \\ \sin(q_1) & \cos(q_1) & L_1\sin(q_1) \\ 0 & 0 & 1 \end{bmatrix}, \tag{5.3}$$

$$\boldsymbol{H}_2^0 = \begin{bmatrix} \cos(q_1+q_2) & -\sin(q_1+q_2) & L_1\cos(q_1)+L_2\cos(q_1+q_2) \\ -\sin(q_1+q_2) & \cos(q_1+q_2) & L_1\sin(q_1)+L_2\sin(q_1+q_2) \\ 0 & 0 & 1 \end{bmatrix}, \tag{5.4}$$

$$\boldsymbol{H}_3^0 = \begin{bmatrix} \cos(q_1+q_2+q_3) & -\sin(q_1+q_2+q_3) & L_1\cos(q_1)+L_2\cos(q_1+q_2)+L_3\cos(q_1+q_2+q_3) \\ -\sin(q_1+q_2+q_3) & \cos(q_1+q_2+q_3) & L_1\sin(q_1)+L_2\sin(q_1+q_2)+L_3\sin(q_1+q_2+q_3) \\ 0 & 0 & 1 \end{bmatrix}, \tag{5.5}$$

$$\boldsymbol{H}_4^0 = \begin{bmatrix} \cos(q_4) & -\sin(q_4) & -\Delta x \\ \sin(q_4) & \cos(q_4) & \Delta y \\ 0 & 0 & 1 \end{bmatrix}, \tag{5.6}$$

$$\boldsymbol{H}_{3a}^3 = \begin{bmatrix} 1 & 0 & 0 \\ 0 & 1 & d_3 \\ 0 & 0 & 1 \end{bmatrix}, \tag{5.7}$$

$$\boldsymbol{H}_{3b}^3 = \begin{bmatrix} 1 & 0 & 0 \\ 0 & 1 & -w_3+d_3 \\ 0 & 0 & 1 \end{bmatrix}. \tag{5.8}$$

We now denote x and y the coordinates of frame Ψ_3 with respect to frame Ψ_0 in x_0 and y_0 direction respectively. We denote θ the rotation of Ψ_3 with respect to frame Ψ_0, where a positive rotation is in counterclockwise direction. The configuration of the end effector, i.e. of frame Ψ_3, can be obtained from (5.5) as

$$\boldsymbol{Y} := \begin{bmatrix} x \\ y \\ \theta \end{bmatrix} = \begin{bmatrix} L_1\cos(q_1)+L_2\cos(q_1+q_2)+L_3\cos(q_1+q_2+q_3) \\ L_1\sin(q_1)+L_2\sin(q_1+q_2)+L_3\sin(q_1+q_2+q_3) \\ q_1+q_2+q_3 \end{bmatrix}. \tag{5.9}$$

Since we will be considering a trajectory where the end effector makes impact with the door, the guard function associated with a open-to-closed transition, presented in Section 2.3.3, should be

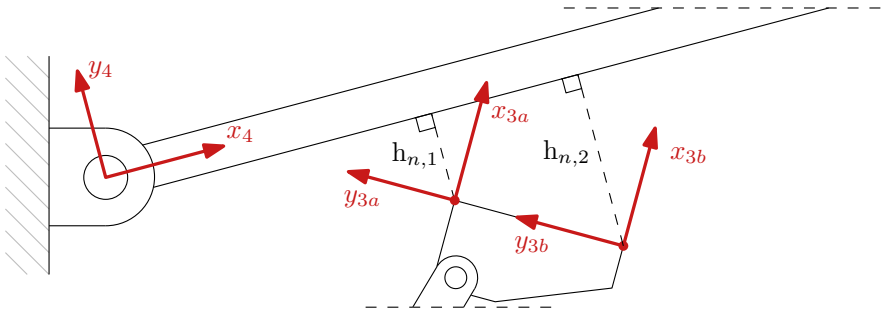

Figure 5.3: *The contact distances* $\mathrm{h}_{n,1}$ *and* $\mathrm{h}_{n,2}$ *related to contact point 1 and 2.*

evaluated. Therefore, the guard functions corresponding with contact point 1 and 2 are given by

$$\gamma^{01} = \mathrm{h}_{n,1}(\boldsymbol{q}) = \begin{bmatrix} 0 & -1 & 0 \end{bmatrix} \boldsymbol{H}_0^4 \boldsymbol{H}_3^0 \boldsymbol{H}_{3a}^3 \begin{bmatrix} 0 \\ 0 \\ 1 \end{bmatrix} - \frac{1}{2} w_4, \tag{5.10}$$

$$\begin{aligned} &= \Delta x \sin(q_4) + \Delta y \cos(q_4) - L_1 \sin(q_1 - q_4) - L_2 \sin(q_1 + q_2 - q_4) \\ &\quad - L_3 \sin(q_1 + q_2 + q_3 - q_4) - d_3 \cos(q_1 + q_2 + q_3 - q_4) - \frac{1}{2} w_4, \end{aligned} \tag{5.11}$$

$$\gamma^{10} = \mathrm{h}_{n,2}(\boldsymbol{q}) = \begin{bmatrix} 0 & -1 & 0 \end{bmatrix} \boldsymbol{H}_0^4 \boldsymbol{H}_3^0 \boldsymbol{H}_{3b}^3 \begin{bmatrix} 0 \\ 0 \\ 1 \end{bmatrix} - \frac{1}{2} w_4, \tag{5.12}$$

$$\begin{aligned} &= \Delta x \sin(q_4) + \Delta y \cos(q_4) - L_1 \sin(q_1 - q_4) - L_2 \sin(q_1 + q_2 - q_4) \\ &\quad - L_3 \sin(q_1 + q_2 + q_3 - q_4) - d_3 \cos(q_1 + q_2 + q_3 - q_4) + w_3 \cos(q_1 + q_2 + q_3 - q_4) \\ &\quad - \frac{1}{2} w_4, \end{aligned} \tag{5.13}$$

respectively. These contact distances are illustrated in Figure 5.3.

5.1.2 Equations of motion

The equations of motion of the system are now presented. Since this chapter is work in progress, the system is modeled without friction. The unilateral constraints are modeled as bilateral for simplicity, and are checked for feasibility during simulation. With $\boldsymbol{\nu} := \boldsymbol{q}$ almost everywhere, the continuous dynamics of the system are given by

$$\boldsymbol{M}(\boldsymbol{q})\dot{\boldsymbol{\nu}} + \boldsymbol{C}(\boldsymbol{q}, \boldsymbol{\nu}) = \boldsymbol{S}\boldsymbol{u} + \sum_{\iota \in \mathcal{I}_{\mathrm{cl}}} \boldsymbol{w}_{n,\iota}(\boldsymbol{q}) \lambda_{n,\iota}, \qquad \forall \iota \in \mathcal{I}, \tag{5.14}$$

$$0 \leq \mathrm{h}_{n,\iota} \perp \lambda_{n,\iota} \geq 0, \tag{5.15}$$

with

$$\mathrm{h}_{n,\iota} := \mathrm{h}_{n,\iota}(\boldsymbol{q}), \tag{5.16}$$

The discrete dynamics are given by

$$\boldsymbol{M}(\boldsymbol{q})(\boldsymbol{\nu}^+ - \boldsymbol{\nu}^-) = \sum_{\iota \in \mathcal{I}_{\mathrm{cl}}} \boldsymbol{w}_{n,\iota}(\boldsymbol{q}) \Lambda_{n,\iota} + \boldsymbol{W}_{t,\iota}(\boldsymbol{q}) \boldsymbol{\Lambda}_{t,\iota}, \tag{5.17}$$

$$0 \leq \mathrm{v}_{n,\iota}^+ \perp \Lambda_{n,\iota} \geq 0, \qquad \forall \iota \in \mathcal{I}_{\mathrm{cl}}, \tag{5.18}$$

with

$$\mathrm{v}_{n,\iota}^{+}(\boldsymbol{q}) := \boldsymbol{w}_{n,\iota}^{T}(\boldsymbol{q})\boldsymbol{\nu}^{+}. \tag{5.19}$$

The mass matrix $\boldsymbol{M}(\boldsymbol{q})$ is given by

$$\boldsymbol{M} = \begin{bmatrix} M_{11} & M_{12} & M_{13} & 0 \\ M_{12} & M_{22} & M_{23} & 0 \\ M_{13} & M_{23} & M_{33} & 0 \\ 0 & 0 & 0 & \bar{I}_4 \end{bmatrix}, \tag{5.20}$$

with

$$\begin{aligned}
M_{11} &= \bar{I}_1 + \bar{I}_2 + \bar{I}_3 + 2L_1(L_3 - c_{3,x})m_3\cos(q_2+q_3) + 2L_1c_{3,y}m_3\sin(q_2+q_3) + L_1L_2(m_2+2m_3)\cos(q_2) \\
&\quad + 2L_2(L_3 - c_{3,x})m_3\cos(q_3) + 2L_2c_{3,y}m_3\sin(q_3), \\
M_{12} &= \bar{I}_2 + \bar{I}_3 + L_1(L_3 - c_{3,x})m_3\cos(q_2+q_3) + L_1c_{3,y}m_3\sin(q_2+q_3) + \frac{1}{2}L_1L_2(m_2+2m_3)\cos(q_2) \\
&\quad + 2L_2(L_3 - c_{3,x})m_3\cos(q_3) + 2L_2c_{3,y}m_3\sin(q_3) \\
M_{13} &= \bar{I}_3 + L_1(L_3 - c_{3,x})m_3\cos(q_2+q_3) + L_1c_{3,y}m_3\sin(q_2+q_3) + L_2(L_3 - c_{3,x})m_3\cos(q_3) \\
&\quad + L_2c_{3,y}m_3\sin(q_3), \\
M_{22} &= \bar{I}_2 + \bar{I}_3 + 2L_2(L_3 - c_{3,x})m_3\cos(q_3) + 2L_2c_{3,y}m_3\sin(q_3), \\
M_{23} &= \bar{I}_3 + L_2(L_3 - c_{3,x})m_3\cos(q_3) + L_2c_{3,y}m_3\sin(q_3), \\
M_{33} &= \bar{I}_3, \\
\bar{I}_1 &= I_1 + (\frac{1}{4}m_1 + m_2 + m_3)L_1^2, \\
\bar{I}_2 &= I_2 + (\frac{1}{4}m_2 + m_3)L_2^2, \\
\bar{I}_3 &= I_3 + m_3\left((L_3 - c_{3,x})^2 + c_{3,y}^2\right),
\end{aligned}$$

where m_1, m_2, m_3 are the masses of link 1 to 3, and I_1, I_2, I_3 are the mass moment of inertia of link 1 to 3. The spring forces, damper forces, and centripetal forces form the generalized forces vector, which is given by

$$\boldsymbol{C} = \begin{bmatrix} C_1 \\ C_2 \\ C_3 \\ C_4 \end{bmatrix}, \tag{5.21}$$

with

$$\begin{aligned}
C_1 &= -\frac{1}{2}L_1L_2(m_2+2m_3)\left(\dot{q}_2^2 + 2\dot{q}_1\dot{q}_2\right)\sin(q_2) + L_1e(q_2+q_3)\left((\dot{q}_1+\dot{q}_2+\dot{q}_2)^2 - \dot{q}_1^2\right) \\
&\quad + L_2e(q_3)\left(\dot{q}_3^2 + 2\dot{q}_1\dot{q}_3 + 2\dot{q}_2\dot{q}_3\right), \\
C_2 &= \frac{1}{2}L_1L_2(m_2+2m_3)\sin(q_2) - L_1e(q_2+q_3)\dot{q}_1^2 + L_2e(q_3)\left(\dot{q}_3^2 + 2\dot{q}_1\dot{q}_3 + 2\dot{q}_2\dot{q}_3\right), \\
C_3 &= -L_1e(q_2+q_3)\dot{q}_1^2 - L_2e(q_3)(\dot{q}_1+\dot{q}_2)^2, \\
C_4 &= c_d\dot{q}_4 + c_kq_4,
\end{aligned}$$

where

$$e(q) = m_3\left(c_{3,y}\cos(q) - (L_3 - c_{3,x})\sin(q)\right).$$

The selection matrix is $\boldsymbol{S} = \begin{bmatrix}\boldsymbol{I}_3 & \boldsymbol{0}_{3\times 1}\end{bmatrix}$. Finally, the jacobians $\boldsymbol{w}_{n,1}^T$ and $\boldsymbol{w}_{n,2}^T$ are defined by $\dot{\mathrm{h}}_{n,1} = \boldsymbol{w}_{n,1}^T\dot{\boldsymbol{q}}$ and $\dot{\mathrm{h}}_{n,2} = \boldsymbol{w}_{n,2}^T\dot{\boldsymbol{q}}$, which give

$$\boldsymbol{w}_{n,1} = \begin{bmatrix} a(\boldsymbol{q}) + b(\boldsymbol{q}) + c(\boldsymbol{q}) + d(\boldsymbol{q}) \\ b(\boldsymbol{q}) + c(\boldsymbol{q}) + d(\boldsymbol{q}) \\ c(\boldsymbol{q}) + d(\boldsymbol{q}) \\ -a(\boldsymbol{q}) - b(\boldsymbol{q}) - c(\boldsymbol{q}) - d(\boldsymbol{q}) + \Delta x\cos(q_4) - \Delta y\sin(q_4) \end{bmatrix}, \tag{5.22}$$

$$\boldsymbol{w}_{n,2} = \begin{bmatrix} a(\boldsymbol{q}) + b(\boldsymbol{q}) + c(\boldsymbol{q}) + d(\boldsymbol{q}) - w_3\sin(q_1+q_2+q_3-q_4) \\ b(\boldsymbol{q}) + c(\boldsymbol{q}) + d(\boldsymbol{q}) - w_3\sin(q_1+q_2+q_3-q_4) \\ c(\boldsymbol{q}) + d(\boldsymbol{q}) - w_3\sin(q_1+q_2+q_3-q_4) \\ -a(\boldsymbol{q}) - b(\boldsymbol{q}) - c(\boldsymbol{q}) - d(\boldsymbol{q}) + \Delta x\cos(q_4) - \Delta y\sin(q_4) + w_3\sin(q_1+q_2+q_3-q_4) \end{bmatrix}, \tag{5.23}$$

with

$$\begin{aligned} a(\boldsymbol{q}) &= -L_1\cos(q_1 - q_4), \\ b(\boldsymbol{q}) &= -L_2\cos(q_1 + q_2 - q_4), \\ c(\boldsymbol{q}) &= -L_3\cos(q_1 + q_2 + q_3 - q_4), \\ d(\boldsymbol{q}) &= d_3\sin(q_1 + q_2 + q_3 - q_4). \end{aligned}$$

The kinematics presented in Section 5.1.1 and the dynamics presented in this section are first derived in [70]. For a more thorough derivation of the kinematics and dynamics, the reader is referred to that work. In the next section a tracking simulation for the example system is simulated and discussed.

5.2 Trajectory tracking with simultaneous impact

Using the system presented in Section 5.1, the results of the trajectory tracking simulation will be discussed in this section. The considered reference trajectory contains a simultaneous impact between the two contact points and the door. First, the design of the reference trajectory will be discussed, where the resulting reference trajectory satisfies the assumptions posed in this work. Then, the simulation results are presented. Here the tracking behavior around the reference trajectory with simultaneous impacts is discussed, and the benefits of the reference spreading error are illustrated. The simulations presented in this section are performed using MATLAB and a hybrid systems toolbox written by the author of [59].

5.2.1 Reference trajectory design

To design the reference trajectory, a Hermite interpolation is used to interpolate between the desired initial state and input and the desired final state and input. The Hermite interpolation makes use of the quintic polynomial functions

$$y(t) = a_0 + a_1 t + a_2 t^2 + a_3 t^3 + a^4 t^4 + a_5 t^5, \tag{5.24}$$

$$\dot{y}(t) = a_1 + 2a_2 t + 3a_3 t^2 + 4a^4 t^3 + 5a_5 t^4, \tag{5.25}$$

$$\ddot{y}(t) = 2a_2 + 6a_3 t + 12a^4 t^2 + 20a_5 t^3, \tag{5.26}$$

where the coefficients of the polynomial a_0 to a_5 are determined by the system

$$\begin{bmatrix} 1 & t_0 & t_0^2 & t_0^3 & t_0^4 & t_0^5 \\ 0 & 1 & 2\,t_0 & 3\,t_0^2 & 4\,t_0^3 & 5\,t_0^4 \\ 0 & 0 & 2 & 6\,t_0 & 12\,t_0^2 & 20\,t_0^3 \\ 1 & t_f & t_f^2 & t_f^3 & t_f^4 & t_f^5 \\ 0 & 1 & 2\,t_f & 3\,t_f^2 & 4\,t_f^3 & 5\,t_f^4 \\ 0 & 0 & 2 & 6\,t_f & 12\,t_f^2 & 20\,t_f^3 \end{bmatrix} \begin{bmatrix} a_0 \\ a_1 \\ a_2 \\ a_3 \\ a_4 \\ a_5 \end{bmatrix} = \begin{bmatrix} y_0 \\ \dot{y}_0 \\ \ddot{y}_0 \\ y_f \\ \dot{y}_f \\ \ddot{y}_f \end{bmatrix}. \tag{5.27}$$

Here t_0 and t_f are the start- and end-time of the trajectory segment, respectively, y_0, $\dot{y}_0$, and $\ddot{y}_0$ the position, velocity and acceleration at the start of the trajectory segment, and y_f, $\dot{y}_f$, and $\ddot{y}_f$ the position, velocity and acceleration at the end of the trajectory segment.

The Hermite interpolation is now used to define a reference trajectory. The reference is defined on task level, i.e., the configuration of the end effector $\boldsymbol{Y}$ is prescribed. Three event times are introduced: $\tau_0 = 0$ is initial time of the reference, $\tau_1 = 1$ is the event time of the simultaneous impact, and $\tau_2 = \tau_f = 2$ is the final time of the reference. The ante-event segment of the reference, $t \in [\tau_0, \tau_1]$, has the initial and final conditions

$$\begin{array}{llllll} x_0 = 0.650 & x_1^- = 0.433 & y_0 = 0 & y_1^- = 0.280 & \theta_0 = \pi/5 & \theta_1^- = \pi/2 \\ \dot{x}_0 = 0 & \dot{x}_1^- = -0.250 & \dot{y}_0 = 0 & \dot{y}_1^- = 0.350 & \dot{\theta}_0 = 0 & \dot{\theta}_1^- = 0 \\ \ddot{x}_0 = 0 & \ddot{x}_1^- = -0.700 & \ddot{y}_0 = 0 & \ddot{y}_1^- = 2 & \ddot{\theta}_0 = 0 & \ddot{\theta}_1^- = 0 \end{array} \tag{5.28}$$

Note that we only define the left limits for $t = t_1$, because the right limits are defined by the discrete dynamics (5.17)-(5.18). During the design of the ante-event segment, we assume the door to be closed, i.e., $q_4 = \dot{q}_4 = \ddot{q}_4$ for all $t \in [\tau_0, \tau_1]$. The conditions (5.28) define the trajectory for $t \in [\tau_0, \tau_1]$ using the hermite interpolation (5.27). This trajectory is now extended, where the final conditions of the left extension are

$$\begin{array}{lll} x_{\text{ext}}^- = 0.353 & y_{\text{ext}}^- = 0.400 & \theta_{\text{ext}}^- = \pi/2 \\ \dot{x}_{\text{ext}}^- = -0.580 & \dot{y}_{\text{ext}}^- = 0.830 & \dot{\theta}_{\text{ext}}^- = 0 \\ \ddot{x}_{\text{ext}}^- = -0.700 & \ddot{y}_{\text{ext}}^- = 2 & \ddot{\theta}_{\text{ext}}^- = 0 \end{array} \tag{5.29}$$

These conditions result in the trajectories illustrated in Figure 5.4. The post-event segment of the trajectory is now designed in a similar fashion. Since the end-effector is constrained to the door during the post-event trajectory, $\mathrm{h}_{n,1} = \mathrm{h}_{n,2} = 0$ (and their derivatives as well). Because of these constraints, a state reduction can be applied. The initial and final conditions for the post-event segment are

$$\begin{array}{llll} (o_{3,x}^4)_{\text{ext}}^+ = 0.650 & (o_{3,x}^4)_2 = 0.433 & (q_4)_{\text{ext}}^+ = 0 & (q_4)_2 = 0.280 \\ (\dot{o}_{3,x}^4)_{\text{ext}}^+ = 0 & (\dot{o}_{3,x}^4)_2 = -0.250 & (\dot{q}_4)_{\text{ext}}^+ = 0 & (\dot{q}_4)_2 = 0.350 \\ (\ddot{o}_{3,x}^4)_{\text{ext}}^+ = 0 & (\ddot{o}_{3,x}^4)_2 = -0.700 & (\ddot{q}_4)_{\text{ext}}^+ = 0 & (\ddot{q}_4)_2 = 2 \end{array} \tag{5.30}$$

where $o_{3,x}^4$ is the position of the Ψ_3 frame in the x-direction of frame Ψ_4, that is the position of the end effector along the door. The conditions in (5.30) are used instead of $\boldsymbol{Y}$, for a more intuitive design process of the trajectory. The super- and subscript $(\cdot)_e x t^+$ indicates the initial condition of the trajectory extension, and the subscript $(\cdot)_2$ indicates the final condition of the post-event trajectory. The post-event reference trajectory resulting from (5.30) is illustrated in Figure 5.4. The entire reference trajectory shown in Figure 5.4 satisfies the assumptions applicable to the reference, specifically:

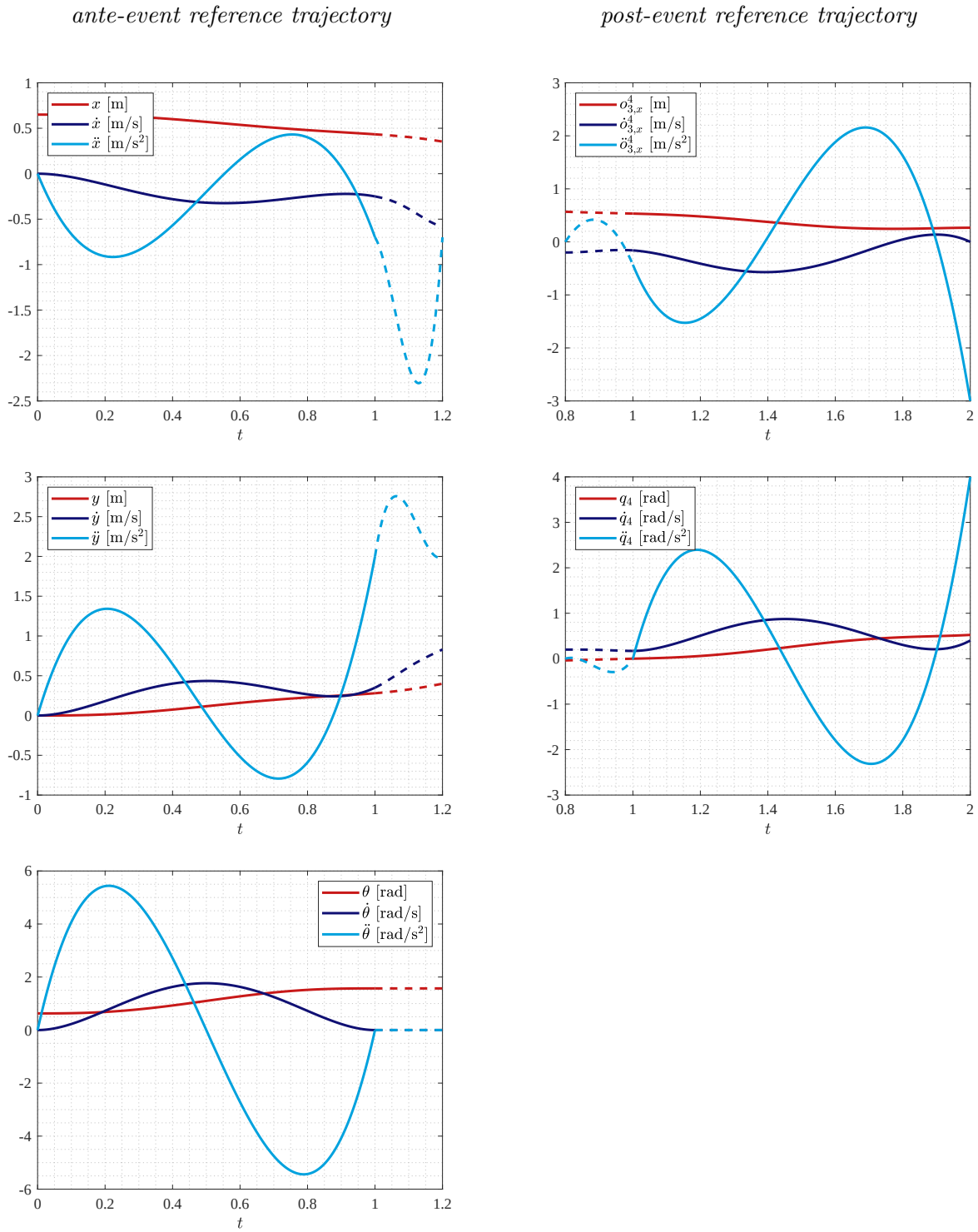

Figure 5.4: *The reference trajectory for $t \in [\tau_0, \tau_2]$. On the left is the ante-event reference trajectory, with in the left-top image x, $\dot{x}$, $\ddot{x}$, the left-middle image y, $\dot{y}$, $\ddot{y}$, and in the left-bottom image θ, $\dot{\theta}$, $\ddot{\theta}$. On the right is the post-event reference trajectory, with in the right-top image $o^4_{3,x}$, $\dot{o}^4_{3,x}$, $\ddot{o}^4_{3,x}$, and in the right-middle image q_4, $\dot{q}_4$, $\ddot{q}_4$. The dashed lines indicate the extensions past τ_1.*

- Assumption 4 (*Transversal guard activations*).

- Assumption 7 (*Growing mode sequences*).
- Assumption 8 (*Guard-transition association*).

Guard-transition association is straightforward in this case, as we only consider position dependent guard functions in this example. We achieve transversality of the guard activations in the reference trajectory by choosing $\dot{y}_1^- > 0$, as can be observed in (5.28).

Since the unilateral constraints are modeled as bilateral constraints, the simulation will return pulling reaction forces when a release occurs. Therefore, to make sure that the mode sequences are growing, the ante-event velocity $\dot{\boldsymbol{q}}^-$ should be chosen in such a way that the impulsive dynamics result in feasible impulsive reaction forces $\Lambda_{n,1}$ and $\Lambda_{n,2}$, i.e., $\Lambda_{n,1} > 0$ and $\Lambda_{n,2} > 0$ for $t = \tau_1$. Also, since we don't want any releases after the event takes place, the post-event accelerations for $t \in [\tau_1, \tau_2]$ should be chosen in such a way, that the post-event reaction forces $\lambda_{n,1}$ and $\lambda_{n,2}$ are feasible as well. Thus, we should also check that $\lambda_{n,1} > 0$ and $\lambda_{n,2} > 0$ for $t \in [\tau_1, \tau_2]$. Since we are interested in tracking the designed reference, the trajectories close to $\boldsymbol{\alpha}$ should also satisfy the conditions mentioned above.

The reference trajectory plotted in Figure 5.4 is found by trial and error, where we keep track of both the impulsive reaction forces $\Lambda_{n,1}$ and $\Lambda_{n,2}$, as well as the continuous reaction forces $\lambda_{n,1}$ and $\lambda_{n,2}$. The reference trajectory generates the impulsive event described in Table 5.1, and the continuous reaction forces plotted in Figure 5.5. Here we observe that both the impulsive event and the post-event trajectory are feasible.

Table 5.1: *Properties of the simultaneous event in the reference trajectory* $(\boldsymbol{\alpha}, \boldsymbol{\mu})$.

i	$s_{i-1} \to s_i$	τ^i [s]	$\Lambda_{n,1}$ [Ns]	$\Lambda_{n,2}$ [Ns]
1	$00 \to 11$	1.0000	1.2572	0.3410

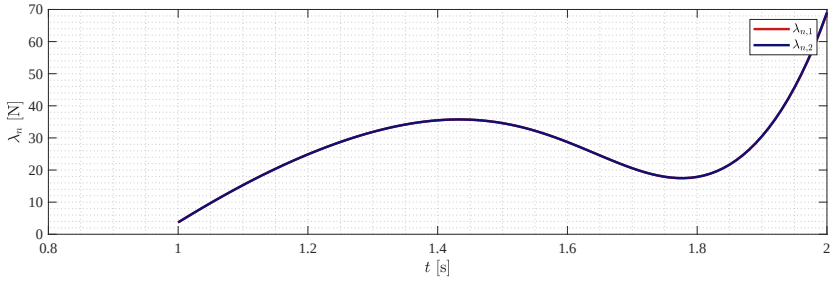

Figure 5.5: *The reaction forces* $\lambda_{n,1}$ *and* $\lambda_{n,2}$ *of the reference trajectory* $\boldsymbol{\alpha}$ *for* $t \in [\tau_1, \tau_2]$.

During the design of the trajectory, some parameters proved to be particularly influential on the feasibility of the trajectory. When considering the impulsive event, the ante-event velocities $\dot{\boldsymbol{q}}^-$ should be chosen in such a way that the impulsive dynamics generate feasible reaction forces. Besides the ante-event velocities in the reference trajectory, the feasibility of the impulsive event is mainly governed by the mass distribution of the system. The positions of the centers of mass, and the weights of the links and end-effector have a significant effect on the impulsive reaction forces. The design of the system can therefore make it easier to find feasible impacts.

Considering the post-event trajectory, the input $\boldsymbol{\mu}$ for $t \in [\tau_1, \tau_2]$ should be chosen in such a way that the reaction forces remain positive. Particularly the inputs close to the event should be chosen carefully. The quintic polynomial shape functions used to define the reference trajectory provide

little control over the evolution of the accelerations $\ddot{\boldsymbol{q}}$, and therefore the inputs $\boldsymbol{\mu}$. Higher order shape functions, that also allow to specify the jerks $\dddot{\boldsymbol{q}}$ of the system, can prove beneficial. Also, since we used exact inverse dynamics to relate the end effector configuration $\boldsymbol{Y}$ to the joint space configuration $\boldsymbol{q}$, the design space of the accelerations is limited. More freedom can be achieved by using loose inverse dynamics, e.g., a QP solver, making the design process of the acceleration profile more intuitive.

5.2.2 Simulation results

A trajectory tracking simulation is performed with the system presented in Section 5.1. First, the system performing the reference trajectory $(\boldsymbol{\alpha}, \boldsymbol{\mu})$ will be shown and discussed. After that, an initial state-and-input perturbation is introduced in the system and the tracking of the reference trajectory is presented.

The reference trajectory defined in task space is now transformed to the state reference $\boldsymbol{\alpha}$, defined in joint space. The reference is simulated, and the result is plotted in Figure 5.6, with its corresponding feedforward $\boldsymbol{\mu}$ plotted in Figure 5.7. In Figure 5.6 we notice the nonsmoothness in the position $\boldsymbol{q}$ and the jump in the velocity $\dot{\boldsymbol{q}}$ at $t = \tau_1 = 1$. The system only enters two different modes, indicated by the bars 0 and 1 above the plots. The ante-event segment 0 in dark blue indicates that both contact points are not in contact, and the post-event segment 1 in light blue indicates that both contact points are in contact. Snapshots of the system performing the reference trajectory can be seen in Appendix D.

Now an initial state-and-input perturbation is introduced into the system. The initial state of the perturbed system is given by

$$\boldsymbol{x}_0^\epsilon = \boldsymbol{\alpha}_0(0) + \epsilon \boldsymbol{z}_0(0), \tag{5.31}$$

where $\epsilon \boldsymbol{z}_0$ is a vector that perturbs the initial state and input. The input of the perturbed trajectory is chosen to be

$$\boldsymbol{u} = {}_{\searrow}\boldsymbol{\mu} + \boldsymbol{K}_i(\boldsymbol{x}^\epsilon - \bar{\boldsymbol{\alpha}}), \tag{5.32}$$

with ${}_{\searrow}\boldsymbol{\mu}$ indicating a pushing sequence feedforward and $\boldsymbol{K}_i$ indicating the feedback gain, where we use $\boldsymbol{K}_1$ in the ante-event segment and $\boldsymbol{K}_2$ in the post-event segment. We now simulate the tracking behavior of the system, choosing a particular perturbation $\epsilon \boldsymbol{z}_0(0)$ and feedback gains K_i. The perturbation and feedback gains are chosen as

$$\epsilon \boldsymbol{z}_0(0) = \begin{bmatrix} -0.05 & -0.03 & -0.02 & 0 & -0.02 & -0.05 & 0.03 & 0 \end{bmatrix}, \tag{5.33}$$

$$\boldsymbol{K}_1 = \begin{bmatrix} 8 & 0 & 0 & 0 & 16 & 0 & 0 & 0 \\ 0 & 8 & 0 & 0 & 0 & 16 & 0 & 0 \\ 0 & 0 & 8 & 0 & 0 & 0 & 16 & 0 \end{bmatrix}, \tag{5.34}$$

$$\boldsymbol{K}_2 = \begin{bmatrix} 100 & 0 & 0 & 0 & 20 & 0 & 0 & 0 \\ 0 & 100 & 0 & 0 & 0 & 20 & 0 & 0 \\ 0 & 0 & 0 & 0 & 0 & 0 & 0 & 0 \end{bmatrix}. \tag{5.35}$$

This results in the tracking behavior plotted in Figure 5.8 and input plotted in Figure 5.9. It can be noticed that another mode is present in the trajectory. The ante-event mode is indicated by segment 0, the post-event mode is indicated by segment 2, and close to the impact time the micro-segment 1 can be observed. This is the loss of simultaneity that occurs as a result of the perturbation. Snapshots of the system tracking the reference trajectory can be seen in Appendix D.

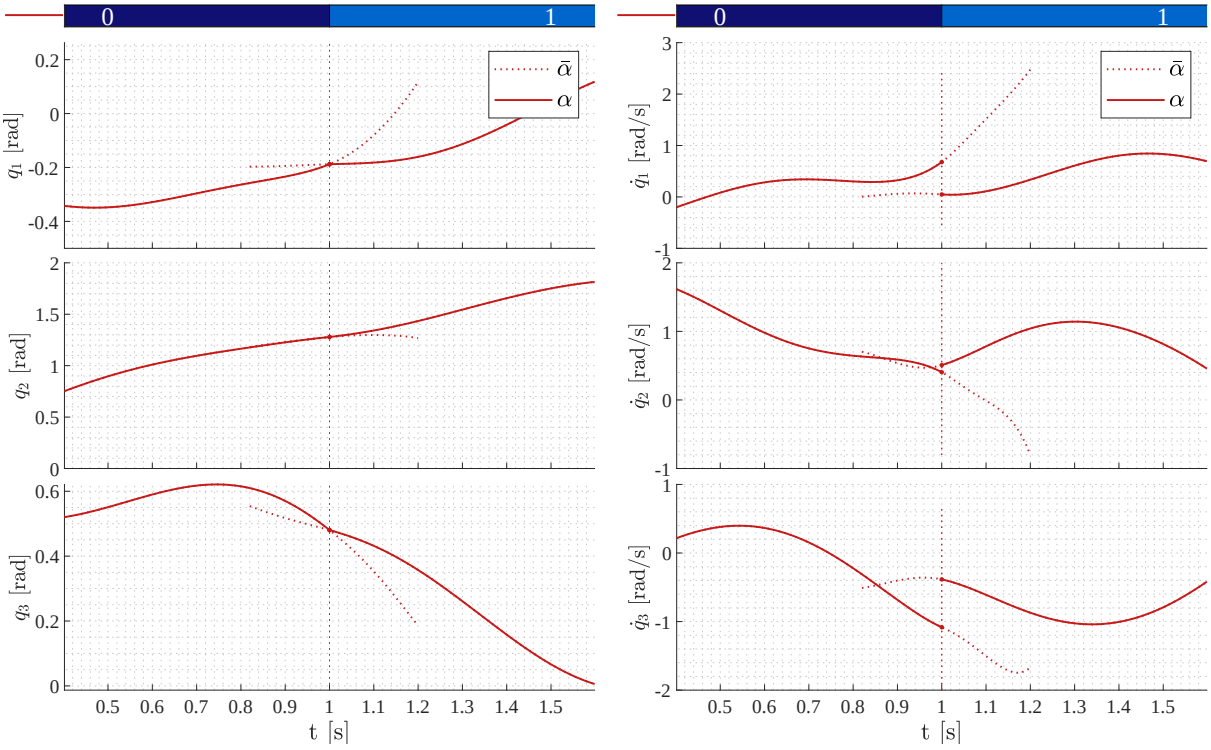

Figure 5.6: *The reference trajectory* $\boldsymbol{\alpha}$*, which is generated from the trajectory shown in Figure 5.4.*

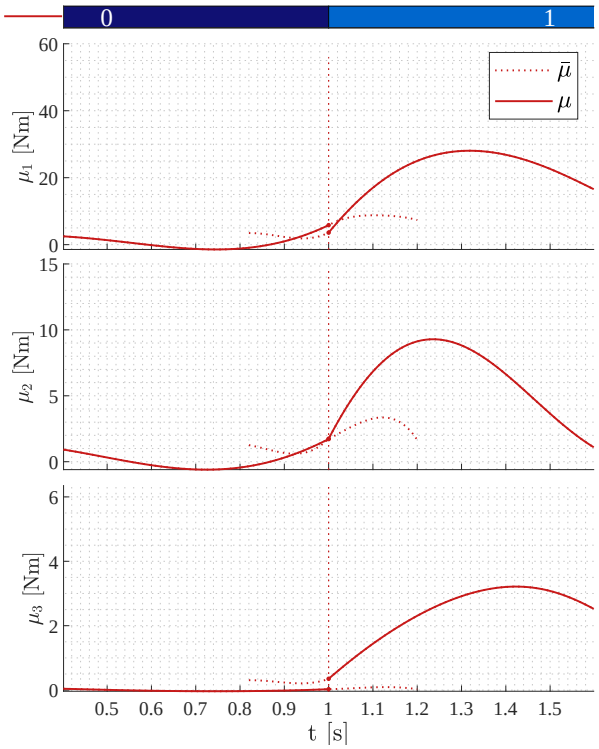

Figure 5.7: *The feedforward* $\boldsymbol{\mu}$ *used to generate* $\boldsymbol{\alpha}$ *shown in Figure 5.6.*

To consider the feasibility of the trajectory, we evaluate the generated reaction forces. First the

two micro-events are considered. The properties of these micro-events are presented in Table 5.2. Notice that for both events $\Lambda_{n,1} \geq 0$ and $\Lambda_{n,2} \geq 0$, meaning that they are feasible.

Table 5.2: *Properties of the micro-events in the perturbed trajectory* $(\boldsymbol{x}^\epsilon, \boldsymbol{u})$.

k	$s^{k-1} \to s^k$	t^k [s]	$\Lambda_{n,1}$ [Ns]	$\Lambda_{n,2}$ [Ns]
1	$00 \to 01$	1.0389	1.2273	0
2	$01 \to 11$	1.0488	0.5247	0.4442

We now evaluate the post-event state, by checking whether $\lambda_{n,1} \geq 0$ and $\lambda_{n,2} \geq 0$ for $t \in [t^1, \tau_2]$, where t^k is the event time of the k-th micro-event. The reaction forces $\lambda_{n,1}$ and $\lambda_{n,2}$ are plotted in Figure 5.10. Here we see that for all $t \in [t^1, \tau_2]$, $\lambda_{n,1} > 0$ and $\lambda_{n,2} > 0$, meaning that also the post-event trajectory is feasible.

5.3 Summary

This chapter discusses the first steps made towards a numerical validation of the theory presented in this work. First, an example system is presented, in the form of an RRR-robot opening a door. While the system can readily be extended to input-dependent guard functions and spatial friction, this example is modeled without these extensions. For this example, the trajectory tracking behavior of a trajectory with simultaneous impacts is discussed. The design of the reference trajectory is presented, and since finding a feasible trajectory turned out not straightforward, insights are given on the key facets of finding a feasibly trajectory. Our aim is to develop these insights into an algorithm or rule of thumb, suitable to straightforwardly finding a feasible reference trajectory with simultaneous impacts. Finally, the simulation results are shown for the feasible trajectory that was found in this chapter. The simulations performed in this chapter do not validate the theory presented in this work. First the example system should be extended with the modeling of spatial friction, and adding releasing motions to the considered trajectories. Then, the LTTHS and PTTHS associated with the NSITHS should be defined for the example system, and compared to the tracking trajectories for both isolated and simultaneous events. One can then numerically validate whether the approximations generated by the LTTHS and PTTHS are indeed first order.

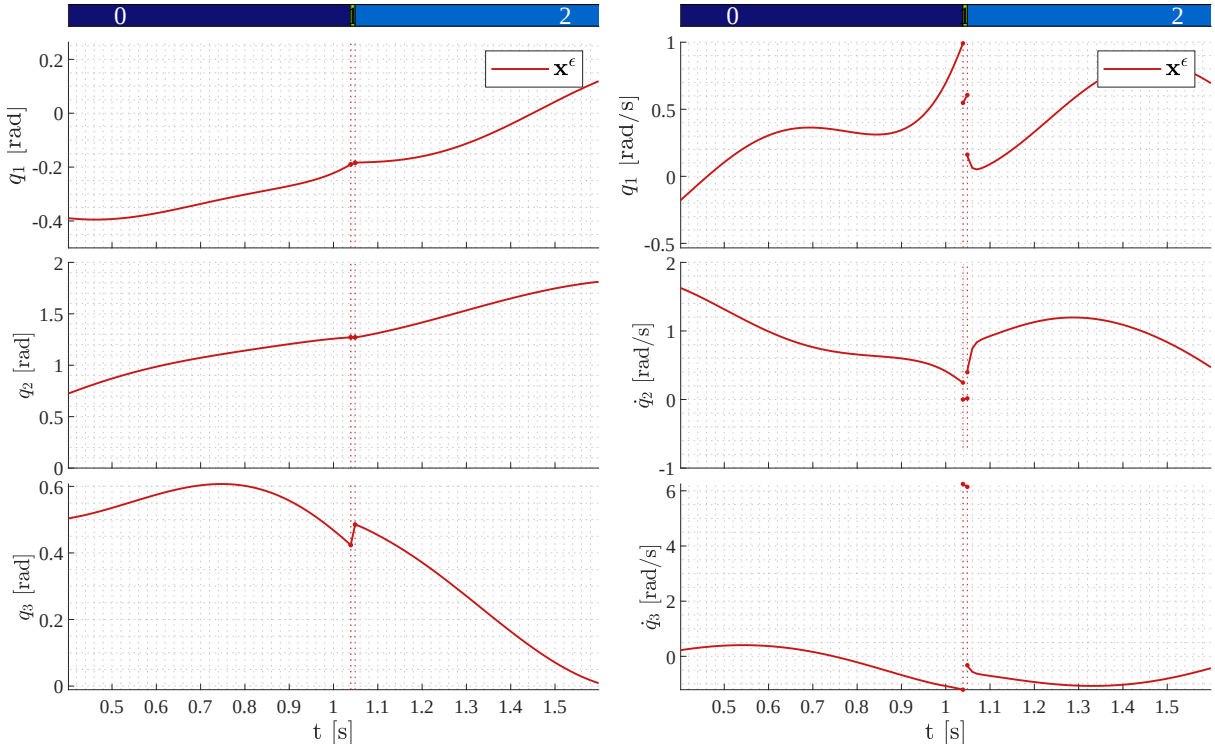

Figure 5.8: *The tracking trajectory $\boldsymbol{x}$ with initial state-and-input perturbation $\epsilon \boldsymbol{z}_0$, which is generated by tracking the reference trajectory $\boldsymbol{\alpha}$ with feedback gains K_1 for the ante-event state and K_2 for the post-event state.*

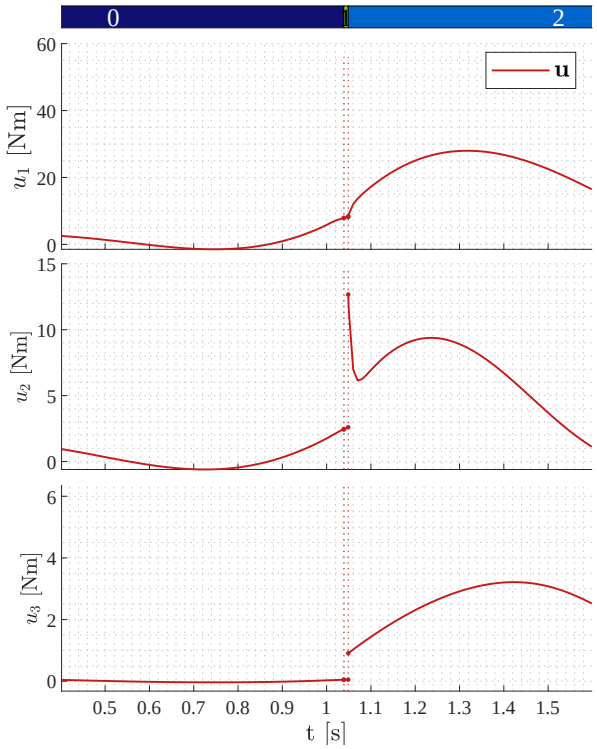

Figure 5.9: *The input $\boldsymbol{u}$ used to generate the tracking trajectory $\boldsymbol{x}$ shown in Figure 5.8, with $\boldsymbol{\alpha}$ as reference.*

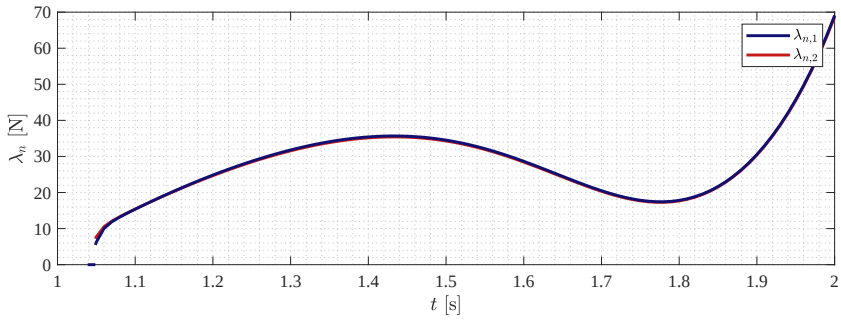

Figure 5.10: *The reaction forces* $\lambda_{n,1}$ *and* $\lambda_{n,2}$ *of the perturbed trajectory* $\boldsymbol{x}^{\epsilon}$ *for* $t \in [t^1, \tau_2]$.

Chapter 6

Conclusions and Recommendations

This chapter concludes this research and contains recommendations for future research. As stated in Section 1.5, the research objective of this work is twofold. Firstly, we aim at finding a model suitable for mechanical systems with unilateral constraints and spatial friction, and extend the sensitivity analysis presented in [59] to be suitable for such models. Secondly, in the cases of simultaneous releases, this work aims at extending the sensitivity analysis to be suitable for trajectories with input-triggered events. These research objectives have been formally defined as:

Simultaneous impacts with friction
Find a model suitable to describe mechanical systems with unilateral constraints and spatial friction. The sensitivity analysis and mathematical notation presented in [59] shall be extended to be compatible with such models.

Simultaneous releases
Extending the sensitivity analysis presented in [59] such that it is suitable for input-triggered events.

In the following sections, the conclusions and recommendations related to these research objectives are given. In Section 6.1, the most important conclusions are drawn and the contribution of this work is summarized. Then, in Section 6.2, a number of suggestions for future research is given.

6.1 Conclusions

In this section, the conclusions that are drawn from this work are presented. The conclusions are subdivided in several subjects, which correspond with the outline of the chapters in this work. Each subject is concluded by the contribution associated with that subject, given in *italic*. Together, these contributions achieve the research objective first presented in Section 1.5.

Modeling. To analyze mechanical systems with unilateral constraints and spatial friction, a suitable model needed to be found. The hybrid system formulation with guard functions has been previously used in modeling mechanical systems with trajectories experiencing impact [59]. In Chapter 2, a hybrid system formulation using guard functions is presented for mechanical systems with trajectories experiencing frictional impacts, releasing motions, and stick/slip transitions. We name this model the nonlinear state-and-input-triggered hybrid system (NSITHS).

A model, suitable to describe mechanical systems with unilateral constraints and spatial friction, is found and presented in the form of an NSITHS.

State-and-input-triggered isolated events. The model presented in Chapter 2 is used to

analyze the effect of perturbations on trajectories of mechanical systems with unilateral constraints and spatial friction. By performing a sensitivity analysis, a model that describes the response of the system on perturbations is obtained. Since the model presented in Chapter 2 contains input-dependent guard functions, the sensitivity analysis presented in [55] does not suffice. Therefore, the sensitivity analysis is extended to be suitable for input-dependent guard functions and jump maps. This sensitivity analysis defines a linear time-triggered hybrid system (LTTHS), which approximates the behavior of the NSITHS for trajectories with isolated events.

The sensitivity analysis and notation presented in [59] is extended to be compatible with the NSITHS, for trajectories with isolated state-and-input-triggered events.

State-and-input-triggered simultaneous events. The approximation of the NSITHS presented in Chapter 3, named the LTTHS, is only valid for trajectories with isolated events. In Chapter 4, the LTTHS is extended to be suitable for nominal trajectories with simultaneous events. Using the approach presented in [67], the jump gain that describes the jumping behavior in the LTTHS is replaced by the positively homogeneous jump gain. This positively homogeneous jump gain approximates the jumping behavior of the trajectories around the nominal trajectory, where loss of simultaneity occurs. Using the positively homogeneous jump gain, the positively homogeneous time-triggered hybrid system (PTTHS) is defined. The PTTHS approximates the behavior of the NSITHS for trajectories with simultaneous events. The work in [59] presents the PTTHS for state-triggered events and state-dependent jump maps, whereas this work presents the PTTHS for state-and-input-triggered events and state-and-input dependent jump gains.

The sensitivity analysis and notation presented in [59] is extended to be compatible with the NSITHS, for trajectories with simultaneous state-and-input-triggered events.

To summarize, this work presents an analysis on the tracking behavior of mechanical systems with unilateral constraints and spatial friction. The analysis is compatible with both state-and-input-dependent guard functions and jump maps, and a class of nominal trajectories that can experience both isolated and simultaneous events. The reader should be aware that the theory is not valid for near-simultaneous events in the nominal trajectory. The analysis results in an approximation of trajectories close to the nominal trajectory, which we claim can be used to assess the local asymptotic stability of the original system. Since the approximation is time-triggered, conventional stability analysis tools can be used to assess the stability of the state-and-input triggered system. Also, the approximation can be used for LQR optimal control settings, or even receding horizon control settings.

6.2 Recommendations

Several research objectives have been addressed in this work. Since research is performed in a particular scope, this work has limitations which are translated into suggestions for future research. Also, due to the continuously progressing nature of research, new potential research subjects have arisen during the writing of this work. In this section, a number of suggestions is made for future research. We presume these suggestions to contribute to the methodology of reference spreading (RS) and the search for a high performance tracking control strategy for mechanical systems physical interaction at non-negligible speed. The recommendations are presented in no particular order.

Numerical validation. The contribution of this work lies in extending the work in [59] to be compatible with state-and-input-dependent guards, and needs to be validated by means of numerical simulation. While first-steps have been taken in performing this validation, the scope of this project did now allow for a complete validation to be finished. A numerical simulation for mechanical

systems with state-triggered events is already available in a planar setting, which can be extended to be suitable for state-and-input-triggered events by implementing releasing motions. When this addition has been made, the next step can be made by including dry friction, resulting in stick/slip transitions and frictional impacts. There is an unsolved problem with the guard function associated with slip-to-stick transitions, which can lead to numerical problems. A solution should be found for this guard function assess stick/slip transitions in the numerical validations. Finally, these simulations should be extended to a 3-dimensional settings, and systems of higher complexity.

General definition positively homogeneous jump gain. One of the main contributions of this is work is the extension of the positively homogeneous to input-dependent guards. While this positively homogeneous jump gain can be defined for any event character, this work solely focuses on character-2 events. The RS control approach would benefit from a general definition of the positively homogeneous jump gain, which can be used to straightforwardly compute the positively homogeneous jump gain for an event of arbitrary character.

Stick/slip impacts. With the goal of designing a high performance control strategy for mechanical systems with unilateral constraints and spatial friction, this work has led to another suggestion for future research. When a contact point impacts a surface, the post-event state of that event could immediately activate a stick/slip-transition related guard function. For a high performance control strategy, we often desire to act on the border between stick and slip, e.g., during a running motion of a robot. Currently, the theory is not applicable to situations where the post-event state of an event immediately activates another guard function. We suggest that future research should entail find a jump gain that can approximate the behavior of such events, under the presence of perturbations.

Trajectory generation. To apply the RS control approach, a nominal trajectory that satisfies the posed assumptions is required. This reference trajectory has proven to be not straightforward to find. We believe that finding a straightforward method for defining this reference trajectory, along with its extensions, is a valuable addition to the RS control approach. The extensions are currently designed in a non-generalizable way. A general algorithm that generates the extensions can lead to improvements in domain of attraction, robustness, and convergence rate. Another approach can be to generate the reference trajectories by the machine learning approach 'learning by demonstration'.

Mathematical accuracy. This work can benefit from more extensive research in the mathematical accuracy of the sensitivity analysis. The stability of the LTTHS is found to imply local asymptotic stability of the associated nonlinear state-triggered hybrid system (NSTHS) in [55]. While we believe it exists, this relation is not yet proven for the LTTHS derived from the NSITHS. Therefore, we suggest investigating this relation as future research. Correspondingly, we believe the same relation can be found between the PTTHS and the NSTHS, and the PTTHS and the NSITHS. In addition, we belief the approximations defined by the LTTHS and PTTHS are of first order. We expect that further investigation in the accuracy of these approximations will lead to a proof for the approximations being first-order. Finally, the jump gains $\boldsymbol{G}$ and $\boldsymbol{J}$ have only been formally derived for character-2 events. We claim that, using an induction-like proof, the derivation of the jump-gain can be extended to events of an arbitrary character.

Bibliography

[1] V. T. Robotics and M. Lab, "Simlab quadruped." `http://www.me.vt.edu/research/laboratories/rmlab/`, 2018.

[2] A. Robotics, "Irb 360 flexpicker." `https://new.abb.com/products/robotics/industrial-robots/irb-360`, 2018.

[3] R. I. Leine and H. Nijmeijer, *Dynamics and Bifurcations of Non-Smooth Mechanical Systems*. Berlin, Heidelberg: Springer-Verlag, 1st ed., 2004.

[4] A. F. Fillippov, *Differential Equations with Discontinuous Righthand Sides*. Dordrecht: Springer-Science, 1st ed., 1988.

[5] R. I. Leine and N. van de Wouw, "Uniform Convergence of Monotone Measure Differential Inclusions: With Application To the Control of Mechanical Systems With Unilateral Constraints," *International Journal of Bifurcation and Chaos*, vol. 18, no. 5, pp. 1435–1457, 2008.

[6] J. J. Moreau and P. O. Panagiotopoulos, *Nonsmooth Mechanics and Applications*. Wien: Springer-Verlag, 1st ed., 1988.

[7] B. Brogliato, *Nonsmooth Mechanics*. Springer, 3rd ed., 1999.

[8] N. van de Wouw, "An introduction to Time-Stepping: a Numerical Technique for Mechanical Systems with Unilateral Constraints," *Unpublished*, pp. 1–27, 2004.

[9] A. J. Van Der Schaft and J. M. Schumacher, "Complementarity modeling of hybrid systems," *IEEE Transactions on Automatic Control*, vol. 43, no. 4, pp. 483–490, 1998.

[10] W. P. M. H. Heemels, *Linear complementarity systems: a study in hybrid dynamics*. PhD thesis, Eindhoven University of Technology, 1999.

[11] C. Glocker, *Set-Valued Force Laws: Dynamics of Non-Smooth Systems*, vol. 1. Zürich: Springer, 1 ed., 2001.

[12] J.-M. Bourgeot and B. Brogliato, "Passivity-based tracking control of multiconstraint complementarity Lagrangian systems," *International Journal of Bifurcation and Chaos*, vol. 15, no. 6, pp. 1839–1866, 2005.

[13] I.-C. Morarescu and B. Brogliato, "Tracking Control of Multiconstraint Complementarity Lagrangian Systems," *International Journal of Bifurcation and Chaos*, vol. 55, no. 6, pp. 1300–1313, 2010.

[14] D. J. Hyun, S. Seok, J. Lee, and S. Kim, "High speed trot-running: Implementation of a hierarchical controller using proprioceptive impedance control on the MIT Cheetah," *International Journal of Robotics Research*, vol. 33, no. 11, pp. 1417–1445, 2014.

[15] B. Morris and J. W. Grizzle, "Hybrid invariant manifolds in systems with impulse effects with application to periodic locomotion in bipedal robots," *IEEE Transactions on Automatic Control*, vol. 54, no. 8, pp. 1751–1764, 2009.

[16] R. Goebel, R. G. Sanfelice, and A. R. Teel, "Hybrid dynamical systems," *IEEE Control Systems Magazine*, vol. 29, no. 2, pp. 28–93, 2009.

[17] J. Ding, J. H. Gillula, H. Huang, M. P. Vitus, W. Zhang, and C. J. Tomlin, "Hybrid Systems in Robotics: Toward Reachability-Based Controller Design," *IEEE Robotics & Automation Magazine*, vol. 18, no. 3, pp. 33–43, 2011.

[18] H. Ye and a. N. Michel, "Stability theory for hybrid dynamical systems," *IEEE Transactions on Automatic Control*, vol. 43, no. 4, pp. 461–474, 1998.

[19] J. Lygeros, K. Johansson, S. Simic, and S. Sastry, "Dynamical properties of hybrid automata," *IEEE Transactions on Automatic Control*, vol. 48, no. 1, pp. 2–17, 2003.

[20] F. L. Pereira and G. N. Silva, "Lyapunov stability of measure driven impulsive systems," *Differential Equations*, vol. 40, no. 8, pp. 1122–1130, 2004.

[21] B. Brogliato, "Absolute stability and the Lagrange-Dirichlet theorem with monotone multivalued mappings," *Systems and Control Letters*, vol. 51, no. 5, pp. 343–353, 2004.

[22] R. Leine and N. van de Wouw, *Stability and Convergence of Mechanical Systems with Unilateral Constraints*, vol. 36. Springer, 2008.

[23] M. K. Camlibel, J.-S. Pang, and J. Shen, "Lyapunov Stability of Complementarity and Extended Systems," *SIAM Journal on Optimization*, vol. 17, no. 4, pp. 1056–1101, 2007.

[24] M. K. Camlibel and N. van de Wouw, "On the Convergence of Linear Passive Complementarity Systems," *IEEE Conference on Decision and Control*, vol. 46th, pp. 5886–5891, 2007.

[25] M. H. Raibert, "Hopping in Legged Systems - Modeling and Simulation for the Two-Dimensional One-Legged Case," *IEEE Transactions on Systems, Man and Cybernetics*, vol. SMC-14, no. 3, pp. 451–463, 1984.

[26] A. Lebaudy, J. Prosser, and M. Kam, "Control Algorithms for a Vertically-Constrained One-Legged Hopping Machine," *Proceedings of the 32nd Conference on Decision and Control*, pp. 2688–2693, 1993.

[27] H. Michalska, M. Ahmadi, and M. Buehler, "Vertical motion control of a hopping robot," *Proceedings of IEEE International Conference on Robotics and Automation*, vol. 3, no. April, pp. 2712–2717, 1996.

[28] P. Gregorio, M. Ahmadi, and M. Buehler, "Design, control, and energetics of an electrically actuated legged robot," *IEEE Transactions on Systems, Man, and Cybernetics, Part B: Cybernetics*, vol. 27, no. 4, pp. 626–634, 1997.

[29] J. W. Grizzle, G. Abba, and F. Plestan, "Asymptotically stable walking for biped robots: Analysis via systems with impulse effects," *IEEE Transactions on Automatic Control*, vol. 46, no. 1, pp. 51–64, 2001.

[30] A. D. Ames, "Human-inspired control of Bipedal walking robots," *IEEE Transactions on Automatic Control*, vol. 59, no. 5, pp. 1115–1130, 2014.

[31] J. Reher, E. A. Cousineau, A. Hereid, C. M. Hubicki, and A. D. Ames, "Realizing dynamic and efficient bipedal locomotion on the humanoid robot DURUS," *Proceedings - IEEE International Conference on Robotics and Automation*, vol. 2016-June, pp. 1794–1801, 2016.

[32] A. Robotics, "Cassie." `http://www.agilityrobotics.com/robots/#cassie`, 2018.

[33] J. W. Grizzle, C. Chevallereau, R. W. Sinnet, and A. D. Ames, "Models, feedback control, and open problems of 3D bipedal robotic walking," *Automatica*, vol. 50, no. 8, pp. 1955–1988, 2014.

[34] N. van de Wouw and R. I. Leine, "Tracking control for a class of measure differential inclusions," *Proceedings IEEE Conference on Decision and Control*, pp. 2526–2532, 2008.

[35] N. van de Wouw and R. I. Leine, "Stability and Control of Lur'e-type Measure Differential Inclusions," *Unpublished*, pp. 129–151, 2010.

[36] R. Naldi and R. G. Sanfelice, "Passivity-based control for hybrid systems with applications to mechanical systems exhibiting impacts," *Automatica*, vol. 49, no. 5, pp. 1104–1116, 2013.

[37] R. G. Sanfelice, J. J. B. Biemond, N. van de Wouw, and W. P. M. H. Heemels, "Tracking control for hybrid systems via embedding of known reference trajectories," *Proceedings of the 2011 American Control Conference*, pp. 869–874, 2011.

[38] R. G. Sanfelice, J. J. Biemond, N. van de Wouw, and W. P. M. H. Heemels, "An embedding approach for the design of state-feedback tracking controllers for references with jumps," *International Journal of Robust and Nonlinear Control*, vol. 24, pp. 1585–1608, 2014.

[39] M. Posa, M. Tobenkin, and R. Tedrake, "Stability Analysis and Control of Rigid Body Systems with Impacts and Friction," *IEEE TRANSACTIONS ON AUTOMATIC CONTROL*, vol. 61, no. 6, pp. 1423–1437, 2016.

[40] Y. Zhao, B. R. Fernandez, and L. Sentis, "A Framework for Planning and Controlling Non-Periodic Bipedal Locomotion," *CoRR*, 2015.

[41] J. J. B. Biemond, N. van de Wouw, W. P. M. H. Heemels, and H. Nijmeijer, "Tracking Control for Hybrid Systems with State-Triggered Jumps," *IEEE Transactions on Automatic Control*, vol. 58, no. 257462, pp. 876–890, 2013.

[42] L. Menini and A. Tornambè, "Asymptotic tracking of periodic trajectories for a simple mechanical system subject to nonsmooth impacts," *IEEE Transactions on Automatic Control*, vol. 46, no. 7, pp. 1122–1126, 2001.

[43] S. Galeani, L. Menini, A. Potini, and A. Tornambè, "Trajectory tracking for a particle in elliptical billiards," *International Journal of Control*, vol. 81, no. 2, pp. 189–213, 2008.

[44] F. Forni, A. R. Teel, and L. Zaccarian, "Follow the bouncing ball: Global results on tracking and state estimation with impacts," *IEEE Transactions on Automatic Control*, vol. 58, no. 6, pp. 1470–1485, 2013.

[45] J. J. B. Biemond, W. P. M. H. Heemels, R. G. Sanfelice, and N. van de Wouw, "Distance function design and Lyapunov techniques for the stability of hybrid trajectories," *Automatica*, vol. 73, pp. 38–46, 2016.

[46] M. Baumann, J. J. Biemond, R. I. Leine, and N. van de Wouw, "Synchronization of impacting mechanical systems with a single constraint," *Physica D: Nonlinear Phenomena*, vol. 362, pp. 9–23, 2018.

[47] J. Kim, H. Shim, and J. H. Seo, "Tracking control for hybrid systems with state jumps using gluing function," *2016 IEEE 55th Conference on Decision and Control, CDC 2016*, pp. 3006–3011, 2016.

[48] T. Yang, F. Wu, and L. Zhang, "Tracking control of hybrid systems with state-triggered jumps and stochastic events and its application," *IET Control Theory & Applications*, vol. 11, no. 7, pp. 1024–1033, 2017.

[49] A. Saccon, N. van de Wouw, and H. Nijmeijer, "Sensitivity analysis of hybrid systems with state jumps with application to trajectory tracking," *Proceedings of the 53rd IEEE Conference on Decision and Control*, pp. 3065–3070, 2014.

[50] M. W. L. M. Rijnen, A. Saccon, and H. Nijmeijer, "On Optimal Trajectory Tracking for Mechanical Systems with Unilateral Constraints," *2015 IEEE 54th Annual Conference on Decision and Control (CDC)*, pp. 2561–2566, 2015.

[51] H. K. Khalil, *Nonlinear Systems*. Englewood Cliffs, NJ: Prentice-Hall, 3rd ed., 1996.

[52] G. P. Incremona, A. Saccon, A. Ferrara, and H. Nijmeijer, "Trajectory tracking of mechanical systems with unilateral constraints: Experimental results of a recently introduced hybrid PD feedback controller," *Proceedings of the IEEE Conference on Decision and Control*, vol. 54rd IEEE, no. Cdc, pp. 920–925, 2015.

[53] M. W. L. M. Rijnen, A. T. van Rijn, H. Dallali, A. Saccon, and H. Nijmeijer, "Hybrid Trajectory Tracking for a Hopping Robotic Leg," *IFAC-PapersOnLine*, vol. 49, no. 14, pp. 107–112, 2016.

[54] N. G. Tsagarakis, S. Morfey, H. Dallali, G. A. Medrano-Cerda, and D. G. Caldwell, "An asymmetric compliant antagonistic joint design for high performance mobility," *IEEE International Conference on Intelligent Robots and Systems*, pp. 5512–5517, 2013.

[55] M. W. L. M. Rijnen, J. Biemond, N. van de Wouw, A. Saccon, and H. Nijmeijer, "Hybrid Systems with State-Triggered Jumps: Sensitivity-Based Stability Analysis with Application to Trajectory Tracking," *Submitted*, pp. 1–16, 2017.

[56] M. Rijnen, E. De Mooij, S. Traversaro, F. Nori, N. van de Wouw, A. Saccon, and H. Nijmeijer, "Control of humanoid robot motions with impacts: Numerical experiments with reference spreading control," *Proceedings - IEEE International Conference on Robotics and Automation*, pp. 4102–4107, 2017.

[57] H. Zhao, J. Horn, J. Reher, V. Paredes, and A. D. Ames, "A hybrid systems and optimization-based control approach to realizing multi-contact locomotion on transfemoral prostheses," *Proceedings of the IEEE Conference on Decision and Control*, vol. 54, no. 2, pp. 1607–1612, 2015.

[58] H. L. Chen, *Trajectory tracking control for mechanical systems experiencing simultaneous impacts*. Master's thesis, Eindhoven University of Technology, 2018.

[59] M. W. L. M. Rijnen, *Enabling motions with impacts in robotic and mechatronic systems*. Eindhoven: Technische Universiteit Eindhoven, 2018.

[60] C. Glocker, "Energetic consistency conditions for standard impacts: Part I: Newton-type inequality impact laws and Kane's example," *Multibody System Dynamics*, vol. 32, no. 4, pp. 445–509, 2014.

[61] A. van Rijn, *Hybrid trajectory tracking for hopping robots*. Master's thesis, Eindhoven University of Technology, 2016.

[62] N. van de Wouw, *Multibody and Nonlinear Dynamics Lecture Notes*. Eindhoven: University of Technology Eindhoven, 2016.

[63] M. Anitescu, "Digital Object Identifier (Optimization-based simulation of nonsmooth rigid multibody dynamics," *Math. Program., Ser. A*, vol. 105, pp. 113–143, 2006.

[64] V. Acary and B. Brogliato, *Numerical Methods for Nonsmooth Dynamical Systems: Applications in Mechanics and Electronics*, vol. 35. Montbonnot: Springer, 2008.

[65] W. M. Haddad, V. Chellaboina, and S. G. Nersesov, *Impulsive and Hybrid Dynamical Systems*. New Jersey: Princeton University Press, 1st ed., 2006.

[66] É. Delassus, "Mémoire sur la théorie des liaisons finies unilatérales," *Annales scientifiques de l'É.N.S.*, vol. 34, no. 3rd, pp. 95–179, 1917.

[67] M. Rijnen, H. L. Chen, N. van de Wouw, A. Saccon, and H. Nijmeijer, "Sensitivity analysis for trajectories of nonsmooth mechanical systems with simultaneous impacts : a hybrid systems perspective," *Submitted*, 2018.

[68] J. P. Hespanha, *Linear Systems Theory*. Princeton, New Jersey: Princeton Press, February 2018. ISBN13: 9780691179575.

[69] T. Apostol, *Multi-Variable Calculus and Linear Algebra with Applications*, vol. 2. New York: John Wiley & Sons, 2nd ed., 1967.

[70] M. W. L. M. Rijnen, "RRR ROBOT OPENING A DOOR SENSITIVITY ANALYSIS OF A PLANAR 4 DOF SYSTEM," *Unpublished*, no. July, pp. 1–14, 2018.

Appendix A

Nonsmooth modeling

A.1 Discrete event set derivation

In this section the discrete event sets $\mathcal{D}$ are defined for a system with one contact point. When the state or input of the system enters a discrete event set, the contact point can change set and a reinitialization of the state can take place.

Open to stick/slip
When a contact point is not in contact, it can trigger a guard function $\gamma^{\text{op}\to\text{cl}}$ to go from open to closed. This guard is defined using the contact distance $\mathrm{h}_{n,\iota}$, where $\mathrm{h}_{n,\iota}$ is the smallest distance between the contact point and the contact surface. When $\mathrm{h}_{n,\iota} > 0$, the contact point is in open-contact. When $\mathrm{h}_{n,\iota} = 0$ with $\dot{h}_{n,\iota} < 0$, the contact point enters the closed-contact mode with a non-zero ante-impact velocity. Therefore the guard function $\gamma^{\text{op}\to\text{cl}}$ is given by

$$\gamma^{\text{op}\to\text{cl}} = h_{n,\iota}(\boldsymbol{q}). \tag{A.1}$$

Since the closing of a contact point at nonzero velocity is an impulsive event, the impulsive dynamics need to be considered to find whether the contact point will slip or stick after the impact. The manifold where $\gamma = 0$ is divided into two regions: a region where the post-impact state is in slip and a region where the post-impact state is in stick. This region is defined by the guard functions $\Gamma_\iota^{\text{sl}\to\text{st}}$ and $\Gamma_\iota^{\text{st}\to\text{sl}}$, where $\Gamma_\iota^{\text{sl}\to\text{st}} < 0, \Gamma_\iota^{\text{st}\to\text{sl}} > 0$ in the region where the impacting contact point goes to slip and $\Gamma_\iota^{\text{sl}\to\text{st}} > 0, \Gamma_\iota^{\text{st}\to\text{sl}} < 0$ in the region where the contact point goes to stick. Both guard functions are equal to zero when the contact point is at the border between stick and slip. This is illustrated in Figure A.1. For post-event slip, we know that $||\mathbf{v}_{t,\iota}^+|| > 0$, and for post-event stick, we know that $\mu\Lambda_{n,\iota} - ||\mathbf{\Lambda}_{t,\iota}|| > 0$. From this we can derive the guard functions

$$\Gamma_\iota^{\text{st}\to\text{sl}} = \mu^2\Lambda_{n,\iota}^2 - \mathbf{\Lambda}_{t,\iota}\mathbf{\Lambda}_{t,\iota}^T, \tag{A.2}$$

$$\Gamma_\iota^{\text{sl}\to\text{st}} = (\mathbf{v}_{t,\iota}^+)^T\mathbf{v}_{t,\iota}^+. \tag{A.3}$$

Slip to stick/open
When a contact point is in closed-contact slip, it can transition to closed-contact stick and it can transition to open-contact. A slipping contact transitions to sticking when the tangential velocity of the contact point is zero, i.e.,

$$||\mathbf{v}_{t,\iota}|| = 0. \tag{A.4}$$

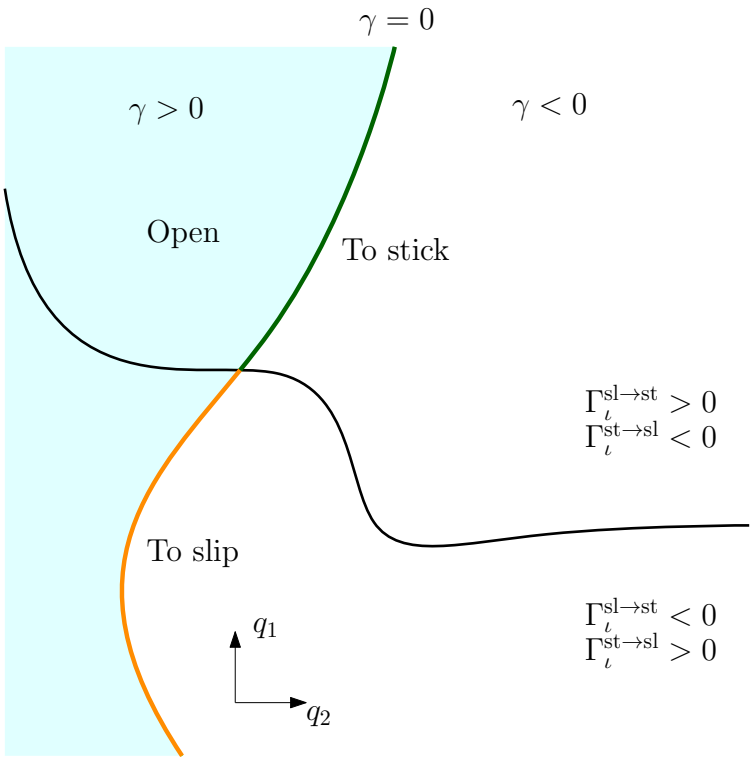

Figure A.1: *The functions $\gamma(\boldsymbol{q}, \dot{\boldsymbol{q}})$ and $\Gamma(\boldsymbol{q}, \dot{\boldsymbol{q}})$ illustrated in the state space of $\boldsymbol{q} \in \mathbb{R}^2$. The light blue area is the state space where the contact is open, and closes contact when it triggers $\gamma = 0$. If it triggers $\gamma = 0$ in the area where $\Gamma_\iota^{sl\to st} < 0, \Gamma_\iota^{st\to sl} > 0$ (orange), then the contact will go to slip. If it triggers $\gamma = 0$ in the area where $\Gamma_\iota^{sl\to st} > 0, \Gamma_\iota^{st\to sl} < 0$ (green), then the contact will go to stick.*

A guard function that can be used to describe this set is

$$\gamma^{\text{sl}\to\text{st}} = \mathbf{v}_{t,\iota}^T \mathbf{v}_{t,\iota}, \tag{A.5}$$

which is equal to zero when $||\mathbf{v}_{t,\iota}|| = 0$, greater than zero when $||\mathbf{v}_{t,\iota}|| > 0$, smaller than zero when $||\mathbf{v}_{t,\iota}|| < 0$, and it is globally differentiable. The time derivative of the guard function is then given by

$$\dot{\gamma}^{\text{sl}\to\text{st}} = \frac{(\dot{\mathbf{v}}_{t,\iota})_1 + (\dot{\mathbf{v}}_{t,\iota})_2}{\sqrt{(\mathbf{v}_{t,\iota})_1^2 + (\mathbf{v}_{t,2})_2^2}}. \tag{A.6}$$

For $\gamma^{\text{sl}\to\text{st}} = 0$, $\dot{\gamma}^{\text{sl}\to\text{st}}$ is undefined because of a division by zero. But we can take the left limit of $\dot{\gamma}^{\text{sl}\to\text{st}}$ to find the direction at which the guard is activated. Using a Taylor expansion w.r.t. the time we can define the limits

$$(\dot{\mathbf{v}}_{t,\iota})_1(\tau + s) = a_1 s + o(s), \tag{A.7}$$
$$(\dot{\mathbf{v}}_{t,\iota})_2(\tau + s) = a_2 s + o(s), \tag{A.8}$$

where τ is the event time where $\gamma = 0$. Note that the Taylor expansions are only physically realistic for $s < 0$. We can then write

$$\dot{\gamma}^{\text{sl}\to\text{st}}(\tau + s) = \frac{(a_1 + a_2)s + o(s)}{\sqrt{(a_1^2 + a_2^2)s^2 + o(s^2)}} \approx \text{Sign}(s)(a_1 + a_2). \tag{A.9}$$

Since we're interested in the left limit, we get

$$\lim_{s\to 0^-} \dot{\gamma}^{\text{sl}\to\text{st}}(\tau+s) = -(a_1^2 + a_2^2), \tag{A.10}$$

which will be non-zero when the guard is activated transversally. This guard function can be used to perform the positive homogenization. For simulations we have to find another solution, because $\gamma^{\text{sl}\to\text{st}}$ cannot become negative. This will lead to problems when we use zero-border crossing detection.

Stick to slip/open
When a contact point is in closed-contact stick, it can transition to closed-contact slip and it can transition to open-contact. A slipping contact transitions to sticking when the tangential reaction force becomes equal to the normal reaction force at that contact point times the friction coefficient, i.e.,

$$\mu\lambda_{n,\iota} = ||\boldsymbol{\lambda}_{t,\iota}||. \tag{A.11}$$

A guard function that can be used to describe this set is

$$\gamma_{\text{st}\to\text{sl}} = \mu^2\lambda_{n,\iota}^2 - \boldsymbol{\lambda}_{t,\iota}\boldsymbol{\lambda}_{t,\iota}^T, \tag{A.12}$$

which is equal to zero when $\mu\lambda_{n,\iota} = ||\boldsymbol{\lambda}_{t,\iota}||$, greater than zero when $\mu^2\lambda_{n,\iota}^2 > ||\boldsymbol{\lambda}_{t,\iota}||$, and it is globally differentiable.

A.2 Proximal Point Formulation

The contact law and friction law defined in the complementarity condition formulation can be redefined to a proximal point formulation. This makes the system compatible with simulation methods as timestepping [64, Chapter 10]. More information on the definition of the proximal point formulation of contact laws and friction laws can be found in [22, Section 5.3].

A.2.1 Signorini's contact law and Poisson's impact law

In Figure **??** a convex set C is illustrated. The normal cone $N_C(\boldsymbol{x})$ of a point $\boldsymbol{x}$ is $N_C(\boldsymbol{x}) = 0$ if $\boldsymbol{x} \in \text{int}(C)$, where int(.) is the interior of a set. An example of this is point $\boldsymbol{x}_3$ in Figure A.2. Defining bd(.) as the boundary of the set, when $\boldsymbol{x} \in \text{bd}(C)$ there are two options. When $\boldsymbol{x}$ is on a smooth part of bd(C), then $N_C(\boldsymbol{x})$ is a ray normal to bd(C) at point $\boldsymbol{x}$ as depicted in at point $\boldsymbol{x}_1$. When $\boldsymbol{x}$ is on a nonsmooth part of bd(C), then $N_C(\boldsymbol{x})$ is a cone starting on the point $\boldsymbol{x}$ whose sides are normal to the left and right approximation of the point $\boldsymbol{x}$ on bd(C). This is illustrated at point $\boldsymbol{x}_2$. The proximal point $\text{prox}_C(\boldsymbol{z})$ of a point $\boldsymbol{z}$, is the point in C closest to the point $\boldsymbol{z}$. The point $\boldsymbol{x}$ is the proximal point to all points $\boldsymbol{z} \in N_C(\boldsymbol{x})$. For a point $\boldsymbol{z} \in C$, $\text{prox}_C(\boldsymbol{z}) = \boldsymbol{z}$ i.e. $\boldsymbol{x}_3$ in Figure A.2.

This formulation can be used to define Signorini's contact law, which is defined as (2.19). The normal cone formulation, as illustrated in Figure A.2, of the contact is given by

$$-\text{h}_{n,\iota} \in N_{C_{n,\iota}}(\lambda_{n,\iota}), \quad \text{with } C_{n,\iota} = (\mathbb{R}^n)^+. \tag{A.13}$$

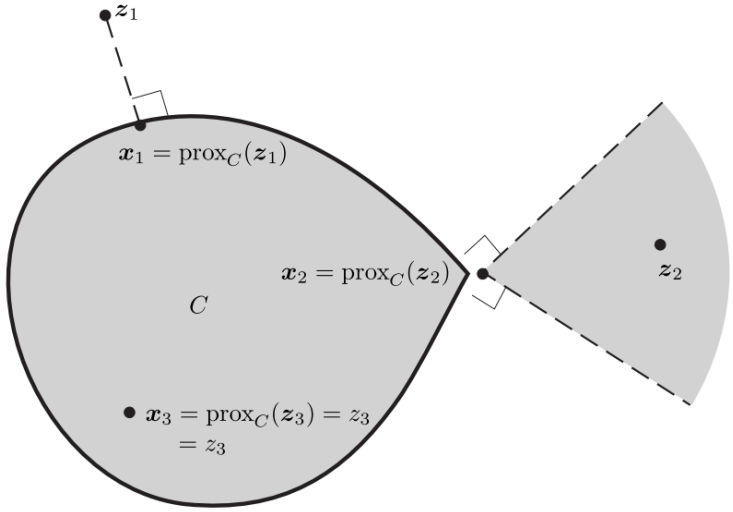

Figure A.2: *An illustration of the normal cone formulation N_C and proximal points formulation $prox_C$.*

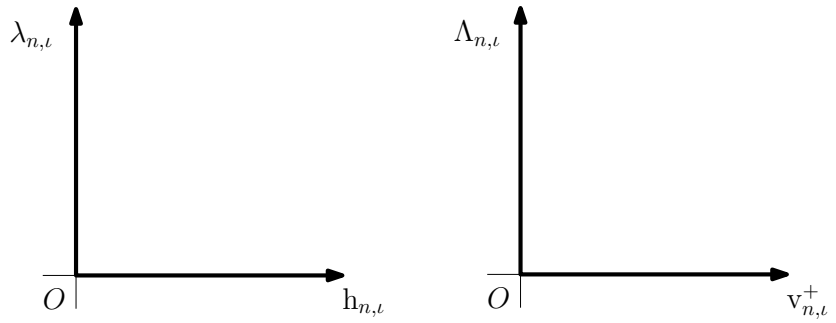

Figure A.3: *In* (a) *Signorini's contact law and in* (b) *Newton's impact law without restitution.*

The set $C_{n,\iota}$ is the set of admissible normal forces according to Signorini's law. See Figure A.3a for an illustration of the set $C_{n,\iota}$ with $\lambda_{n,\iota} \in C_{n,\iota}$ and $\text{h}_{n,\iota} \in N_{C_{n,\iota}}(\lambda_{n,\iota})$. Now using the fact that

$$\boldsymbol{x} = \text{prox}_C(\boldsymbol{x} - r\boldsymbol{y}), r > 0 \iff -\boldsymbol{y} \in N_C(\boldsymbol{x}), \tag{A.14}$$

rewriting (A.13) to a proximal point formulation gives

$$\lambda_{n,\iota} = \text{prox}_{C_{n,\iota}}(\lambda_{n,\iota} - r\text{h}_{n,\iota}), \quad \text{with } C_{n,\iota} = (\mathbb{R}^n)^+ \text{ and } r > 0. \tag{A.15}$$

Similarly for the Poisson's impact law illustrated in Figure A.3b, we find the proximal point formulation

$$\Lambda_{n,\iota} = \text{prox}_{C_{n,\iota}}(\Lambda_{n,\iota} - r\text{v}^+_{n,\iota}), \quad \text{with } C_{n,\iota} = (\mathbb{R}^n)^+ \text{ and } r > 0. \tag{A.16}$$

A.2.2 Coulomb's friction law

Now we define the normal cone formulation of Coulomb's friction law

$$-\mathbf{v}_{t,\iota} \in N_{C_{t,\iota}}(\boldsymbol{\lambda}_{t,\iota}) \quad \forall \iota \in \mathcal{I}_a, \quad \text{with } C_{t,\iota}(\lambda_{n,\iota}) = \{\boldsymbol{\lambda}_{t,\iota} \mid ||\boldsymbol{\lambda}_{t,\iota}|| \leq \mu\lambda_{n,\iota}\}, \tag{A.17}$$

which is illustrated in Figure A.4.

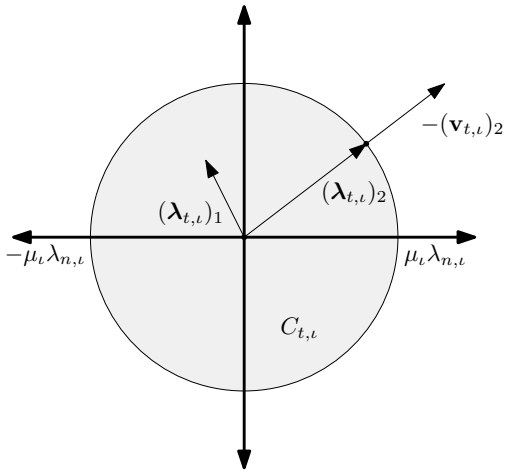

Figure A.4: *The friction disk with two seperate friction forces* $\boldsymbol{\lambda}_{t,1}$ *and* $\boldsymbol{\lambda}_{t,2}$*.* $\boldsymbol{\lambda}_{t,1} = \mu\lambda_{n,1}$*, resulting in a tangential velocity* $\mathbf{v}_{t,\iota} > 0$*.* $\boldsymbol{\lambda}_{t,2} < \mu\lambda_{n,2}$*, leading to a tangential velocity* $\mathbf{v}_{t,\iota} = 0$*.*

C_t is the set of all admitted friction forces. The tangential velocity $\mathbf{v}_{t,\iota}$ is directed opposite to the friction force $\boldsymbol{\lambda}_{t,\iota}$ for isotropic friction.

Now using the fact that

$$\boldsymbol{x} = \text{prox}_C(\boldsymbol{x} - r\boldsymbol{y}), r > 0 \iff -\boldsymbol{y} \in N_C(\boldsymbol{x}), \tag{A.18}$$

we can rewrite the normal cone to a proximal point formulation

$$\boldsymbol{\lambda}_{t,\iota} = \text{prox}_{C_{t,\iota}}(\boldsymbol{\lambda}_{t,\iota} - r\mathbf{v}_{t,\iota}) \quad \text{with } C_{t,\iota}(\lambda_{n,\iota}) = \{\boldsymbol{\lambda}_{t,\iota} \mid ||\boldsymbol{\lambda}_{t,\iota}|| \leq \mu\lambda_{n,\iota}\} \text{ and } r > 0. \tag{A.19}$$

Similarly, for the impact dynamics we can formulate

$$\boldsymbol{\Lambda}_{t,\iota} = \text{prox}_{C_{t,\iota}}(\boldsymbol{\Lambda}_{t,\iota} - r\mathbf{v}_{t,\iota}^+) \quad \text{with } C_{t,\iota}(\lambda_{n,\iota}) = \{\boldsymbol{\Lambda}_{t,\iota} \mid ||\boldsymbol{\Lambda}_{t,\iota}|| \leq \mu\Lambda_{n,\iota}\} \text{ and } r > 0. \tag{A.20}$$

A.2.3 System dynamics with contact law and friction law

The flow dynamics is then described by

$$\boldsymbol{M}(\boldsymbol{q})\dot{\boldsymbol{\nu}} + \boldsymbol{H}(\boldsymbol{q}, \boldsymbol{\nu}) = \boldsymbol{S}(\boldsymbol{q})\boldsymbol{u} + \sum_{i \in \mathcal{I}_c} \left(\boldsymbol{w}_{n,\iota}(\boldsymbol{q})\lambda_{n,\iota} + \boldsymbol{W}_{t,\iota}(\boldsymbol{q})\boldsymbol{\lambda}_{t,\iota}\right), \tag{A.21}$$

$$\lambda_{n,\iota} = \text{prox}_{C_{n,\iota}}(\lambda_{n,\iota} - rh_{n,\iota}), \tag{A.22}$$

$$\boldsymbol{\lambda}_{t,\iota} = \text{prox}_{C_{t,\iota}}(\boldsymbol{\lambda}_{t,\iota} - r\mathbf{v}_{t,\iota}), \tag{A.23}$$

with

$$C_{n,\iota} = (\mathbb{R}^n)^+ \text{ and } r > 0, \tag{A.24}$$

$$C_{t,\iota}(\lambda_{n,\iota}) = \{\boldsymbol{\lambda}_{t,\iota} \mid ||\boldsymbol{\lambda}_{t,\iota}|| \leq \mu\lambda_{n,\iota}\} \text{ and } r > 0. \tag{A.25}$$

The impulsive dynamics that take place when a contact point opens or closes contact is described by

$$\boldsymbol{M}(\boldsymbol{q})(\boldsymbol{\nu}^{+}-\boldsymbol{\nu}^{-})=\sum_{\iota\in\mathcal{I}_c}\left(\boldsymbol{w}_{n,\iota}(\boldsymbol{q})\Lambda_{n,\iota}+\boldsymbol{W}_{t,\iota}(\boldsymbol{q})\boldsymbol{\Lambda}_{t,\iota}\right), \tag{A.26}$$

$$\Lambda_{n,\iota}=\mathrm{prox}_{C_{n,\iota}}(\Lambda_{n,\iota}-r\zeta_{n,\iota}^{+}), \tag{A.27}$$

$$\boldsymbol{\Lambda}_{t,\iota}=\mathrm{prox}_{C_{t,\iota}}(\boldsymbol{\Lambda}_{t,\iota}-r\mathbf{v}_{t,\iota}^{+}) \tag{A.28}$$

with

$$C_{n,\iota}=(\mathbb{R}^{n})^{+}\text{ and }r>0, \tag{A.29}$$

$$C_{t,\iota}(\lambda_{n,\iota})=\{\boldsymbol{\Lambda}_{t,\iota}\mid||\boldsymbol{\Lambda}_{t,\iota}||\leq\mu\Lambda_{n,\iota}\}\text{ and }r>0. \tag{A.30}$$

Appendix B

Frictional Impacts in Mechanical Systems

B.1 Reference trajectories with impact away from slip-stick border

Let us now look at the case where a contact point goes from open to closed away from $\Gamma = 0$, where $\Gamma = 0$ represents the stick/slip border. This is illustrated in Figure B.1. The goal is to prove that for an event away from Γ, a sufficiently small perturbation cannot cause the trajectory to hit $\gamma = 0$ at a perturbed ante-impact state $\boldsymbol{x}^-(t^\epsilon)$ where Γ changes sign in comparison with the unperturbed ante-impact state $\boldsymbol{\alpha}^-(\tau)$. From [67, p. 6] we know that based on the continuity property of γ and $\boldsymbol{f}$, the perturbed impact state can be written as

$$\boldsymbol{x}(t^\epsilon) = \boldsymbol{\alpha}(\tau) + \epsilon\dot{\boldsymbol{\alpha}}(\tau)\frac{\partial t^\epsilon}{\partial \epsilon} + \epsilon \boldsymbol{z}(\tau) + o(\epsilon), \tag{B.1}$$

for sufficiently small ϵ. The shortest distance between $\Gamma = \Gamma(\boldsymbol{\alpha}(\tau))$ and $\Gamma = 0$ on the manifold where $\gamma = 0$ is defined as the constant δ_Γ, which is also illustrated in Figure B.1.

Let's define a point in the state $\boldsymbol{x}_{\gamma=0,\Gamma=0}$ where $\gamma(\boldsymbol{x}_{\gamma=0,\Gamma=0}) = 0$ and $\Gamma(\boldsymbol{x}_{\gamma=0,\Gamma=0}) = 0$. We are evaluating nominal trajectories which impact away from $\Gamma = 0$, i.e. $\Gamma(\boldsymbol{\alpha}(\tau)) \neq \Gamma(\boldsymbol{x}_{\gamma=0,\Gamma=0})$. Since Γ is continuously differentiable, we know

$$||\Gamma(\boldsymbol{\alpha}(\tau)) - \Gamma(\boldsymbol{x}_{\gamma=0,\Gamma=0})|| \leq \kappa||\boldsymbol{\alpha}(\tau) - \boldsymbol{x}_{\gamma=0,\Gamma=0}||, \tag{B.2}$$

where $\kappa > 0$ [22]. Now, since $\Gamma(\boldsymbol{\alpha}(\tau)) \neq \Gamma(\boldsymbol{x}_{\gamma=0,\Gamma=0})$, we know that $||\Gamma(\boldsymbol{\alpha}(\tau)) - \Gamma(\boldsymbol{x}_{\gamma=0,\Gamma=0})|| > 0$ and therefore from (B.2) that $||\boldsymbol{\alpha}(\tau) - \boldsymbol{x}_{\gamma=0,\Gamma=0}|| > 0$, i.e. $\delta_\Gamma > 0$. Finally, from (B.1), we find

$$||\boldsymbol{x}(t^\epsilon) - \boldsymbol{\alpha}(\tau)|| = ||\epsilon\dot{\boldsymbol{\alpha}}(\tau)\frac{\partial t^\epsilon}{\partial \epsilon} + \epsilon \boldsymbol{z}(\tau) + o(\epsilon)||. \tag{B.3}$$

Since $\delta_\Gamma > 0$ and $\lim_{\epsilon\to 0} ||\boldsymbol{x}(t^\epsilon) - \boldsymbol{\alpha}(\tau)|| = 0$, there always exists an ϵ such that $||\boldsymbol{x}(t^\epsilon) - \boldsymbol{\alpha}(\tau)|| < \delta_\Gamma$.

In other words, this proves that if $\boldsymbol{f}$, γ and Γ are continuous and the nominal trajectory makes impact away from the slip-stick post-impact mode border $\Gamma = 0$, then there always exists a range of ϵ such that the perturbed state will have the same post-impact mode as the nominal trajectory.

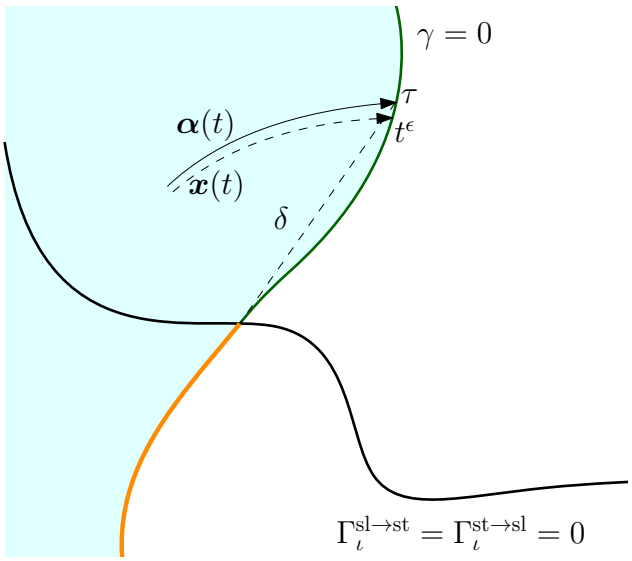

Figure B.1: *The guard functions γ and Γ in the state space of $\boldsymbol{q}$. A transition from open to closed is made away from Γ. $\boldsymbol{\alpha}(t)$ is the nominal trajectory and $\boldsymbol{x}(t)$ a perturbed trajectory of the contact point up to the transition.*

B.2 Post-impact accelerations in open-to-stick transitions

The mode transition from stick to slip happens when a guard is triggered at acceleration level,

$$\gamma^{\text{st}\to\text{sl}} = \mu_\iota^2 \lambda_{n,\iota}^2 - \boldsymbol{\lambda}_{t,\iota}\boldsymbol{\lambda}_{t,\iota}^T, \tag{B.4}$$

and the post-impact mode is determined by the guard functions defined at velocity level

$$\Gamma_\iota^{\text{st}\to\text{sl}} = \mu_\iota^2 \Lambda_{n,\iota}^2 - \boldsymbol{\Lambda}_{t,\iota}\boldsymbol{\Lambda}_{t,\iota}^T, \tag{B.5}$$

$$\Gamma_\iota^{\text{sl}\to\text{st}} = (\mathbf{v}_{t,\iota}^+)^T \mathbf{v}_{t,\iota}^+. \tag{B.6}$$

Since the jump map from open to stick is

$$\boldsymbol{M}(\boldsymbol{q})(\dot{\boldsymbol{q}}^+ - \dot{\boldsymbol{q}}^-) = \boldsymbol{w}_{n,\iota}(\boldsymbol{q})\Lambda_{n,\iota} + \boldsymbol{W}_{t,\iota}(\boldsymbol{q})\boldsymbol{\Lambda}_{t,\iota}, \tag{B.7}$$

$$\mathrm{v}_{n,\iota}^+ = 0, \tag{B.8}$$

$$\mathbf{v}_{t,\iota}^+ = 0, \tag{B.9}$$

which is on velocity level, the post-impact reaction forces of the open-to-stick event can be in the stick-to-slip jump set, causing an immediate transition to slip. This is demonstrated using the flow dynamics of the stick mode at the time-instant of the transition,

$$\boldsymbol{M}(\boldsymbol{q}^+)\ddot{\boldsymbol{q}}^+ + \boldsymbol{H}(\boldsymbol{q}^+, \dot{\boldsymbol{q}}^+) = \boldsymbol{S}(\boldsymbol{q}^+)\boldsymbol{u}^+ + \sum_{\iota\in\mathcal{I}_c} \left(\boldsymbol{w}_{n,\iota}(\boldsymbol{q}^+)\lambda_{n,\iota}^+ + \boldsymbol{W}_{t,\iota}(\boldsymbol{q}^+)\boldsymbol{\lambda}_{t,\iota}^+\right), \tag{B.10}$$

$$\boldsymbol{w}_{n,\iota}^T(\boldsymbol{q}^+)\ddot{\boldsymbol{q}}^+ + \dot{\boldsymbol{w}}_{n,\iota}^T(\boldsymbol{q}^+)\dot{\boldsymbol{q}}^+ = 0, \tag{B.11}$$

$$\boldsymbol{W}_{t,\iota}^T(\boldsymbol{q}^+)\ddot{\boldsymbol{q}}^+ + \dot{\boldsymbol{W}}_{t,\iota}^T(\boldsymbol{q}^+)\dot{\boldsymbol{q}}^+ = 0. \tag{B.12}$$

We can deduce from (B.8)-(B.9) and (B.11)-(B.12) that the normal acceleration of the transition contact point $\boldsymbol{w}_{n,\iota}^T(\boldsymbol{q}^+)\ddot{\boldsymbol{q}}^+$ and the tangential acceleration of the transitioning contact point $\boldsymbol{W}_{t,\iota}^T(\boldsymbol{q}^+)\ddot{\boldsymbol{q}}^+$ are both equal to zero. From (B.10) we then notice that $\lambda_{n,\iota}^+$ and $\boldsymbol{\lambda}_{t,\iota}^+$ depend continuously on $\boldsymbol{u}^+$

and can therefore instantly lead to $\mu_\iota^2 \lambda_{n,\iota}^2 - \boldsymbol{\lambda}_{t,\iota} \boldsymbol{\lambda}_{t,\iota}^T > 0$ for certain $\boldsymbol{u}^+$. For these inputs the contact point will immediately start slipping after the open-to-stick transition. These areas are illustrated in Figure B.2

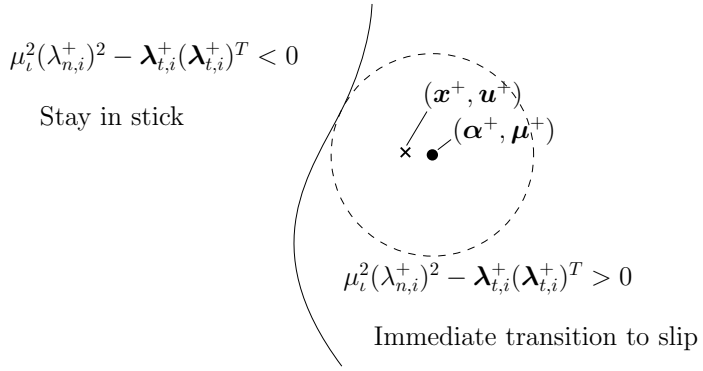

Figure B.2: *The border between an open-to-stick event that stays in stick and an open-to-stick event that immediately starts slipping is illustrated in this figure. The post event state and input indicated in the figure is in the* $\mu_\iota^2(\lambda_{n,\iota}^+)^2 - \boldsymbol{\lambda}_{t,\iota}^+(\boldsymbol{\lambda}_{t,\iota}^+)^T > 0$ *area, causing the contact point to immediately start slipping.*

Using the continuity of the system's flow dynamics and the function $\mu_\iota^2(\lambda_{n,\iota}^+)^2 - \boldsymbol{\lambda}_{t,\iota}^+(\boldsymbol{\lambda}_{t,\iota}^+)^T$, we can show that if we choose $\boldsymbol{\mu}^+$ such that $\boldsymbol{\alpha}^+, \boldsymbol{\mu}^+$ is not on $\mu_\iota^2(\lambda_{n,\iota}^+)^2 - \boldsymbol{\lambda}_{t,\iota}^+(\boldsymbol{\lambda}_{t,\iota}^+)^T = 0$ then there always exists a range of perturbations ϵ such that the perturbed post-impact is on the same side of $\mu_\iota^2(\lambda_{n,\iota}^+)^2 - \boldsymbol{\lambda}_{t,\iota}^+(\boldsymbol{\lambda}_{t,\iota}^+)^T = 0$ as the unperturbed trajectory similarly to Section B.1.

Appendix C

Sensitivity Analysis for Input-Dependent Guards

C.1 Linearized jump gain for isolated events

The perturbed state is defined as

$$\boldsymbol{x}(t,\epsilon) = \boldsymbol{x}(t_0,\epsilon) + \int_{t_0}^{t} \boldsymbol{f}(\boldsymbol{x}(s,\epsilon),\boldsymbol{u}(s,\epsilon),s)ds. \tag{C.1}$$

Then

$$\frac{\partial \boldsymbol{x}(t,\epsilon)}{\partial \epsilon} = \frac{\partial \boldsymbol{x}_0}{\partial \epsilon} + \int_{t_0}^{t} \left(\frac{\partial \boldsymbol{f}}{\partial \boldsymbol{x}} \frac{\partial \boldsymbol{x}}{\partial \epsilon} + \frac{\partial \boldsymbol{f}}{\partial \boldsymbol{u}} \frac{\partial \boldsymbol{u}}{\partial \epsilon} \right) ds, \tag{C.2}$$

$$\frac{\partial^2 \boldsymbol{x}}{\partial t \partial \epsilon} = \frac{\partial \boldsymbol{f}}{\partial \boldsymbol{x}} \frac{\partial \boldsymbol{x}}{\partial \epsilon} + \frac{\partial \boldsymbol{f}}{\partial \boldsymbol{u}} \frac{\partial \boldsymbol{u}}{\partial \epsilon}, \tag{C.3}$$

which we can write as

$$\frac{\partial^2 \boldsymbol{x}}{\partial t \partial \epsilon} = D_1 \boldsymbol{f}(\boldsymbol{x}(t,\epsilon),\boldsymbol{u}(t,\epsilon),t) \cdot \frac{\partial \boldsymbol{x}}{\partial \epsilon} + D_2 \boldsymbol{f}(\boldsymbol{x}(t,\epsilon),\boldsymbol{u}(t,\epsilon),t) \cdot \frac{\partial \boldsymbol{u}}{\partial \epsilon}, \tag{C.4}$$

with $D_i \boldsymbol{f}$ the derivative of $\boldsymbol{f}$ wrt the ith term of $\boldsymbol{f}$. Evaluating (C.4) at $\epsilon = 0$ results in the flow dynamics of the positive homogenization

$$\dot{\boldsymbol{z}} = D_1 \boldsymbol{f}(\boldsymbol{\alpha}(t),\boldsymbol{\mu}(t),t) \cdot \boldsymbol{z}(t) + D_2 \boldsymbol{f}(\boldsymbol{\alpha}(t),\boldsymbol{\mu}(t),t) \cdot \boldsymbol{v}(t), \tag{C.5}$$

where

$$\boldsymbol{z}(t) = \left. \frac{\partial \boldsymbol{x}(t,\epsilon)}{\partial \epsilon} \right|_{\epsilon=0}, \text{ and } \boldsymbol{v}(t) = \left. \frac{\partial \boldsymbol{u}(t,\epsilon)}{\partial \epsilon} \right|_{\epsilon=0}. \tag{C.6}$$

When we consider a single jump

$$\boldsymbol{x}^+(t^\epsilon,\epsilon) = \boldsymbol{g}(\boldsymbol{x}^-(t^\epsilon,\epsilon),t^\epsilon), \tag{C.7}$$

using a Taylor approximation on the left-hand side of (C.7) with respect to ϵ and around $\epsilon = 0$, we can write

$$\boldsymbol{x}^+(t^\epsilon,\epsilon) = \boldsymbol{\alpha}^+(t^\epsilon) + \epsilon \boldsymbol{z}^+(t^\epsilon) + o(\epsilon), \tag{C.8}$$

$$\boldsymbol{u}^+(t^\epsilon,\epsilon) = \boldsymbol{\mu}^+(t^\epsilon) + \epsilon \boldsymbol{v}^+(t^\epsilon) + o(\epsilon), \tag{C.9}$$

where $\boldsymbol{\alpha}(t)$ is a nominal reference trajectory that satisfies the dynamics of the system and $\boldsymbol{\mu}(t)$ an input that achieves this reference trajectory. Now we expand this in terms of ϵ, so with

$$\Delta = \left.\frac{\partial t^\epsilon}{\partial \epsilon}\right|_{\epsilon=0}, \tag{C.10}$$

we get

$$\boldsymbol{\alpha}^+(t^\epsilon) = \boldsymbol{\alpha}^+(\tau) + \epsilon\dot{\boldsymbol{\alpha}}^+(\tau)\Delta + o(\epsilon), \tag{C.11}$$
$$\boldsymbol{\mu}^+(t^\epsilon) = \boldsymbol{\mu}^+(\tau) + \epsilon\dot{\boldsymbol{\mu}}^+(\tau)\Delta + o(\epsilon), \tag{C.12}$$
$$\boldsymbol{z}^+(t^\epsilon) = \boldsymbol{z}^+(\tau) + \epsilon\dot{\boldsymbol{z}}^+(\tau)\Delta + o(\epsilon), \tag{C.13}$$
$$\boldsymbol{v}^+(t^\epsilon) = \boldsymbol{v}^+(\tau) + \epsilon\dot{\boldsymbol{v}}^+(\tau)\Delta + o(\epsilon), \tag{C.14}$$

which when substituted into (C.8) and (C.9) gives,

$$\boldsymbol{x}^+(t^\epsilon, \epsilon) = \boldsymbol{\alpha}^+(\tau) + \epsilon\dot{\boldsymbol{\alpha}}^+(\tau)\Delta + \epsilon\boldsymbol{z}^+(\tau) + o(\epsilon). \tag{C.15}$$
$$\boldsymbol{u}^+(t^\epsilon, \epsilon) = \boldsymbol{\mu}^+(\tau) + \epsilon\dot{\boldsymbol{\mu}}^+(\tau)\Delta + \epsilon\boldsymbol{v}^+(\tau) + o(\epsilon). \tag{C.16}$$

To find Δ, we evaluate the ante impact guard function

$$\gamma^-(\boldsymbol{x}^-(t^\epsilon), \boldsymbol{u}^-(t^\epsilon), t^\epsilon) = 0. \tag{C.17}$$

In previous work, the guard function γ was not dependent on $\boldsymbol{u}(t^\epsilon)$ because friction and release was not considered. We now expand $\gamma(\boldsymbol{x}(t^\epsilon), \boldsymbol{u}(t^\epsilon), t^\epsilon)$ wrt ϵ, giving

$$\gamma(\boldsymbol{x}(t^\epsilon), \boldsymbol{u}(t^\epsilon), tt^\epsilon) = \gamma(\boldsymbol{\alpha}(\tau), \boldsymbol{\mu}(\tau), \tau) + \epsilon\left[\frac{\partial\gamma}{\partial\epsilon}(\boldsymbol{\alpha}(\tau), \boldsymbol{\mu}(\tau), \tau)\right]_{\epsilon=0} + o(\epsilon), \tag{C.18}$$
$$= \gamma(\boldsymbol{\alpha}(\tau), \boldsymbol{\mu}(\tau), \tau) + \epsilon\left[\frac{\partial\gamma}{\partial\boldsymbol{x}}\left(\frac{\partial\boldsymbol{x}}{\partial\epsilon} + \frac{\partial\boldsymbol{x}}{\partial tt^\epsilon}\frac{dt^\epsilon}{d\epsilon}\right) + \frac{\partial\gamma}{\partial\boldsymbol{u}}\left(\frac{\partial\boldsymbol{u}}{\partial\epsilon} + \frac{\partial\boldsymbol{u}}{\partial t^\epsilon}\frac{dt^\epsilon}{d\epsilon}\right) + \frac{\partial\gamma}{\partial t^\epsilon}\frac{dt^\epsilon}{d\epsilon}\right]_{\epsilon=0} + o(\epsilon). \tag{C.19}$$

By definition $\gamma(\tau) = 0$, so we can rewrite (C.19) to

$$\gamma(\boldsymbol{x}(t^\epsilon), \boldsymbol{u}(t^\epsilon), t^\epsilon) = \epsilon\left[D_1\gamma\cdot(\overline{\boldsymbol{z}}(\tau) + \dot{\boldsymbol{\alpha}}(\tau)\Delta) + D_2\gamma\cdot(\overline{\boldsymbol{v}}(\tau) + \dot{\boldsymbol{\mu}}(\tau)\Delta) + D_3\cdot\gamma\Delta\right] \tag{C.20}$$

Now we can evaluate (C.19) using (C.20), which gives

$$\epsilon\left[D_1\gamma^-\cdot\left(\boldsymbol{z}^-(\tau) + \dot{\boldsymbol{\alpha}}^-(\tau)\Delta\right) + D_2\gamma^-\cdot\left(\boldsymbol{v}^-(\tau) + \dot{\boldsymbol{\mu}}^-(\tau)\Delta\right) + D_3\gamma^-\cdot\Delta\right] = 0. \tag{C.21}$$

From (C.21) we can determine the expression for Δ,

$$\Delta = -\frac{D_1\gamma^-\cdot\boldsymbol{z}^-(\tau) + D_2\gamma^-\cdot\boldsymbol{v}^-(\tau)}{\dot{\gamma}^-}, \tag{C.22}$$

with

$$\gamma^- = \gamma^-(\boldsymbol{\alpha}^-(\tau), \boldsymbol{\mu}^-(\tau), \tau), \tag{C.23}$$
$$\dot{\gamma}^- = D_1\gamma^-\cdot\dot{\boldsymbol{\alpha}}^- + D_2\gamma^-\cdot\dot{\boldsymbol{\mu}}^- + D_3\gamma^-. \tag{C.24}$$

To find the expression for the right hand side of (C.7), we now expand $\boldsymbol{g}(\boldsymbol{x}^-(t^\epsilon, \epsilon), \boldsymbol{u}^-(t^\epsilon, \epsilon), t^\epsilon)$ with respect to ϵ as

$$\boldsymbol{g}(\boldsymbol{x}^-, \boldsymbol{u}^-, t^\epsilon) = \boldsymbol{g}(\boldsymbol{\alpha}^-(\tau), \tau) + \epsilon \left[\frac{\partial \boldsymbol{g}}{\partial \epsilon}\right] + o(\epsilon), \tag{C.25}$$

$$= \boldsymbol{\alpha}^+(\tau) + \epsilon \left[\frac{\partial \boldsymbol{g}}{\partial \boldsymbol{x}}\left(\frac{\partial \boldsymbol{x}}{\partial \epsilon} + \frac{\partial \boldsymbol{x}}{\partial t^\epsilon}\frac{dt^\epsilon}{d\epsilon}\right) + \frac{\partial \boldsymbol{g}}{\partial \boldsymbol{u}}\left(\frac{\partial \boldsymbol{u}}{\partial \epsilon} + \frac{\partial \boldsymbol{u}}{\partial t^\epsilon}\frac{dt^\epsilon}{d\epsilon}\right) + \frac{\partial \boldsymbol{g}}{\partial t^\epsilon}\frac{dt^\epsilon}{d\epsilon}\right]_{\epsilon=0} + o(\epsilon), \tag{C.26}$$

$$= \boldsymbol{\alpha}^+(\tau) + \epsilon \left[D_1\boldsymbol{g} \cdot \left(\boldsymbol{z}^- + \dot{\boldsymbol{\alpha}}^-\Delta\right) + D_2\boldsymbol{g} \cdot \left(\boldsymbol{v}^- + \dot{\boldsymbol{\mu}}(\tau)\Delta\right) + D_3\boldsymbol{g} \cdot \Delta\right] + o(\epsilon). \tag{C.27}$$

For small ϵ, we can rewrite (C.7), (C.22) and (C.27) to a general jump map with counter k as

$$\boldsymbol{x}^+(t^\epsilon, \epsilon) = \boldsymbol{g}(\boldsymbol{x}^-, \boldsymbol{u}^-, t^\epsilon) =: \boldsymbol{g}^-, \tag{C.28}$$

$$\Delta = -\frac{D_1\gamma \cdot \boldsymbol{z}^-(\tau) + D_2\gamma \cdot \boldsymbol{v}^-(\tau)}{\dot{\gamma}}, \tag{C.29}$$

$$\boldsymbol{g}^- = \boldsymbol{\alpha}^+(\tau) + \epsilon \left[D_1\boldsymbol{g}^- \cdot \left(\boldsymbol{z}^-(\tau) + \dot{\boldsymbol{\alpha}}^-\Delta\right) + D_2\boldsymbol{g}^- \cdot \left(\boldsymbol{v}^-(\tau) + \dot{\boldsymbol{\mu}}^-\Delta\right) + D_3\boldsymbol{g}^- \cdot \Delta\right]. \tag{C.30}$$

From (C.15) we get

$$\boldsymbol{z}^+(\tau) = \frac{1}{\epsilon}\left(\boldsymbol{x}^+(t^\epsilon) - \boldsymbol{\alpha}^+(\tau)\right) - \dot{\boldsymbol{\alpha}}^+(\tau)\Delta, \tag{C.31}$$

and by equating (C.28) and (C.30) we find an expression for $\overline{\boldsymbol{x}}^+(t^\epsilon, \epsilon)$ which we can substitute into (C.31) resulting in

$$\boldsymbol{z}^+(\tau) = D_1\boldsymbol{g}^- \cdot \left(\boldsymbol{z}^-(\tau) + \dot{\boldsymbol{\alpha}}^-\Delta\right) + D_2\boldsymbol{g}^- \cdot \left(\boldsymbol{v}^-(\tau) + \dot{\boldsymbol{\mu}}^-\Delta\right) + D_3\boldsymbol{g}^- \cdot \Delta - \dot{\boldsymbol{\alpha}}^-(\tau)\Delta. \tag{C.32}$$

Now, by substituting (C.29) into (C.32), we get

$$\boldsymbol{z}^+(\tau) = -\left(D_1\boldsymbol{g}^- \cdot \boldsymbol{f}^- + D_2\boldsymbol{g}^- \cdot \dot{\boldsymbol{\mu}}^- + D_3\boldsymbol{g}^- \cdot 1 - \boldsymbol{f}^+\right)\frac{D_1\gamma^- \cdot \boldsymbol{z}^- + D_2\gamma^- \cdot \boldsymbol{v}^-}{\dot{\gamma}^-} + D_1\boldsymbol{g}^- \cdot \boldsymbol{z}^- + D_2\boldsymbol{g}^- \cdot \boldsymbol{v}^-, \tag{C.33}$$

$$\boldsymbol{z}^+(\tau) = \left(D_1\boldsymbol{g}^- - \left(\dot{\boldsymbol{g}}^- - \boldsymbol{f}^+\right)\frac{D_1\gamma^-}{\dot{\gamma}^-}\right) \cdot \boldsymbol{z}^- + \left(D_2\boldsymbol{g}^- - \left(\dot{\boldsymbol{g}}^- - \boldsymbol{f}^+\right)\frac{D_2\gamma^-}{\dot{\gamma}^-}\right) \cdot \boldsymbol{v}^-, \tag{C.34}$$

with

$$\dot{\boldsymbol{g}}^- = D_1\boldsymbol{g}^- \cdot \boldsymbol{f}^- + D_2\boldsymbol{g}^- \cdot \dot{\boldsymbol{\mu}}^- + D_3\boldsymbol{g}^- \cdot 1, \tag{C.35}$$

$$\boldsymbol{f}^+ = \boldsymbol{f}(\boldsymbol{\alpha}^+(\tau), \boldsymbol{\mu}^+(\tau), \tau), \tag{C.36}$$

$$\boldsymbol{f}^- = \boldsymbol{f}(\boldsymbol{\alpha}^-(\tau), \boldsymbol{\mu}^-(\tau), \tau). \tag{C.37}$$

Now, using

$$\boldsymbol{G}(\tau) = D_1\boldsymbol{g}^- - \left(\dot{\boldsymbol{g}}^- - \boldsymbol{f}^+\right)\frac{D_1\gamma^-}{\dot{\gamma}^-}, \tag{C.38}$$

$$\boldsymbol{J}(\tau) = D_2\boldsymbol{g}^- - \left(\dot{\boldsymbol{g}}^- - \boldsymbol{f}^+\right)\frac{D_2\gamma^-}{\dot{\gamma}^-}, \tag{C.39}$$

we can write

$$\boldsymbol{z}^+(\tau) = \boldsymbol{G}\boldsymbol{z}^- + \boldsymbol{J}\boldsymbol{v}^-. \tag{C.40}$$

C.2 Linearized jump gain for simultaneous events

We now assume that we find the first order approximation of the perturbed post-impact state of two simultaneous jumps, by considering these jumps after each other as

$$
\begin{aligned}
{}^{s^{k+1}}\boldsymbol{z}(\tau) &= \boldsymbol{G}^{k+1\ s^k}\boldsymbol{z} + \boldsymbol{J}^{k+1\ s^k}\boldsymbol{v} && \text{(C.41)}\\
{}^{s^{k+1}}\boldsymbol{z}(\tau) &= \boldsymbol{G}^{k+1}\left(\boldsymbol{G}^{k\ s^{k-1}}\boldsymbol{z} + \boldsymbol{J}^{k\ s^{k-1}}\boldsymbol{v}\right) + \boldsymbol{G}^{k+1\ s^k}\boldsymbol{v}, && \text{(C.42)}\\
&= \boldsymbol{G}^{k+1}\boldsymbol{G}^{k\ s^{k-1}}\boldsymbol{z} + \boldsymbol{G}^{k+1}\boldsymbol{J}^{k\ s^{k-1}}\boldsymbol{v} + \boldsymbol{J}^{k+1\ s^k}\boldsymbol{v}. && \text{(C.43)}
\end{aligned}
$$

We prove that this is true by deriving an expression for the post-impact state of two simultaneous jumps, and comparing it with (C.43). Now we evaluate the jump map of two jumps at the same time instant τ,

$$
{}^{s^{k+1}}\boldsymbol{x}^\epsilon(t^{k+1}) = {}^{s^{k+1}\leftarrow s^k}\boldsymbol{g}({}^{s^k}\boldsymbol{x}^\epsilon(t^{k+1}), {}^{s^k}\boldsymbol{u}^\epsilon(t^{k+1}), t^{k+1}), \tag{C.44}
$$

with

$$
{}^{s^k}\boldsymbol{x}^\epsilon(t^{k+1}) = \int_{t^k}^{t^{k+1}} \left[{}^{s^k}\boldsymbol{f}\left({}^{s^k}\boldsymbol{x}^\epsilon(), {}^{s^k}\boldsymbol{u}^\epsilon(t)\right)\right] dt + {}^{s^k}\boldsymbol{g}({}^{s^{k-1}}\boldsymbol{x}^\epsilon(t^k), {}^{s^{k-1}}\boldsymbol{u}^\epsilon(t^k), t^k). \tag{C.45}
$$

We rewrite the integral in (C.45) to

$$
\int_{t^k}^{t^{k+1}} {}^{s^k}\boldsymbol{f}(t,\epsilon)dt = \boldsymbol{F}(t^{k+1},\epsilon) - \boldsymbol{F}(t^k,\epsilon) = \boldsymbol{\Phi}(t^k, t^{k+1}, \epsilon), \tag{C.46}
$$

where ${}^{s^k}\boldsymbol{f}\left({}^{s^k}\boldsymbol{x}^\epsilon(t), {}^{s^k}\boldsymbol{u}^\epsilon(t)\right)$ can be written as ${}^{s^k}\boldsymbol{f}(t,\epsilon)$, because $\boldsymbol{x}^\epsilon$ and $\boldsymbol{u}^\epsilon$ depend solely on t and ϵ. We now expand $\boldsymbol{\Phi}$ with respect to ϵ, which results in

$$
\begin{aligned}
\boldsymbol{\Phi}(t^k, t^{k+1}, \epsilon) &= \boldsymbol{\Phi}(\tau^k, \tau^{k+1}, \epsilon) + \epsilon \left.\frac{\partial \boldsymbol{\Phi}}{\partial \epsilon}\right|_{\epsilon=0} + o(\epsilon), && \text{(C.47)}\\
&= \boldsymbol{F}(\tau,0) - \boldsymbol{F}(\tau,0) + \left[{}^{s^k}\boldsymbol{f}(t^{k+1},\epsilon)\frac{dt^{k+1}}{d\epsilon} - {}^{s^k}\boldsymbol{f}(t^{k+1},\epsilon)\frac{dt^k}{d\epsilon} + \int_{t^k}^{t^{k+1}} \frac{\partial^{s^k}\boldsymbol{f}}{\partial\epsilon}dt\right]_{\epsilon=0}, && \text{(C.48)}\\
&= {}^{s^k}\boldsymbol{f}(\Delta^{k+1} - \Delta^k), && \text{(C.49)}
\end{aligned}
$$

since $\tau^k = \tau^{k+1} = \tau$, and $\left.\int_{t^k}^{t^{k+1}} \frac{\partial^{s^k}\boldsymbol{f}(t,\epsilon)}{\partial\epsilon}dt\right|_{\epsilon=0} = 0$. Here ${}^{s^k}\boldsymbol{f} = {}^{s^k}\boldsymbol{f}({}^{s^k}\boldsymbol{\alpha}(\tau), {}^{s^k}\boldsymbol{\mu}(\tau), \tau)$. Note that ϵ is assumed sufficiently small, such that we can write t as a function of ϵ. By expanding (C.44) with respect to ϵ, we find

$$
{}^{s^{k+1}}\boldsymbol{x}^\epsilon(t^{k+1}) = {}^{s^{k+1}}\boldsymbol{\alpha}(\tau) + \epsilon \left.\frac{\partial^{s^{k+1}}\boldsymbol{g}({}^{s^k}\boldsymbol{x}^\epsilon(t^{k+1}), {}^{s^k}\boldsymbol{u}^\epsilon(t^{k+1}), t^{k+1})}{\partial\epsilon}\right|_{\epsilon=0} + o(\epsilon), \tag{C.50}
$$

with

$$
\left.\frac{\partial^{s^{k+1}}\boldsymbol{g}}{\partial\epsilon}\right|_{\epsilon=0} = \left[\frac{\partial^{s^{k+1}}\boldsymbol{g}}{\partial\boldsymbol{x}}\left(\frac{\partial^{s^k}\boldsymbol{x}}{\partial\epsilon} + \frac{\partial^{s^k}\boldsymbol{x}}{\partial t}\frac{\mathrm{d}t^{k+1}}{\mathrm{d}\epsilon}\right) + \frac{\partial^{s^{k+1}}\boldsymbol{g}}{\partial\boldsymbol{u}}\left(\frac{\partial^{s^k}\boldsymbol{u}}{\partial\epsilon} + \frac{\partial^{s^k}\boldsymbol{u}}{\partial t}\frac{\mathrm{d}t^{k+1}}{\mathrm{d}\epsilon}\right) + \frac{\partial^{s^{k+1}}\boldsymbol{g}}{\partial t}\frac{\mathrm{d}t^{k+1}}{\mathrm{d}\epsilon}\right]_{\epsilon=0}, \tag{C.51}
$$

$$\left.\frac{\partial^{s^{k+1}}\boldsymbol{g}}{\partial\epsilon}\right|_{\epsilon=0} = \Bigg[D_1{}^{s^{k+1}}\boldsymbol{g}\left(\frac{\partial\boldsymbol{\Phi}}{\partial\epsilon}+D_1{}^{s^k}\boldsymbol{g}\left(\frac{\partial^{s^{k-1}}\boldsymbol{x}}{\partial\epsilon}+\frac{\partial^{s^{k-1}}\boldsymbol{x}}{\partial t}\frac{\mathrm{d}t^k}{\mathrm{d}\epsilon}\right)+D_2{}^{s^k}\boldsymbol{g}\left(\frac{\partial^{s^{k-1}}\boldsymbol{u}}{\partial\epsilon}+\frac{\partial^{s^{k-1}}\boldsymbol{u}}{\partial t}\frac{\mathrm{d}t^k}{\mathrm{d}\epsilon}\right)$$
$$+D_3{}^{s^k}\boldsymbol{g}\frac{\mathrm{d}t^k}{\mathrm{d}\epsilon}\right)+D_2{}^{s^{k+1}}\boldsymbol{g}\left(\frac{\partial^{s^k}\boldsymbol{u}}{\partial\epsilon}+\frac{\partial^{s^k}\boldsymbol{u}}{\partial t}\frac{\mathrm{d}t^{k+1}}{\mathrm{d}\epsilon}\right)+D_3{}^{s^{k+1}}\boldsymbol{g}\frac{\mathrm{d}t^{k+1}}{\mathrm{d}\epsilon}\Bigg]_{\epsilon=0}, \quad \text{(C.52)}$$

$$\left.\frac{\partial^{s^{k+1}}\boldsymbol{g}}{\partial\epsilon}\right|_{\epsilon=0} = D_1{}^{s^{k+1}}\boldsymbol{g}\cdot\left({}^{s^k}\dot{\boldsymbol{\alpha}}(\Delta^{k+1}-\Delta^k)+D_1{}^{s^k}\boldsymbol{g}\cdot\left({}^{s^{k-1}}\boldsymbol{z}+{}^{s^{k-1}}\dot{\boldsymbol{\alpha}}\Delta^k\right)+D_2{}^{s^k}\boldsymbol{g}\cdot\left({}^{s^{k-1}}\boldsymbol{v}+{}^{s^{k-1}}\dot{\boldsymbol{\mu}}\Delta^k\right)\right.$$
$$\left.+D_3{}^{s^k}\boldsymbol{g}\cdot\Delta^k\right)+D_2{}^{s^{k+1}}\boldsymbol{g}\cdot\left({}^{s^k}\boldsymbol{v}+{}^{s^k}\dot{\boldsymbol{\mu}}\Delta^{k+1}\right)+D_3{}^{s^{k+1}}\boldsymbol{g}\cdot\Delta^{k+1}. \quad \text{(C.53)}$$

We now substitute (C.53) into (C.50), which we in turn substitute into (C.31) to get

$${}^{s^{k+1}}\boldsymbol{z}(\tau) = D_1{}^{s^{k+1}}\boldsymbol{g}\cdot{}^{s^k}\boldsymbol{f}\Delta^{k+1}-D_1{}^{s^{k+1}}\boldsymbol{g}\cdot{}^{s^k}\boldsymbol{f}\Delta^k+D_1{}^{s^{k+1}}\boldsymbol{g}\cdot\left(D_1{}^{s^k}\boldsymbol{g}\cdot\left({}^{s^{k-1}}\boldsymbol{z}+{}^{s^{k-1}}\boldsymbol{f}\Delta^k\right)\right.$$
$$\left.+D_2{}^{s^k}\boldsymbol{g}\cdot\left({}^{s^{k-1}}\boldsymbol{v}+{}^{s^{k-1}}\dot{\boldsymbol{\mu}}\Delta^k\right)+D_3{}^{s^k}\boldsymbol{g}\cdot\Delta^k\right)+D_2{}^{s^{k+1}}\boldsymbol{g}\cdot\left({}^{s^k}\boldsymbol{v}+{}^{s^k}\dot{\boldsymbol{\mu}}\Delta^{k+1}\right)+\left(D_3{}^{s^{k+1}}\boldsymbol{g}-{}^{s^{k+1}}\boldsymbol{f}\right)\Delta^{k+1}, \quad \text{(C.54)}$$

with ${}^{s^k}\boldsymbol{f}={}^{s^k}\boldsymbol{f}({}^{s^k}\boldsymbol{\alpha}(\tau),{}^{s^k}\boldsymbol{\mu}(\tau),\tau)$. The five terms in (C.54) can be rewritten into

$$D_1{}^{s^{k+1}}\boldsymbol{g}\cdot{}^{s^k}\boldsymbol{f}\Delta^{k+1} = -\frac{D_1{}^{s^{k+1}}\boldsymbol{g}\cdot{}^{s^{k+1}}\boldsymbol{f}}{\dot{\gamma}^{k+1}}\left(D_1\gamma^{k+1}\cdot\left(\boldsymbol{G}^{k\ s^{k-1}}\boldsymbol{z}+\boldsymbol{J}^{k\ s^{k-1}}\boldsymbol{v}\right)+D_2\gamma^{k+1}\cdot{}^{s^k}\boldsymbol{v}\right), \quad \text{(C.55)}$$

$$-D_1{}^{s^{k+1}}\boldsymbol{g}\cdot{}^{s^k}\boldsymbol{f}\Delta^k = \frac{D_1{}^{s^{k+1}}\boldsymbol{g}\cdot{}^{s^k}\boldsymbol{f}}{\dot{\gamma}^k}\left(D_1\gamma^k\cdot{}^{s^{k-1}}\boldsymbol{z}+D_2\gamma^k\cdot{}^{s^{k-1}}\boldsymbol{v}\right), \quad \text{(C.56)}$$

$$D_1{}^{s^{k+1}}\boldsymbol{g}\cdot\left(D_1{}^{s^k}\boldsymbol{g}\cdot\left({}^{s^{k-1}}\boldsymbol{z}+{}^{s^{k-1}}\boldsymbol{f}\Delta^k\right)+D_2{}^{s^k}\boldsymbol{g}\cdot\left({}^{s^{k-1}}\boldsymbol{v}+{}^{s^{k-1}}\dot{\boldsymbol{\mu}}\Delta^k\right)+D_3{}^{s^k}\boldsymbol{g}\cdot\Delta^k\right)=$$
$$D_1{}^{s^{k+1}}\boldsymbol{g}\cdot\left(-\frac{D_1{}^{s^k}\boldsymbol{g}\cdot{}^{s^{k-1}}\boldsymbol{f}}{\dot{\gamma}^k}D_1\gamma^k-\frac{D_2{}^{s^k}\boldsymbol{g}\cdot{}^{s^{k-1}}\dot{\boldsymbol{\mu}}}{\dot{\gamma}^k}D_1\gamma^k-\frac{D_3{}^{s^k}\boldsymbol{g}\cdot 1}{\dot{\gamma}^k}D_1\gamma^k+D_1{}^{s^k}\boldsymbol{g}\right)\cdot{}^{s^{k-1}}\boldsymbol{z}$$
$$+D_1{}^{s^{k+1}}\boldsymbol{g}\cdot\left(-\frac{D_1{}^{s^k}\boldsymbol{g}\cdot{}^{s^{k-1}}\boldsymbol{f}}{\dot{\gamma}^k}D_2\gamma^k-\frac{D_2{}^{s^k}\boldsymbol{g}\cdot{}^{s^{k-1}}\dot{\boldsymbol{\mu}}}{\dot{\gamma}^k}D_2\gamma^k-\frac{D_3{}^{s^k}\boldsymbol{g}\cdot 1}{\dot{\gamma}^k}D_2\gamma^k+D_2{}^{s^k}\boldsymbol{g}\right)\cdot{}^{s^{k-1}}\boldsymbol{v}, \quad \text{(C.57)}$$

$$D_2{}^{s^{k+1}}\boldsymbol{g}\cdot\left({}^{s^k}\boldsymbol{v}+{}^{s^k}\dot{\boldsymbol{\mu}}\Delta^{k+1}\right) = -\frac{D_2{}^{s^{k+1}}\boldsymbol{g}\cdot{}^{s^k}\dot{\boldsymbol{\mu}}}{\dot{\gamma}^{k+1}}D_1\gamma^{k+1}\cdot\boldsymbol{G}^{k\ s^{k-1}}\boldsymbol{z}-\frac{D_2{}^{s^{k+1}}\boldsymbol{g}\cdot{}^{s^k}\dot{\boldsymbol{\mu}}}{\dot{\gamma}^{k+1}}D_1\gamma^{k+1}\cdot\boldsymbol{J}^{k\ s^{k-1}}\boldsymbol{v}$$
$$+\left(D_2{}^{s^{k+1}}\boldsymbol{g}-\frac{D_2{}^{s^{k+1}}\boldsymbol{g}\cdot{}^{s^k}\dot{\boldsymbol{\mu}}}{\dot{\gamma}^{k+1}}D_2\gamma^{k+1}\right)\cdot{}^{s^k}\boldsymbol{v}, \quad \text{(C.58)}$$

$$\left(D_3{}^{s^{k+1}}\boldsymbol{g}\cdot 1-{}^{s^{k+1}}\boldsymbol{f}\right)\Delta^{k+1} = -\frac{D_3{}^{s^{k+1}}\boldsymbol{g}\cdot 1+{}^{s^{k+1}}\boldsymbol{f}}{\dot{\gamma}^{k+1}}\left(D_1\gamma^{k+1}\cdot\left(\boldsymbol{G}^{k\ s^{k-1}}\boldsymbol{z}+\boldsymbol{J}^{k\ s^{k-1}}\boldsymbol{v}\right)+D_2\gamma^{k+1}\cdot{}^{s^k}\boldsymbol{v}\right). \quad \text{(C.59)}$$

When we substitute the equations above into (C.54), after reordering the expression we get

$$
\begin{aligned}
{}^{s^{k+1}}\boldsymbol{z}(\tau) = &\left(\frac{{}^{s^{k+1}}\boldsymbol{f} - D_1{}^{s^{k+1}}\boldsymbol{g} \cdot {}^{s^k}\boldsymbol{f} - D_2{}^{s^{k+1}}\boldsymbol{g} \cdot {}^{s^k}\dot{\boldsymbol{\mu}} - D_3{}^{s^{k+1}}\boldsymbol{g} \cdot 1}{\dot{\gamma}^{k+1}} D_1\gamma^{k+1} \cdot \boldsymbol{G}^k \right. \\
&\left. + D_1{}^{s^{k+1}}\boldsymbol{g} \cdot \frac{{}^{s^k}\boldsymbol{f} - D_1{}^{s^k}\boldsymbol{g} \cdot {}^{s^{k-1}}\boldsymbol{f} - D_2{}^{s^k}\boldsymbol{g} \cdot {}^{s^{k-1}}\dot{\boldsymbol{\mu}} - D_3{}^{s^k}\boldsymbol{g} \cdot 1}{\dot{\gamma}^k} D_1\gamma^{k+1} + D_1{}^{s^{k+1}}\boldsymbol{g} D_1{}^{s^k}\boldsymbol{g} \cdot 1 \right) {}^{s^{k-1}}\boldsymbol{z} \\
&+ \left(\frac{{}^{s^{k+1}}\boldsymbol{f} - D_1{}^{s^{k+1}}\boldsymbol{g} \cdot {}^{s^k}\boldsymbol{f} - D_2{}^{s^{k+1}}\boldsymbol{g} \cdot {}^{s^k}\dot{\boldsymbol{\mu}} - D_3{}^{s^{k+1}}\boldsymbol{g} \cdot 1}{\dot{\gamma}^{k+1}} D_1\gamma^{k+1} \cdot \boldsymbol{J}^k \right. \\
&\left. + D_1{}^{s^{k+1}}\boldsymbol{g} \cdot \frac{{}^{s^k}\boldsymbol{f} - D_1{}^{s^k}\boldsymbol{g} \cdot {}^{s^{k-1}}\boldsymbol{f} - D_2{}^{s^k}\boldsymbol{g} \cdot {}^{s^{k-1}}\dot{\boldsymbol{\mu}} - D_3{}^{s^k}\boldsymbol{g} \cdot 1}{\dot{\gamma}^k} D_2\gamma^{k+1} + D_1{}^{s^{k+1}}\boldsymbol{g} D_2{}^{s^k}\boldsymbol{g} \cdot 1 \right) {}^{s^{k-1}}\boldsymbol{v} \\
&+ \left(\frac{{}^{s^{k+1}}\boldsymbol{f} - D_1{}^{s^{k+1}}\boldsymbol{g} \cdot {}^{s^k}\boldsymbol{f} - D_2{}^{s^{k+1}}\boldsymbol{g} \cdot {}^{s^k}\dot{\boldsymbol{\mu}} - D_3{}^{s^{k+1}}\boldsymbol{g} \cdot 1}{\dot{\gamma}^{k+1}} D_2\gamma^{k+1} \right) {}^{s^k}\boldsymbol{v}, \quad \text{(C.60)}
\end{aligned}
$$

from which we can isolate $\boldsymbol{G}^k$, and $\boldsymbol{J}^k$ resulting in

$$
\begin{aligned}
{}^{s^{k+1}}\boldsymbol{z}(\tau) = &\left(\frac{{}^{s^{k+1}}\boldsymbol{f} - D_1{}^{s^{k+1}}\boldsymbol{g} \cdot {}^{s^k}\boldsymbol{f} - D_2{}^{s^{k+1}}\boldsymbol{g} \cdot {}^{s^k}\dot{\boldsymbol{\mu}} - D_3{}^{s^{k+1}}\boldsymbol{g} \cdot 1}{\dot{\gamma}^{k+1}} D_1\gamma^{k+1} + D_1{}^{s^{k+1}}\boldsymbol{g} \cdot 1 \right) \boldsymbol{G}^k \, {}^{s^{k-1}}\boldsymbol{z} \\
&+ \left(\frac{{}^{s^{k+1}}\boldsymbol{f} - D_1{}^{s^{k+1}}\boldsymbol{g} \cdot {}^{s^k}\boldsymbol{f} - D_2{}^{s^{k+1}}\boldsymbol{g} \cdot {}^{s^k}\dot{\boldsymbol{\mu}} - D_3{}^{s^{k+1}}\boldsymbol{g} \cdot 1}{\dot{\gamma}^{k+1}} D_1\gamma^{k+1} + D_1{}^{s^{k+1}}\boldsymbol{g} \cdot 1 \right) \boldsymbol{J}^k \, {}^{s^{k-1}}\boldsymbol{v} \\
&+ \left(\frac{{}^{s^{k+1}}\boldsymbol{f} - D_1{}^{s^{k+1}}\boldsymbol{g} \cdot {}^{s^k}\boldsymbol{f} - D_2{}^{s^{k+1}}\boldsymbol{g} \cdot {}^{s^k}\dot{\boldsymbol{\mu}} - D_3{}^{s^{k+1}}\boldsymbol{g} \cdot 1}{\dot{\gamma}^{k+1}} D_2\gamma^{k+1} + D_2{}^{s^{k+1}}\boldsymbol{g} \cdot 1 \right) {}^{s^k}\boldsymbol{v}, \quad \text{(C.61)}
\end{aligned}
$$

which is equal to

$$
{}^{s^{k+1}}\boldsymbol{z}(\tau) = \boldsymbol{G}^{k+1}\boldsymbol{G}^k \, {}^{s^{k-1}}\boldsymbol{z} + \boldsymbol{G}^{k+1}\boldsymbol{J}^k \, {}^{s^{k-1}}\boldsymbol{v} + \boldsymbol{J}^{k+1} \, {}^{s^k}\boldsymbol{v}. \quad \text{(C.62)}
$$

Here we see that (C.62) is equal to (C.43). This proves that for any k, the first-order approximation of the post-impact state of two simultaneous jumps at τ can be found by evaluating the two jumps separately. Since k is a variable in this proof, using an induction-like proof, this holds for any amount of jumps as well. This is illustrated in Figure C.1.

When we take $k = 1$, we show that the jumps from 0 to 2 can be described by evaluating the jump from 0 to 1 and the jump 1 to 2 in succession. This also holds for $k = 2$. The jump from 0 to 3 can be described by evaluating the jump from 0 to 2 and the jump from 2 to 3 in succession. This indicates that we can use (C.62) to find an expression for the approximation of the post-impact state for l simultaneous jumps, with $l \in \mathbb{Z}$. Also, we show that multiple constant jump gains will result in a total jump which can also be described by a constant jump gain.

Intuitively, for l simultaneous jumps, we can find the approximation of the post-impact state using

$$
{}^{l\leftarrow 0}\boldsymbol{z}(\tau) = {}^{l\leftarrow 0}\boldsymbol{L}(\boldsymbol{z}^0(\tau), \boldsymbol{v}(\tau), \tau) = {}^{l\leftarrow 0}\boldsymbol{G}\boldsymbol{z}^0(\tau) + \sum_{i=0}^{l-1} \left({}^{l\leftarrow i+1}\boldsymbol{G} \, {}^{i+1\leftarrow i}\boldsymbol{J}\boldsymbol{v}^i(\tau) \right), \quad \text{(C.63)}
$$

where the superscript

$$
b \leftarrow a = b \leftarrow (b-1) \leftarrow \cdots \leftarrow (a+1) \leftarrow a, \quad \text{(C.64)}
$$

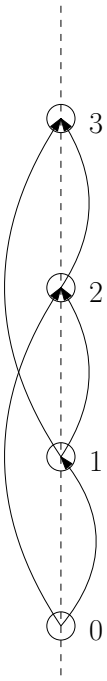

Figure C.1: *This figure illustrates how the derivation of the jump gain for two simultaneous jumps can be extended intuitively to a jump gain for an arbitrary number of simultaneous jumps.*

and

$$ {}^{b\leftarrow a}\boldsymbol{G} = {}^{b\leftarrow(b-1)}\boldsymbol{G}\cdots\ {}^{(a+2)\leftarrow(a+1)}\boldsymbol{G}^{(a+1)\leftarrow a}\boldsymbol{G}, \tag{C.65} $$

$$ {}^{b\leftarrow a}\boldsymbol{J} = {}^{b\leftarrow(b-1)}\boldsymbol{J}\cdots\ {}^{(a+2)\leftarrow(a+1)}\boldsymbol{J}^{(a+1)\leftarrow a}\boldsymbol{J}, \tag{C.66} $$

with slight abuse of notation, in the sense that $b-1$ indicates the mode-descriptor that describes the mode before the mode that is desribed by b.

C.3 Positive homogeneity

The approximation of the perturbed trajectory $\boldsymbol{x}$ can be found using $\boldsymbol{\alpha}+\epsilon\boldsymbol{z}$, with

$$ \begin{aligned} {}^{s^{k-1}}\dot{\boldsymbol{z}} &= {}^{s^{k-1}}\boldsymbol{A}(t)^{s^{k-1}}\boldsymbol{z} + {}^{s^{k-1}}\boldsymbol{B}(t)^{s^{k-1}}\boldsymbol{v}, \\ {}^{s^k}\boldsymbol{z} &= {}^{s^k\leftarrow s^{k-1}}\boldsymbol{H}\left({}^{s^{k-1}}\boldsymbol{z}, {}^{s^{k-1}}\boldsymbol{v}, t\right), \\ {}^{s^k}\dot{\boldsymbol{z}} &= {}^{s^k}\boldsymbol{A}(t)^{s^k}\boldsymbol{z} + {}^{s^k}\boldsymbol{B}(t)^{s^{k-1}}\boldsymbol{v}, \end{aligned} \tag{C.67} $$

where

$$ {}^{s^k}\boldsymbol{A}(t) = D_1{}^{s^k}\boldsymbol{f}\left({}^{s^k}\boldsymbol{\alpha}(t), {}^{s^k}\boldsymbol{\mu}(t), t\right), \tag{C.68} $$

$$ {}^{s^k}\boldsymbol{B}(t) = D_2{}^{s^k}\boldsymbol{f}\left({}^{s^k}\boldsymbol{\alpha}(t), {}^{s^k}\boldsymbol{\mu}(t), t\right). \tag{C.69} $$

When we look at (C.67), the continuous dynamics of the system are linear. Because of the positively homogeneous jump gain $\boldsymbol{H}$ however, this linearity property is lost. We can see this by looking at

the general solution of (C.67). A system $\boldsymbol{f}(\boldsymbol{x}, \boldsymbol{u}, t)$ with state $\boldsymbol{x}$ and input $\boldsymbol{u}$ is linear if $\boldsymbol{f}(\boldsymbol{x}_1, \boldsymbol{v}_1) + \boldsymbol{f}(\boldsymbol{x}_2, \boldsymbol{v}_2) = \boldsymbol{f}(\boldsymbol{x}_1 + \boldsymbol{x}_2, \boldsymbol{v}_1 + \boldsymbol{v}_2)$. The solutions of (C.67) before the jump are in the form of

$$ {}^{s^{k-1}}\boldsymbol{z}_1(\tau) = {}^{s^{k-1}}\boldsymbol{\phi}(t, t_0)^{s^{k-1}}\boldsymbol{z}_1(t_0) + \int_{t_0}^{\tau} \left[{}^{s^{k-1}}\boldsymbol{\phi}(t, s)^{s^{k-1}}\boldsymbol{B}(s)\boldsymbol{v}_1(s) \right] ds, \tag{C.70} $$

$$ {}^{s^{k-1}}\boldsymbol{z}_2(\tau) = {}^{s^{k-1}}\boldsymbol{\phi}(t, t_0)^{s^{k-1}}\boldsymbol{z}_2(t_0) + \int_{t_0}^{\tau} \left[{}^{s^{k-1}}\boldsymbol{\phi}(t, s)^{s^{k-1}}\boldsymbol{B}(s)\boldsymbol{v}_2(s) \right] ds, \tag{C.71} $$

with t_0 the initial time and τ the jump time. When we add these solutions together we find

$$ {}^{s^{k-1}}\boldsymbol{z}_1(\tau) + {}^{s^{k-1}}\boldsymbol{z}_2(\tau) = {}^{s^{k-1}}\boldsymbol{\phi}(t, t_0) \left({}^{s^{k-1}}\boldsymbol{z}_1(t_0) + {}^{s^{k-1}}\boldsymbol{z}_2(t_0) \right) + \int_{t_0}^{\tau} \left[{}^{s^{k-1}}\boldsymbol{\phi}(t, s)^{s^{k-1}}\boldsymbol{B}(s) \left(\boldsymbol{v}_1(s) + \boldsymbol{v}_2(s) \right) \right] ds, \tag{C.72} $$

which is equal to the solution of ${}^{s^{k-1}}\boldsymbol{z}_3(t_0) = {}^{s^{k-1}}\boldsymbol{z}_1(t_0) + {}^{s^{k-1}}\boldsymbol{z}_2(t_0)$ with $\boldsymbol{v}_3(t) = \boldsymbol{v}_1(t) + \boldsymbol{v}_2(t)$, i.e., the linearity property holds. When ${}^{s^{k-1}}\boldsymbol{z}_1$ jumps with $\boldsymbol{G}^1(\boldsymbol{z}, \tau)$ and ${}^{s^{k-1}}\boldsymbol{z}_1(\tau)$ jumps with $\boldsymbol{G}^2(\boldsymbol{z}, \tau)$ we find the solutions post jump to be

$$ {}^{s^k}\boldsymbol{z}_1(\tau) = {}^{s^k}\boldsymbol{\phi}(t, t_0)\ \boldsymbol{G}^1({}^{s^{k-1}}\boldsymbol{z}_1(t_0), \tau) + \int_{t_0}^{\tau} \left[{}^{s^k}\boldsymbol{\phi}(t, s)^{s^k}\boldsymbol{B}(s)\boldsymbol{v}_1(s) \right] ds, \tag{C.73} $$

$$ {}^{s^k}\boldsymbol{z}_2(\tau) = {}^{s^k}\boldsymbol{\phi}(t, t_0)\ \boldsymbol{G}^2({}^{s^{k-1}}\boldsymbol{z}_2(t_0), \tau) + \int_{t_0}^{\tau} \left[{}^{s^k}\boldsymbol{\phi}(t, s)^{s^k}\boldsymbol{B}(s)\boldsymbol{v}_2(s) \right] ds, \tag{C.74} $$

which when added together results in

$$ {}^{s^k}\boldsymbol{z}_1(\tau) + {}^{s^k}\boldsymbol{z}_2(\tau) = {}^{s^k}\boldsymbol{\phi}(t, t_0) \left(\boldsymbol{G}^{1s^{k-1}}\boldsymbol{z}_1 + \boldsymbol{J}^{1s^{k-1}}\boldsymbol{v}_1 + \boldsymbol{G}^{2s^{k-1}}\boldsymbol{z}_2 + \boldsymbol{J}^{2s^{k-1}}\boldsymbol{v}_2 \right) + \int_{t_0}^{\tau} \left[{}^{s^k}\boldsymbol{\phi}(t, s)^{s^k}\boldsymbol{B}(s) \left(\boldsymbol{v}_1(s) + \boldsymbol{v}_2(s) \right) \right] ds. \tag{C.75} $$

Here we see that the solution of ${}^{s^{k-1}}\boldsymbol{z}_3(t_0) = {}^{s^{k-1}}\boldsymbol{z}_1(t_0) + {}^{s^{k-1}}\boldsymbol{z}_2(t_0)$ with $\boldsymbol{v}_3(t) = \boldsymbol{v}_1(t) + \boldsymbol{v}_2(t)$, which jumps with $\boldsymbol{G}_3(\boldsymbol{z}, \tau)$, is only the equal to (C.75) if $\boldsymbol{G}_1(\boldsymbol{z}, \tau) = \boldsymbol{G}_2(\boldsymbol{z}, \tau) = \boldsymbol{G}_3(\boldsymbol{z}, \tau)$. In other words, the system only maintains its linearity after jump if the jump maps are equal for each ante jump state. Because this is generally not true, we show that the system is positive homogeneous for any jump gains. A system $\boldsymbol{f}(\boldsymbol{x}, \boldsymbol{u})$ with state $\boldsymbol{x}$ and input $\boldsymbol{u}$ is called positively homogeneous of order κ, when $\alpha^\kappa \boldsymbol{f}(\boldsymbol{x}, \boldsymbol{u}) = \boldsymbol{f}(\alpha\boldsymbol{x}, \alpha\boldsymbol{u})$. If we multiply (C.73) with a constant α, we find

$$ {}^{s^k}\boldsymbol{z}_1(\tau) = \alpha^{s^k}\boldsymbol{\phi}(t, t_0)\ \left(\boldsymbol{G}^{1s^{k-1}}\boldsymbol{z}_1 + \boldsymbol{J}^{1s^{k-1}}\boldsymbol{v}_1 \right) + \alpha \int_{t_0}^{\tau} \left[{}^{s^k}\boldsymbol{\phi}(t, s)^{s^{k-1}}\boldsymbol{B}(s)\boldsymbol{v}_1(s) \right] ds. \tag{C.76} $$

If we now look at the solution for $\boldsymbol{z}_4(t_0) = \alpha\boldsymbol{z}_1(t_0)$ with $\boldsymbol{v}_4(t) = \alpha\boldsymbol{v}_1(t)$ jumping with $\boldsymbol{G}^4(\tau)$, and using the fact that $\boldsymbol{G}^4(\tau) = \boldsymbol{G}^1(\tau)$, we find the same solution as (C.76). This shows that the system (C.67) is positively homogeneous of order zero, for any jump gain ${}^{s^k \leftarrow s^{k-1}}\boldsymbol{H}\left({}^{s^{k-1}}\boldsymbol{z}, {}^{s^{k-1}}\boldsymbol{z}, t \right)$. Hence the name, positively homogeneous jump gain.

Appendix D

Trajectory Tracking Visualization

This chapter visualizes the simulations performed in Section 5.2. First the reference trajectory is visualized with snapshots of the system performing the nominal motion Figure D.1. Then the same visualization is shown in Figure D.2 for a trajectory with an initial state-and-input perturbation, which tracks the reference trajectory.

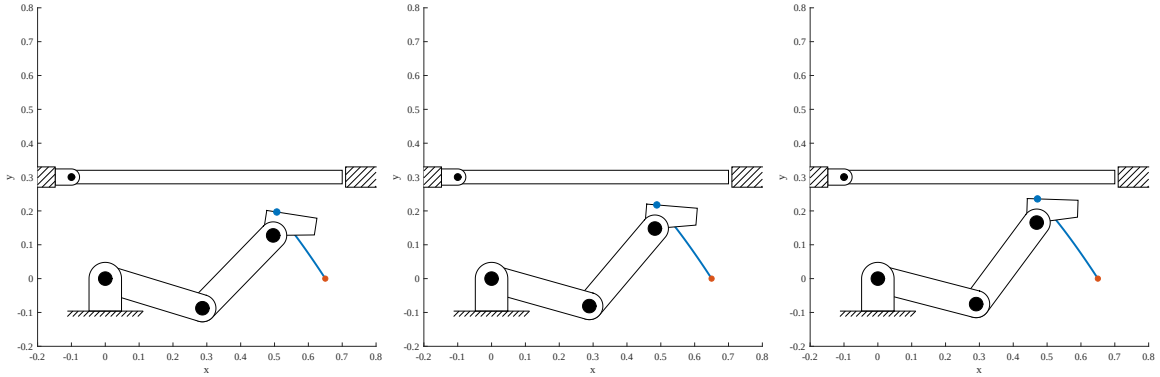

$t = 0.666$ $t = 0.733$ $t = 0.800$

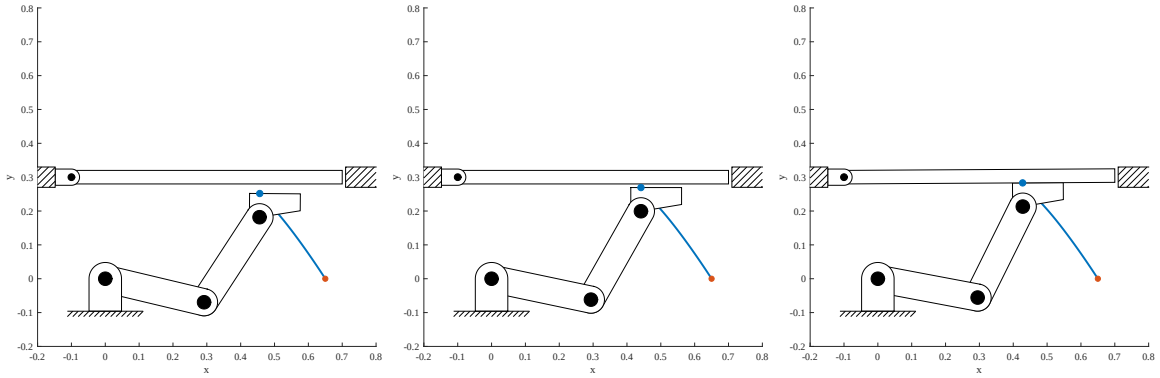

$t = 0.866$ $t = 0.933$ $t = 1.000$

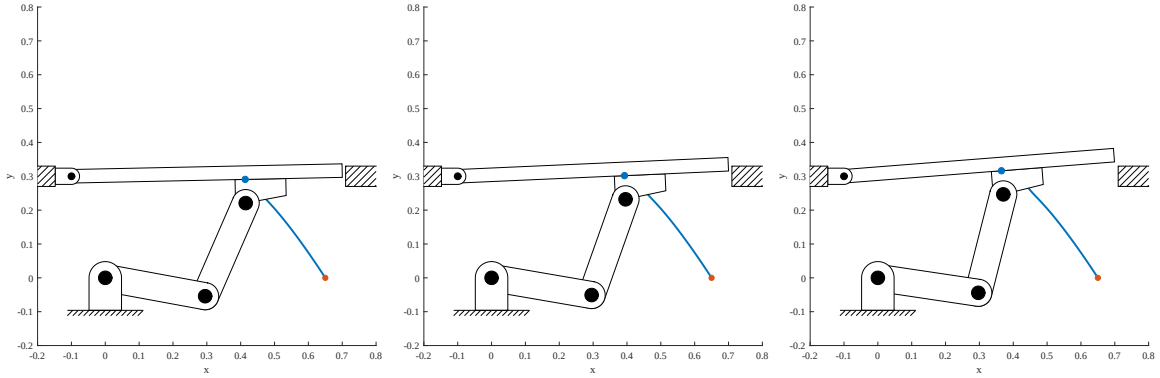

$t = 1.066$ $t = 1.133$ $t = 1.200$

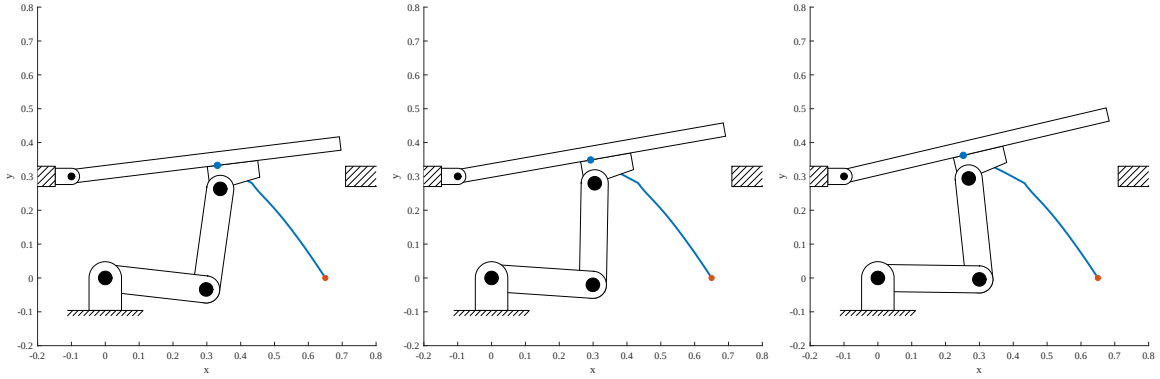

$t = 1.266$ $t = 1.333$ $t = 1.400$

Figure D.1: *Snapshots of the system in Section 5.1 performing the reference trajectory in Section 5.2.*

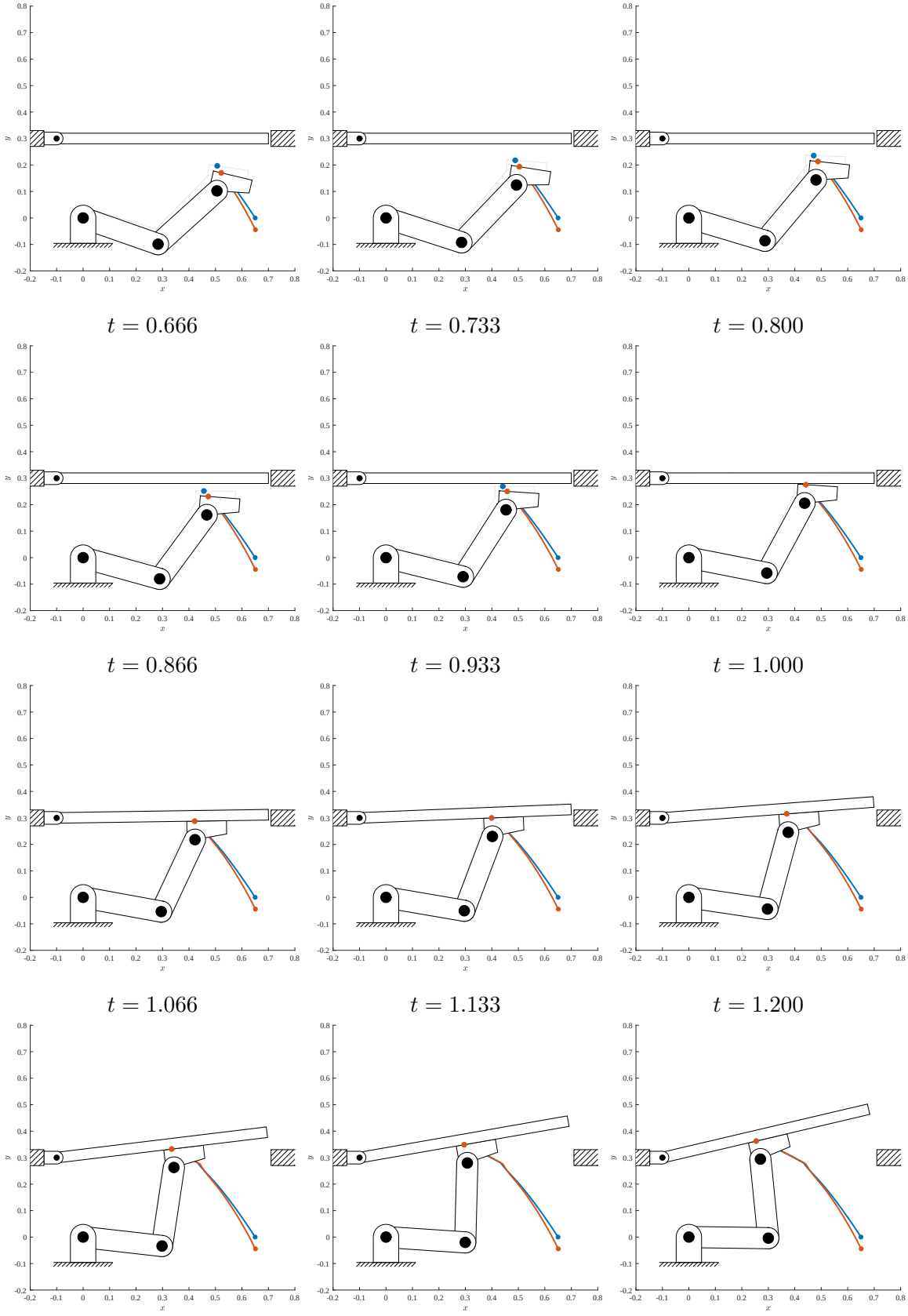

Figure D.2: *Snapshots of the tracking behavior of the system in Section 5.1, tracking the reference trajectory in Section 5.2.*

Appendix E

Code of Scientific Conduct

Declaration concerning the TU/e Code of Scientific Conduct for the Master's thesis

I have read the TU/e Code of Scientific Conduct[i].

I hereby declare that my Master's thesis has been carried out in accordance with the rules of the TU/e Code of Scientific Conduct

Date

08-01-2019

Name

Menno Bokman

ID-number

0784690

Signature

Submit the signed declaration to the student administration of your department.

[i] See: http://www.tue.nl/en/university/about-the-university/integrity/scientific-integrity/
The Netherlands Code of Conduct for Academic Practice of the VSNU can be found here also.
More information about scientific integrity is published on the websites of TU/e and VSNU

January 15 2016